Quantum Transport in Nanowires with Spin-Orbit Interaction: effect of quasi-bound states

Alba Pascual Gil

Directed by Sebastián Bergeret and Vitaly Golovach

Material Physics Department
PhD Program of Physics of Nanostructures and Advanced Materials
University of the Basque Country (UPV/EHU)

December, 2019

A Pepa y José Luis

Agradecimientos

Primero quisiera agradecer a Sebastián Bergeret por su dirección y ayuda en estos cuatro años como supervisor de mi tesis. Tu perspectiva, optimismo y paciencia me han servido de gran ayuda e inspiración para seguir este camino y crecer como persona. Gracias por acogerme en el grupo de *Mesoscopic Physics* durante esta etapa de mi vida. Así mismo, quiero agradecer a Vitaly Golovach todo el apoyo tanto académico como personal que me ha permitido llevar a cabo esta tesis. Aspiro a tener al menos la mitad de tu generosidad como persona y tu amor por la ciencia.

Quisiera también extender este agradecimiento al resto del grupo de *Mesoscopic Physics* del Centro de Física de Materiales. Gracias Dario Bercioux por tus consejos al inicio de mi estancia y también gracias Tineke van den Berg por tu apoyo y amistad. Finalmente, gracias al resto de estudiantes y compaeros de despacho, Cristina, Mikel, Bogusz, Xian-Peng y Julie, por todos los ratos compartidos en este peródo de mi vida.

A nivel más personal, quiero dar las gracias a mis padres por transmitirme sus valores y apoyarme en todo momento para poder hacer siempre lo que yo quisiera. A mi familia por su amor incodicional y a mi hermana Clara por su paciencia infinita. A mi pequeña familia en Donostia por todos esos momentos inolvidables y debates acalorados en las comidas y *coffee breaks*. En especial gracias a Moritz, Patri y Tomáš, no sería hoy quien soy hoy en día sin vosotros. Gracias también a Chusa y Mateo por darme refugio espiritual, a Paloma por aportarle ese toque de humor a mi vida, a Yaiza por completarme, y al resto de amigos que me han acompañado en este viaje. Finalmente, gracias a mi pareja Juan Carlos por estar ahí siempre.

Acknowledgements

First of all, I would like to thank Sebastián Bergeret for all the guidance during the past four years as my PhD supervisor. Your vision, optimism and patience have been of great help and an inspiration to grow as a person. Thank you for welcoming me into the Mesoscopic Physics group during the duration of my stay. I would also like to thank Vitaly Golovach for all his help not only on an academic level but also on a personal one. I aspire to have your generosity as a person and your passion for science.

I would like to extend this acknowledgement to the rest of the Mesoscopip Physics group from the Materials Physics Center in Donostia. Thank you Dario Bercioux for all your advice in the early stages of my stay here and Tineke van den Berg for all your support and friendship. Finally, thanks to the rest of students and office mates, Cristina, Mikel, Bogusz, Xian-Peng and Julie, for all this time spent together.

On a more personal note, I would like to thank my parents for their upbringing and encouragement to pursue my dreams. To my family for their unconditional love and my sister Clara for her infinite patience. To my little family in Donostia for every unforgettable moment and every heated discussion during coffee breaks. And specially, thank you Moritz, Patri and Tomáš, I wouldn't be me today without you. Thank you Chusa and Mateo for offering me spiritual refuge, to Paloma for the spot of humor in my life, to Yaiza for completing me and to the rest of my friends wherever they are for accompanying me during this journey. Last but not least, thank you Juan Carlos for being there always.

Resumen

Esta tesis tiene como objetivo el estudio de transporte en nanohilos semiconductores con interacción espín-órbita e impurezas. A día de hoy estos nanohilos son de los materiales más versátiles para el diseño de dispositivos cuánticos. Ejemplo de ello, es el intenso estudio de los fermiones de Majorana, que pueden detectarse en los extremos de nanohilos, cuando éstos están en contacto con un superconductor [1, 2, 3, 4, 5, 6, 7]. Crucial para la aparición de los fermiones de Majorana es la interacción espín-órbita y el bajo nivel de desorden en los nanohilos. De hecho, el desorden en nanohilos cuánticos afecta fuertemente a la conductancia de los modos de Majorana [8, 9, 10, 11, 12, 13, 14].

Por otro lado, las estructuras semiconductoras con interacción espín-órbita nos llevan atrás en el tiempo hasta la propuesta de Datta y Das de un transistor [15], que propone el control sobre la interacción espín-órbita por medio de un *gate* para rotar el espín del electrón y así controlar el transporte de carga entre dos electrodos ferromagnéticos. Los intentos de fabricar tal dispositivo han topado con varios problemas [16, 17, 18], incluída la baja eficiencia en la inyección de espín del ferromagneto en el semiconductor, pero también con la relajación del espín inducida por el *scattering* del electrón debido al desorden en el dispositivo.

De los ejemplos anteriores se desprende que el estudio del desorden requiere especial atención. En particular en respuesta a la pregunta de cómo afecta el desorden al transporte de carga y espín en un nanohilo cuasi-unidimensional. Esta pregunta es absolutamente no trivial. En los nanohilos, el desplazamiento está confinado en una dirección y los portadores de carga solo pueden desplazarse en la dirección ortogonal a la del potencial de confinamiento. La combinación del confinamiento con la presencia de la interacción espín-órbita de tipo Rashba induce el acoplamiento entre subbandas. Esto afecta fuertemente al transporte en el

hilo cuántico, llegando por ejemplo a suprimir la modulación de espín para valores grandes de la interacción Rashba [19, 20, 21, 22]. Por otro lado, la presencia de una impureza puede llevar a la formación de estados cuasi-ligados localizados entorno a la impureza. En trabajos previos se ha demostrado que la presencia de modos evanescentes lleva a fenómenos poco usuales en el transporte electrónico, como por ejemplo la perfecta transmisión en el umbral energético en el que una nueva subbanda es accesible y comienza a propagar. También se ha observado que cerca, pero por debajo de este umbral, la aparición de estados cuasi-ligados localizados en torno a una impureza atractiva es responsable del bloqueo total de canales de transmisión [23, 24]. La combinación de ambos efectos nunca ha sido tratada.

En esta tesis abordamos este tema y presentamos un estudio teórico exhaustivo del transporte electrónico en nanohilos cuánticos semiconductores con interacción espín-órbita en la presencia de impurezas. Modelamos el nanohilo cuántico como un sistema cuasi-unidimensional en el que el movimiento de los electrones está confinado en la dirección perpendicular a la de propagación. La competición entre la interacción espín-órbita, el confinamiento lateral y la impureza hace que el problema sea altamente no-trivial. Para hacer frente a este problema usamos una combinación de técnicas y aproximaciones que nos permiten identificar novedosas propiedades del transporte de carga y del transporte de espín. Específicamente, describimos la conductancia mediante el formalismo de Landauer-Büttiker, extendiéndolo para el caso de campos dependientes del espín. Describimos el transporte a través de este formalismo en función de los coeficientes de scattering. Para calcular los coeficientes de la matriz de scattering usamos la ecuación de Lippmann-Schwinger, un método ampliamente usado en el tratamiento del scattering en la mecánica cuántica.

Una de las principales dificultades en el tratamiento de la interacción espín-órbita en un potencial de confinamiento es la hibridación de las subbandas. Para superar este problema introducimos la transformación de Schrieffer-Wolff, una transformación de *gauge* que elimina esta hibridación manteniendo la complicación de los efectos de Rashba en la función de onda transformada.

Combinando las técnicas mencionadas calculamos de forma analítica la coductancia para el transporte de carga y espín en un nanohilo con interacción de tipo Rashba en presencia de una impureza puntual.

Encontramos que la impureza acopla estados propagantes y estados evanescentes en el nanohilo cuántico, induciendo estados cuasi-ligados localizados entorno a la impureza. Por otra parte, la interacción espín-órbita de tipo Rashba permite distintos mecanismos de transporte electrónico. Como consecuencia, la conductancia presenta transmisión balística perfecta en la energía umbral donde el siguiente canal se vuelve transmisivo. Además, por debajo de dicha energía umbral la conductancia presenta una reducción significativa. Demostramos que para las subbandas más bajas en esta energía resonante, todos los electrones inyectados en el nanohilo cuántico en un estado preparado de tal manera que su espín se alínea en cierta dirección preferente, solo tienen una forma de transmitir a través de la impureza: mediante un proceso en el que su espín salta a la orientación opuesta. No solo es ésta la única forma de propagar hacia el otro lado de la impureza, sino que la probabilidad de que suceda este proceso de inversión del espín aumenta notablemente respecto a la probabilidad fuera de la resonancia. Es más, en la energía exacta de la resonancia, mientras la probabilidad de transmisión manteniendo la misma orientación en el espín se reduce hasta cero, la probabilidad de transmisión con inversión del espín es máxima.

Más allá del transporte de carga, también derivamos expresiones para las corrientes de espín en el nanohilo y derivamos una expresión para el torque de espín-órbita inducido por la impureza. Demostramos que este torque depende completamente de los procesos de inversión del espín en el scattering. Otro resultado clave de esta tesis es la relación subyacente entre el campo de gauge $SU(2)$ y la transmisión con inversión del espín.

La tesis está organizada de la siguiente manera: el Capítulo 1 es la introduccion a la tesis. En los Capítulos 2 y 3 extendemos esta introducción para hablar de conceptos generales que son usados a lo largo del resto de la tesis. En particular, en el Capítulo 2 proporcionamos un breve repaso sobre el tratamiento teórico del scattering en nanohilos mediante la ecuación de Lippmann-Schwinger. En el Capítulo 3 introducimos la interacción espín-órbita en sistemas de baja dimensionalidad como 2DEG y nanohilos. En este último caso explicamos la dificultad de diagonalizar el Hamiltoniano correspondiente debido a la hibridación de las subbandas.

En el Capítulo 4 introducimos el formalismo de Landauer-Büttiker para la descripción del transporte cuántico. Extendemos la derivación habitual para incluir un sistema con interacción espín-órbita de tipo Rashba y como consecuencia el sistema mantiene no solo corrientes de carga sino también

de espín. También en este captulo introducimos el concepto de voltaje de espín en los bornes conectados al nanohilo. La ausencia de conservación de la corriente de espín en ambos lados de la impureza es interpretada como un torque de espín-órbita que surge de los mecanismos de transmisión y reflexión que invierten el spín inducidos por la impureza debido a la interacción espín-órbita. El principal resultado de este capítulo es la expresión para las corrientes y el torque escritos en función de los coeficientes de transmisión.

En el Capítulo 5 calculamos los coeficientes de scattering explícitamente para el nanohilo. Para ello, aplicamos una transformación de gauge y derivamos una expresión para los coeficientes que es exacta hasta segundo orden en la perturbación. Como primer paso, eliminamos el término responasable de la hibridación de las subbandas debido a la interacción espín-órbita de Rashba empleando una transformación de Schrieffer-Wolff. Esto nos permite obtener los estados de scattering en todo el nanohilo mediante la ecuación de Lippmann-Schwinger del Capítulo 2. Como segundo paso, calculamos los coeficientes de transmisión que resultan ser dependientes del espín debido a la interacción espín-órbita. Identificamos dos tipos de mecanismos de transmisión: unos que mantienen la orientación del espín y otros que la invierten en el sentido opuesto cuando la partícula sufre scattering.

En el Capítulo 6 presentamos los principales resultados de las propiedades del transporte en el nanohilo. Nos centramos tanto en la corriente de carga como en la de espín. Mostramos que para la conductancia aparecen notables características relacionadas con la presencia de estados cuasi-ligados localizados en torno a la impureza. Enseñamos cómo una impureza no magnética puede invertir el espín como consecuencia de la interacción de Rashba, y cómo la probabilidad de transmisión con inversión del espín refleja un comportamiento resonante similar. Además, demostramos que cuando el sistema está en la resonancia, la única transmisión permitida es mediante la inversión del espín y debatimos como esta transmisión que es físicamente medible depende de factores de la simatría del campo de gauge $SU(2)$.

Cada capítulo tiene su propia conclusión, pero de todas formas resumimos toda la tesis en el Capítulo Chapter 7, dónde también discutimas líneas futuras de investigación basadas en los métodos desarrollados en esta tesis.

Contents

Chapter 1

Introduction

Nanowires with spin-orbit interaction provide one of the most versatile playgrounds for quantum design available to date in condensed matter. A prominent example is the realization of Majorana fermions (MF) as solutions of the Bogoliubov-de Gennes equation, combining a particle-like and a hole-like excitation into a superposition of states, localized at an end of a nanowire. Such zero-energy modes were first proposed theoretically [1, 2] and then followed by a large number of experiments [3, 4, 5, 6, 7] showing solid evidence for these elusive fermionic states. The spin-orbit interaction plays an important role in these structures, allowing to convert the usual s-wave pairing of electrons with opposite spins into a p-wave pairing of electrons with equal spins. The mechanism of this singlet-to-triplet conversion of superconducting pairing correlations relies solely on the interplay between the spin-orbit interaction and a homogeneous Zeeman field, which act together to create a space-dependent effective exchange field of a helical type [25], equivalent to an SU(2) 'electric' field in the Yang-Mills field theory [26]. This Yang-Mills electric field, which is the product of Zeeman energy times spin-orbit interaction strength, can be extracted from transport measurements in the Coulomb blockade regime of a quantum dot defined in the nanowire by electrical gating [27]. While signatures of MF have been observed in nanowire-superconducting structures, the measurement of the helical gap has proven to be more difficult [28, 29]. Another key premise for this is ballistic electron transport, however the quantized conductance measurements have proved to be difficult due to strong electron backscattering [30, 31]. Furthermore, disorder in Majorana nanowires can

strongly affect conductance of the zero modes. [8, 9, 10, 11, 12, 13, 14].

On the other hand, the spin-orbit interaction couples efficiently the electron spin to its orbital degrees of freedom, making it possible to affect the spin by engineering the scalar potential along the path of the electron. One can envision designs in which the desired effect of the spin-orbit interaction is strongly enhanced, which can be used to improve device functionality. The idea of using the spin-orbit interaction to rotate the electron spin goes back to the Datta-Das transistor [15], in which the control over the spin-orbit interaction was proposed to be used to modulate the conductance of a ferromagnet-semiconductor-ferromagnet device. Attempts to implement this transistor [16, 17, 18] faced several problems, including the low spin injection efficiency from ferromagnet into semiconductor and the detrimental effect of the scattering of the electron on disorder, which leads to spin relaxation. The interplay between superconductivity and spin-dependent fields also plays a fundamental role in the emerging field of superconducting spintronics [32, 33, 34, 35].

Beside possible applications of semiconducting systems with spin-orbit interaction, there are still fundamental questions regarding the electronic transport in such structures that still require a theoretical analysis. In nanowires, an open question is how a defect may affect the spin and charge transport in a quasi one dimensional wire. The answer to this question is far from trivial in a quasi-one-dimensional quantum wire formed by applying a confining potential to a 2DEG . On the one hand the combination of the quantization of motion along the orthogonal axis and the presence of an intrinsic Rashba spin-orbit interaction gives rise to inter-subband mixing that can strongly affect transport properties of the nanowire, for instance suppressing spin-modulation for large values of Rashba coupling [19, 20, 21, 22]. On the other hand the presence of a scattering center, as for example an impurity, may lead to formation of quasi-bound states localized around the impurity. Previous studies have shown that the presence of evanescent modes leads to unusual properties in the transport such as perfect transparency when the Fermi energy approaches subband minima and the blocking of channels due to quasi-bound states localized around an attractive impurity [23, 24]. Combination of both spin-orbit interaction and impurity scattering remains almost unexplored .

In this thesis we address this issue and present a thorough theoretical study of the electronic transport in semiconducting nanowires with Rashba

spin-orbit coupling in the presence of impurities. We model the nanowire as a quasi-one-dimensional system where the motion of the electrons is confined in the direction perpendicular to the transport direction. The interplay between the spin-orbit coupling, confinement and impurity potential, makes the problem highly non-trivial. We tackle this issue through a combination of theoretical techniques and approximations, which allows us to identify striking novel properties of both the charge and spin transport. Specifically, we describe the conductance by using the well established Landauer-Büttiker formalism, which we extend for the case of spin-dependent fields. Within this formalism the transport is described in terms of the scattering coefficients. In order to calculate these coefficients we use the Lippmann-Schwinger equation, a widely used method to treat scattering in quantum mechanics [36, 37, 38, 20, 39]. One of the main difficulties when dealing with spin-orbit coupling in a confining potential is the intermixing of subbands. In order to overcome this problem we introduce the Schrieffer-Wolff transformation with which we gauge away this intermixing while still accounting for its effects.

By the combination of the above techniques we compute the charge and spin conductances of the Rashba nanowire in the presence of a point-like impurity. We find that the impurity couples evanescent and propagating states in the nanowires, inducing quasi-bound states; while the Rashba spin-orbit interaction allows for different spin-dependent mechanisms for electronic transport. As a result, the charge conductance presents perfect ballistic transmission at the threshold energy for a channel that becomes propagating. In addition, below this threshold energy there appears a dip in the conductance as a consequence of the quasi-bound states strongly suppressing transmission. We prove that for the lowest subbands at this resonant energy all electrons injected in a prepared spin-up state scatter from the impurity to a spin-down state. Furthermore, this spin-flip mechanism is not only the only transmission allowed at resonant energy but it is also enhanced. We derive the expressions for the spin currents in the nanowire and find out and expression for the spin-orbit torque induced by the impurity and the spin-flip mechanisms for transport. While the effects of Rashba spin-orbit coupling in the charge conductance are quite relevant, our key result consists in finding the underlying relation between the spin-flip transmission and the $SU(2)$ field.

The thesis is organized as follows:

In Chapters 2 and 3 we extend the introduction, by discussing general

concepts used in the rest of the thesis. In particular, in Chapter 2 we provide a brief overview of scattering in semiconducting nanowires and the Lippmann-Schwinger equation, our theoretical tool to determine the scattering coefficients. In Chapter 3 we discuss the spin-orbit coupling in low dimensional systems as 2DEGs and quasi 1D nanowires. In the latter case we explain the difficulty of diagonalizing the Hamiltonian due to the subband intermixing.

In Chapter 4 we introduce the Landauer-Büttiker formalism for the description of quantum transport. We extend the customary derivation to a system with Rashba spin-orbit coupling. This automatically extends the formalism to a spin-dependent situation. The system now supports both spin and charge currents and we introduce the concept of spin-bias in the leads connected to the nanowire. The non-conservation of the spin-current at both sides of the impurity is interpreted as a spin-orbit torque arising from the spin-flip transmission mechanisms induced in the impurity by the Rashba spin-orbit coupling. The main result of this chapter is the expression for the currents and torque in terms of the scattering coefficients.

In Chapter 5 we calculate the scattering coefficients explicitly for the nanowire. In order to do this we perform a gauge transformation and derive an expression for the coefficients accurate up to second order of perturbation in the spin-orbit coupling strength. As a first step, we gauge away the intermixing of subbands due to Rashba spin-orbit interaction by performing a Schrieffer-Wolff transformation. This allows us to obtain the scattering states in the whole wire by means of the Lippmann-Schwinger equation following the discussion of Chapter 2. In a second step, we calculate the transmission coefficients, which are now spin-dependent due to the Rashba spin-orbit coupling. We identify two types of transmissions: one that preserves the spin of the scattered particle and one that flips it.

In Chapter 6 we present the main results for the transport properties of the nanowire. We focus on both, charge and spin currents. We show that the conductance presents striking features related to the presence of quasi-bound states localized around the impurities. We show that a non-magnetic impurity can flip spin as a consequence of Rashba spin-orbit coupling, and that the spin-flip transmission reflects similar resonant behavior. As a result, we prove that at the resonant energy the only transmission allowed is through the spin-flip mechanism and we discuss how this measurable transmission $SU(2)$ symmetry factors. This result paves the way for a sensitive interference technique to measure the SU(2) gauge field in nanowires.

Each chapter has its own conclusion section. Nevertheless we briefly summarize the whole thesis in Chapter 7.

Chapter 2

Theoretical description of transport in semiconducting nanowires

Semiconductors are at the heart of modern electronics. In particular, they are important building blocks of nanostructures with versatile applications due to the accurate control of electronic transport via doping and external electric fields [40]. Furthermore, the advances in growth techniques such as molecular beam epitaxy (MBE) and patterning techniques, allows to create high-quatlity, meaning higher electron mobility, heterostructures that exhibit quantum confinement effects and a variety of quantum phenomena. The discovery of conductance quantization in low-dimensional systems (see Fig. 2.1)launches an intensive research of transport properties related to the charge of the electron [41]. In addition, the field of spintronics extended the research to spin-dependent transport phenomena, and the use of semicoductors for the design, and fabrication of novel spin-based electronic devices. The idea behind possible applications in this field relies on the control of the spin dynamics and relaxation by means of external fields.

The cornerstone of many of the advances in these fields are two-dimentional electron gas (2DEG) typically formed at the interface of III-V semiconductor heterostructure which lead to the observation of new interesting phenomena, absent in bulk systems, such as Shubnikov-de Haas oscillations [42, 43], the integer [44] and fractional quantum Hall effect [45, 46, 46, 47] and the quantized conductance [48, 49].

In a two-dimensional electron gas electrons are confined to a narrow

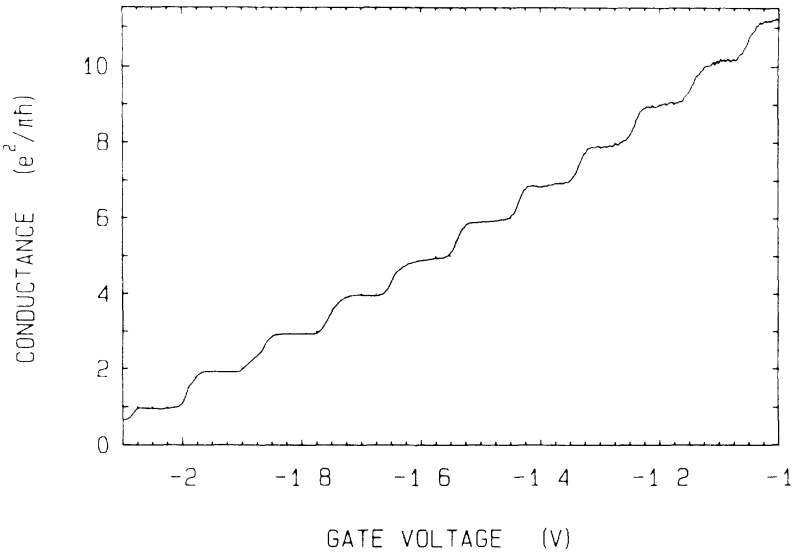

Figure 2.1: Quantized conductance for a point-contact as a function of gate voltage in a GaAs/InGaAs heterostructure. The conductance changes in quantized steps of $2e^2/h$. This figure taken from [48].

quantum well (QW) along the growth direction. Electrons can only move in the plane perpendicular to that direction. Transport properties, and band structure of 2DEGs can be modified by introducing dopants during growth, which contribute with electrons or holes to the QW, and by carefully choosing the materials in the quantum well and the barriers [47].

The two ways of realizing 2DEGs are by band inversion and heterostructure based systems. In Fig. 2.2 we can see the electrostatic potential $V_z(z)$ (along the growth direction z) experienced by conduction band electrons in two situations: one shows a triangular quantum well, which forms, e.g., at the interface between n-doped AlGaAs and undoped GaAs and the other square quantum well, where a thin layer of the semiconducting material supporting the 2DEG, here GaAs, is sandwiched between layers of a different semiconducting material, here AlGaAs [50, 51].

In the first case, the Fermi energy of both will align at the interface of the semiconductors, where translational invariance is broken, with electrons coming out from the n-AlGaAs leaving behind an accumulation of holes which leads to a bending of the conduction and valence band [52]. For large enough hole concentration, the conduction band dips below the Fermi

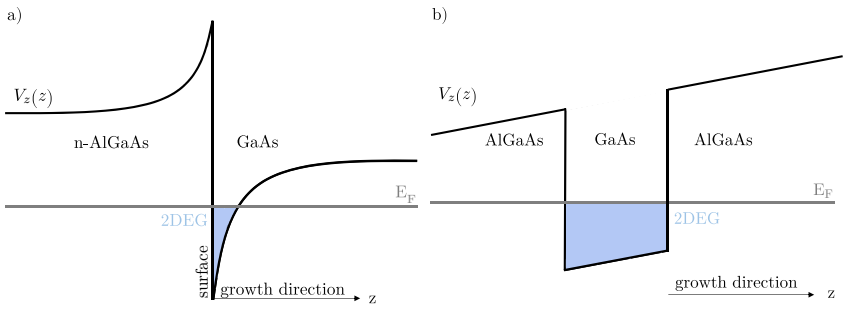

Figure 2.2: (a) Triangular quantum well in an inversion layer semiconductor heteroestructure. (b) Square quantum well in sandwich-like heteroestructure.

energy at the surface. We can see then, that the electron density is sharply peaked near the GaAs-AlGaAs interface forming a thin conduction layer of thickness comparable to the Fermi wavelength, that is the two-dimensional electron gas, hence the name inversion layer. This layer is formed naturally, however, the mobility of layer-inversion 2DEGs is severely limited. Furthermore, since the electrons live at this interface, the quality of the 2DEG is highly dependent on details of fabrication. To achieve higher mobilities the quantum well has to be deeper [53, 54].

This can be done by introducing dopants in sandwiches of materials with differing bandgaps. When two such engineered materials with unequal bandgaps are brought into contact, the Fermi energy of the two materials will align and can form a quantum well. To align the chemical potential in the InGaAs/InAs/InGaAs sandwich structure, charge is transferred from remote dopants, introduced during growth, and into the quantum well.

With the help of gate electrodes (external electric fields), or by clever sample fabrication, a large variety of potential energy structures can be achieved in the 2DEG. This way the motion of electrons can be further confined within the 2DEG semiconductor heterostructure plane leads to (quasi) one-dimensional quantum wires and zero dimensional quantum dots. Quantum confinement gives rise to new and fundamentally important physics phenomenon, it is therefore interesting to study quantum transport through these quantum confined mesoscopic systems [55].

The main focus in this thesis is the theoretical study of transport through a quantum nanowire in the presence of an impurity or defect. Therefore we summarize in this chapter the main theoretical tools for its description.

2.1 Theoretical approach to scattering in nanowires

Quantum wires have been proposed as basic elements in the design of many quantum devices. Because of their size the electronic transport rely on a full quantum mechanical approach rather than a classical one. The most important parameters (or length scales) that describe a semiconductor are the phase coherence length ℓ_ϕ , Fermi wavelength λ_F, and the mean free path ℓ_e of electrons. In a mesoscopic device the ℓ_ϕ is much larger than the physical dimensions (length L and width W) of the device, while the λ_F is comparable to these dimensions. If ℓ_e is much larger than L and W the device is in the ballistic regime in which electrons propagate through the device without being scattered, either elastically or inelastically, by impurities or phonons respectively.

In this thesis we are interested in transport through a nanowire in the presence of an impurity or defect. In particular we describe how the electronic transport is affected by the presence of the impurity, or in other words how the nanowire conductance depends on impurity and intrinsic properties of the wire. Because it is essential for our next analysis, we introduce here the Lippmann-Schwinger equation, which we will use for the description of quantum scattering .

We start discussing this approach in a general 3D situation and then we focus on scattering on a delta-potential in a purely 1D system. We will discuss the limitations of the Born approximation. Finally we focus on a more realistic nanowire described by a transverse confining potential

The main goal in scattering theory is to obtain the wave functions describing the scattering particle given a proper boundary conditions imposed, by the incoming particle. We can then begin by constructing the solution of the Schrödinger equation meeting these two criteria in formal terms.

2.1.1 The Lippmann-Schwinger Equation: theoretical description

Following Ref.[56], we consider a system described by the following Hamiltonian

$$\mathcal{H} = H_0 + V \ , \tag{2.1}$$

with $H_0 = \frac{p^2}{2m_e^*}$ describes the free electrons with mass $m_e^*$and V representing the scattering potential.

The goal is to find a solution for the states $|\psi\rangle$ of the Schrdinger equation:

$$\mathcal{H}|\psi\rangle = E|\psi\rangle \ , \tag{2.2}$$

such that in the limiting of a vanishing potential $V \to 0$ the solution recovered would be that of the unperturbed system $H_0|\phi\rangle = E|\phi\rangle$, i.e. $|\psi\rangle \to |\phi\rangle$. Formally one can write

$$|\psi\rangle = \frac{V}{E - H_0}|\psi\rangle \ . \tag{2.3}$$

Then one can write the solution to Eq. (2.2) as a sum of the particular solution $|\phi\rangle$ and the homogeneous solution in Eq.(2.3) as follows,

$$|\psi\rangle = \frac{1}{E - H_0}V|\psi\rangle + |\phi\rangle \ . \tag{2.4}$$

Some complications arise from the singular nature of $[E - \mathcal{H}_0]^{-1}$ as the continuous spectrum of $\mathcal{H}_0$ will include E. This problem can be circumvented by substituting $E \to E \pm \mathrm{i}\epsilon$ as a way to encode the boundary conditions for integration, so one may write the so-called Lippmann-Schwinger equation as follows,

$$|\psi^{(\pm)}\rangle = |\phi\rangle + \frac{1}{E - \mathcal{H}_0 \pm \mathrm{i}\epsilon}V|\psi^{(\pm)}\rangle \ , \tag{2.5}$$

The physical meaning of $(\pm)$ will be discussed later by evaluating $|\psi^{(\pm)}\rangle$ at long distances. For the moment, we write the Lippmann-Schwinger equation in the coordinate basis,

$$\langle \mathbf{r}|\psi^{(\pm)}\rangle = \langle \mathbf{r}|\phi\rangle + \int d\mathbf{r}'\langle \mathbf{r}|\frac{1}{E - \mathcal{H}_0 \pm \mathrm{i}\epsilon}|\mathbf{r}'\rangle\langle \mathbf{r}'|V|\psi^{(\pm)}\rangle \ . \tag{2.6}$$

In order to solve this integral equation one must first evaluate the kernel defined by,

$$G_\pm(\mathbf{r}, \mathbf{r}') = \langle \mathbf{r}|\frac{1}{E - H_0 \pm \mathrm{i}\epsilon}|\mathbf{r}'\rangle\langle \mathbf{r}'| \ , \tag{2.7}$$

which is nothing more than the Green's function for the Helmholtz equation,

$$\left(\nabla^2 + k^2\right) G_\pm(\mathbf{r}, \mathbf{r}') = \frac{2m_e^*}{\hbar^2}\delta(\mathbf{r}, \mathbf{r}') \ . \tag{2.8}$$

The difficulty of most scattering problems lies in finding the proper Green's function that solves Eq. (2.8) for the system. For the moment, in our derivation we may not write explicitly $G_{\pm}(\mathbf{r},\mathbf{r}')$ so that Eq. (2.6) reads,

$$\langle \mathbf{r}|\psi^{(\pm)}\rangle = \langle \mathbf{r}|\phi\rangle + \int d\mathbf{r}' G_{\pm}(\mathbf{r},\mathbf{r}')\langle \mathbf{r}'|V|\psi^{(\pm)}\rangle \ . \tag{2.9}$$

Notice that the wavefunction $\langle \mathbf{r}|\psi^{(\pm)}\rangle$ in the presence of the scatterer is written as a sum of the incident wave $\langle \mathbf{r}|\phi\rangle$ and a term that represents the scattering interaction. In most physical systems one works with the positive solution for the Green's function $G_{+}(\mathbf{r},\mathbf{r}')$ as it satisfies the so called outgoing boundary conditions (as opposed to the negative solution $G_{-}(\mathbf{r},\mathbf{r}')$ corresponding to the less intuitive incoming boundary conditions). This means that $G_{+}(\mathbf{r},\mathbf{r}')$ garantees an outgoing flow from $\mathbf{r}'$ to $\mathbf{r}$ choosing $E - H_0 + \mathrm{i}\epsilon$ in Eq. (6.4), while $G_{-}(x,x')$ on the other hand leads to an incoming current from $\mathbf{r}$ to $\mathbf{r}'$ choosing $E - H_0 - \mathrm{i}\epsilon$. From here on, we assume the positive case and drop the $(\pm)$ sign reference in our description for notation simplicity.

Now, in order to evaluate the specific behavior of $\langle \mathbf{r}|\psi^{(\pm)}\rangle$ more explicitly let us consider a local potential, that is a potential diagonal in the coordinate representation. The potential V is considere to be local if it can be written as

$$\langle \mathbf{r}'|V|\mathbf{r}''\rangle = V(\mathbf{r}')\,\delta(\mathbf{r}' - \mathbf{r}''') \ , \tag{2.10}$$

and as a result,

$$\begin{aligned}\langle \mathbf{r}'|V|\psi^{(\pm)}\rangle &= \int d\mathbf{r}''\langle \mathbf{r}'|V|\mathbf{r}''\rangle\langle \mathbf{r}''|\psi^{(\pm)}\rangle \\ &= V(\mathbf{r}')\langle \mathbf{r}'|\psi^{(\pm)}\rangle \ .\end{aligned} \tag{2.11}$$

If we define the incident wavefunction to be a plane wave $\phi(\mathbf{r}) = \langle \mathbf{r}|\phi\rangle$,then the equation Eq. (2.9) simplifies to,

$$\psi(\mathbf{r}) = \phi(\mathbf{r}) + \int d\mathbf{r}' G(\mathbf{r},\mathbf{r}')\,V(\mathbf{r}')\,\psi(\mathbf{r}') \ , \tag{2.12}$$

giving the scattering states for an incoming particle evaluated at position x. For a finite range potential, the scattering state inside the support region will have a contribution limited to this space. So in effect the Lippmann-Schwinger equation provides a way to study scattering processes as a result

of a scatterer (the finite range potential) at a point far away the range of the potential. Eq. (2.12) equation can also be written in matrix notation,

$$|\psi\rangle = |\phi\rangle + GV|\psi\rangle \ , \tag{2.13}$$

and sometimes it is more convenient for clarity sake. From now on, and specially in the next section, both notations will appear indistinctly.

In summary, we have introduce the Lippmann-Schwinger both in integral form Eq. (2.12) and in matrix form Eq. (2.13). This is an iterative equation that we will try to solve in the next section for a simple 1D model system in two different ways, first introducing the Born approximation and then by direct integration.

2.1.2 Scattering in a 1D system

The Lippmann-Schwinger is a recursive equation and in most cases its exact solution is a rather difficult task. Therefore to solve (2.12) we write its solution in an recursive way, such that

$$|\psi_{new}\rangle = |\phi\rangle + GV|\psi_{old}\rangle \ . \tag{2.14}$$

In zero order approximation $|\psi_{old}\rangle = |\phi\rangle$, and from Eq. (2.14) we obtain the first order approximation: $|\psi_{new}\rangle = (1 + GV)\,|\phi\rangle$. After iteration of this procedure one can formally write the solution of Eq. (2.14) as:

$$|\psi\rangle = (1 + GV + GVGV + GVGVGV + ...)\,|\phi\rangle \ , \tag{2.15}$$

which is known as the Born series.

The physical picture associated to Eq. (2.15) is that of a free electron propagation, described by G, suffering instantaneous collisions, described by V. The first Born approximation consist in truncating the series at firts order of V, $|\psi\rangle = (1 + GV)\,|\phi\rangle$. One must note that the Born series does not necessarily converge and the Born approximation fails in the description of certain scattering phenomena.

To illustrate how the Born approximation fails we consider the following 1D case,

$$\mathcal{H} = \frac{p_x^2}{2m_e^*} + V\,(x) \ , \tag{2.16}$$

where V is a delta potential $V = v_0\delta\,(x - x_0)$. Here, v_0 represents the strength of the potential and x_0 the position of the scatterer center. We

first solve the problem via the first Born approximation, meaning that in Eq. (2.12) the wavefunction inside the integral is approximated to be $\psi(x') \approx \phi(x')$, which means the interaction with the scatterer is weak. In order to obtain the solution for the scattering states we need the Green's function as a solution of Eq. (2.8) with outgoing boundary conditions in 1D (see Appendix A). This reads:

$$G(x,x') = -\frac{m_e^*}{\hbar^2}\frac{\mathrm{i}}{k}\mathrm{e}^{\mathrm{i}k|x-x'|} \,. \tag{2.17}$$

If we assume that the incoming wave is a plane wave $\phi(x) = \mathrm{e}^{\mathrm{i}kx}$, then following the asymptotic form of the wavefunction for the transmission on the right side of the potential ($x \to +\infty$) we get

$$\psi(x) = \mathrm{e}^{\mathrm{i}kx} + \frac{\mathrm{i}}{k}\frac{m_e^*}{\hbar^2}v_0\mathrm{e}^{\mathrm{i}kx} \,, \tag{2.18}$$

which means that the transmission probability of an incident wave $\phi(x)$ is given by $\psi(x) = \phi(x)\,t$, resulting in the transmission coefficient under the first Born approximation:

$$t = 1 - \frac{\mathrm{i}}{k}\frac{m_e^*}{\hbar^2}v_0. \tag{2.19}$$

In contrast, by direct integration of Eq. (2.12) with the delta-potential we obtain,

$$\psi(x) = \phi(x) + v_0 G(x,x_0)\,\psi(x_0) \,, \tag{2.20}$$

by evaluating Eq. (2.20) at the scatterer center $x = x_0$ it is possible to obtain the wavefunction at the point of the scatterer:

$$\psi(x_0) = \frac{\phi(x_0)}{1 - v_0 G(x_0,x_0)} \,, \tag{2.21}$$

by substituting Eq. (2.21) in Eq. (2.20) it is possible to obtain the full solution for the scattering states along the whole system as follows,

$$\psi(x) = \phi(x) + \frac{v_0 G(x,x_0)\,\phi(x_0)}{1 - v_0 G(x_0,x_0)} \,. \tag{2.22}$$

Substituting Eq. (2.17) in Eq. (2.22) and consider an incoming plane wave $\phi(x) = \mathrm{e}^{\mathrm{i}kx}$, and looking at the asymptotic form of the wavefunction for the transmission ($x \to +\infty$) we can write,

$$\psi(x) = \mathrm{e}^{\mathrm{i}kx} - \frac{\frac{\mathrm{i}}{k}\frac{m_e^*}{\hbar^2}v_0}{1 - \frac{\mathrm{i}}{k}\frac{m_e^*}{\hbar^2}v_0}\mathrm{e}^{\mathrm{i}kx} \,, \tag{2.23}$$

and from here the transmission coefficient in this case for the direct integration of Eq. (2.12) will be

$$t = 1 - \frac{\frac{\mathrm{i}}{k}\frac{m_e^*}{\hbar^2}v_0}{1 - \frac{\mathrm{i}}{k}\frac{m_e^*}{\hbar^2}v_0} \,, \tag{2.24}$$

which is a renormalized version of the transmission coefficient obtained for the first Born approximation case in Eq. (2.19). One can clearly see that in the first Born approximation to this system Eq. (2.19) fails to reproduce the bound state that occurs in Eq. (2.24) for $\frac{\mathrm{i}}{k}\frac{m_e^*}{\hbar^2}v_0 = 1$. This renormalization is trivial as $G(x_0, x_0)$ is a purely real quantity but if this is not the case the transmission coefficient will present resonances in the denominator as we will see for the following quasi-1D problem system. We can conclude that 1st Born approximation is not enough to represent the nuances of the system, specially when working on more complex problems like the quasi-1D system that we will introduce in the following section.

2.1.3 Scattering in a quasi-1D system

In previous section we could see that first Born approximation is not the best approach to describe the nuances of the scattering problem. Indeed, the Lippmann-Schwinger equation leads to more accurate results. However, this approach presents its own problems when dealing with systems higher dimensionality as we will see in this section.

When an electron scatters elastically from an impurity in an open geometry, such as the scattering from a potential-energy barrier or well, it scatters into a traveling wave which propagates away from the defect. In contrast, if the electron is restricted to a wire such that confinement subbands are formed, the incident electron can elastically scatter into evanescent modes available in the wire. We consider a 2DEG system as described in this chapter, formed by a lateral confinement along the y-axis,and that allows free propagation along the x-axis and is translationally invariant along this latter axis. The full Schrodinger equation as described [23] is,

$$\left[-\frac{\hbar^2}{2m_e^*}\left(\frac{\partial^2}{\partial x^2} + \frac{\partial^2}{\partial y^2}\right) + V_{conf}(y) + V_{\mathrm{imp}}(x, y)\right]\psi(x, y) = E\psi(x, y) \,, \tag{2.25}$$

where the confinement potential $V_{conf}(y)$ depends only on the transverse direction y and $V_{\text{imp}}(x,y)$ describes the potential of any impurity in the quasi-1D system. If we had considered a 1D problem along y in the regions where there are no defects, the confinement potential would give rise to a set of normal modes $\Phi_n(y)$ satisfying a 1D Schrödinger equation such that,

$$\left[-\frac{\hbar^2}{2m_e^*}\frac{\partial^2}{\partial y^2}+V_{conf}(y)\right]\Phi_n(y)=E_n\Phi_n(y)\ , \tag{2.26}$$

where n is the subband index and E_n are the subband (quantized) energies. The subband lateral modes $\Phi_n(y)$ form a complete and orthogonal basis such that

$$\sum_n \Phi_n(y)\,\Phi_n^*(y')=\delta(y-y')\ , \tag{2.27}$$

and

$$\int dy\Phi_m^*(y)\,\Phi_n(y)=\delta_{mn}\ . \tag{2.28}$$

Therefore, the general solution of (2.25) can be expanded in this set, and

$$\psi(x,y)=\sum_n c_n\Phi_n(y)\,\mathrm{e}^{\mathrm{i}k_n x}\ , \tag{2.29}$$

where $k_n=\sqrt{2m_e^*(E-E_n)/\hbar^2}$ is the momentum for the n-th subband and c_n are constants. Depending on the energy E, the modes with $E_n>E$ do not propagate and become evanescent modes which decay with $\mathrm{e}^{-\kappa_n x}$ where $\kappa_n=\sqrt{2m_e^*(E_n-E)/\hbar^2}$. Energies where a subband becomes propagating will be called thresholds E_n,and their specific form depends on the type of confinement potential. In the case of a harmonic confinement potential such that $V_{conf}(y)=(1/2)m_e^*\omega_0^2y^2$, the solutions of Eq.(2.26) are,

$$\Phi_n(y)=\frac{1}{\sqrt{2^n n!\sqrt{\pi}\lambda_y}}\mathrm{e}^{-y^2/2\lambda_y^2}H_n(y/\lambda_y)\ , \tag{2.30}$$

with H_n as the Hermite polynomials and $\lambda_y=\sqrt{\hbar/m_e^*\omega_0}$ as the characteristic length of the harmonic oscillator of corresponding energy levels $E_n=\hbar\omega_0(n+1/2)$.

While Bagwell [23] uses this description to solve the scattering problem with an infinite number of coupled modes by wavematching at the boundary set by the impurity potential, our goal is to describe the scattering from an

impurity potential $V_{\text{imp}}(x,y)$ and the influence of the evanescent modes in such a confined system using the Lippmann-Schwinger equation[24]. So the Lippmann-Schwinger equation for the quasi-1D scattering problem reads,

$$\psi(x,y) = \phi(x,y) + \int G^{Q1D}(x,y;x',y')\, V_{\text{imp}}(x',y')\, \psi(x',y')\, dx'dy' \ , \quad (2.31)$$

where the Green's function is given by,

$$\begin{aligned} G^{Q1D}(x,y;x',y') &= \sum_n \Phi_n(y)\, \Phi_n(y')\, G_n^{1D}(x,x') \\ &= -\sum_n \Phi_n(y)\, \Phi_n(y')\, \frac{m_e^*}{\hbar^2} \frac{\mathrm{i}}{k_n} \mathrm{e}^{\mathrm{i}k_n|x-x'|} \ , \end{aligned} \quad (2.32)$$

and the impurity potential $V_{\text{imp}}(x',y')$ has to be localized and short-ranged in order to solve such a system. It is our intention to use a δ-like potential to model the impurity potential, but one must be extremely careful with such potential in 2D as the transitions between all the modes lead to divergences in the integral calculation. For this reason we choose to work with a regularized δ potential. The precise profile of the potential is unimportant as long as the electron wave function $\psi(x,y)$ changes little over the length scale of $V_{\text{imp}}(x,y)$.

For simplicity, and for future convenience, we model such point-like scatterers by a constant potential inside a circle of small radius $\boldsymbol{r} = (x,y)$,

$$V_{\text{imp}}(\boldsymbol{r}) = \begin{cases} V_0, & |\boldsymbol{r} - \boldsymbol{r}_0| < a, \\ 0, & \text{otherwise} \ , \end{cases} \quad (2.33)$$

where V_0 is the potential hight/depth, $\boldsymbol{r}_0$ is the position of the impurity, and a is the range of the potential.

We shall regard Eq. (2.33) as being in the limit of a delta-like function, which is obtained by simultaneously sending $a \to 0$ and $V_0 \to \infty$ while maintaining $V_0 a^2$ constant. Formally, we write Eq. (2.33) as

$$V_{\text{imp}}(\boldsymbol{r}) = v_0 \delta(\boldsymbol{r} - \boldsymbol{r}_0) \ , \quad (2.34)$$

where $v_0 = \pi a^2 V_0$ is the relevant parameter that gives the strength of the point-like scatterer.

We solve the Lippmann-Schwinger equation in Eq.(2.31), for the Green's function and scatterer given by Eq.(2.32) and Eq.(2.34) respectively with

$\boldsymbol{r}_0 = (x_0, y_0)$. And obtain the following transmission coefficient as a result:

$$t_{mn} = \delta_{mn} - \mathrm{i}\frac{\frac{m_e^*}{\hbar^2}v_0}{1 + \mathrm{i}v_0\frac{m_e^*}{\hbar^2}\sum_n \frac{\Phi_n^2}{k_n}} \left[\frac{\mathrm{e}^{\mathrm{i}(k_n - k_m)x_0}}{\sqrt{k_m k_n}}\right] \Phi_m^*(y_0)\Phi_n(y_0) \ .$$

One must notice that the denominator of Eq.(2.35) includes a sum over the infinite set of states, in contrast to Eq.(2.23)). While the latter supports a bound state, the poles of the denominator in Eq.(2.35) are associated with *quasi-bound states* (QBS). The description of quasi-bound states was first introduced by Bagwell [23]. The presence of quasi-bound states is associated with resonances in the transmission related to the presence of evanescent modes (see Fig.2.3). Close to the threshold energy, where a new channel is opened in the typical ballistic nanowire, the attractive potential is able to couple the propagating channel with the evanescent channel about to become propagating. As the evanescent mode is associated with a decaying length(corresponding to the evanescent κ_n), these states are not properly bound as opposed to the stable bound-state of a delta-scatterer in Eq.(2.23), as discussed by other authors [57, 58, 59].

For energies close to resonances associated with quasi-bound states, the condition that the electron wave function is nearly constant in the neighborhood of $\boldsymbol{r}_0$ also means that the impurity is weakly binding ($v_0 \ll \hbar^2/m_e^*$). Indeed, if the impurity was strongly binding ($v_0 \gg \hbar^2/m_e^*$), then the wave function inside the impurity region would resemble to some extent the wave function of a particle in a box, *i.e.* changing sizeably over the length scale a (or even a smaller length scale $a\hbar^2/v_0 m_e^*$). It is clear that in the case of a strongly binding impurity a quasi-bound resonance can, in principle, appear in the energy range of interest, say, between the first and the second modes of the wire. The incident electrons will admix quite a large portion of the strongly oscillating wave function inside the scatterer; the closer to the resonance the more admixed. In that case, the outcome of the scattering event does depend on the precise profile of $V_{\mathrm{imp}}(\boldsymbol{r})$ and writing Eq. (2.34) would not be legitimate. Hence, the strongly binding impurity case is beyond the limits of our calculation and cannot be treated via the Lippmann-Schwinger equation. Then we must bear in mind throughout this work that we are always referring to weakly binding impurities.

The study of scattering in quasi-1D systems was widely covered either numerically or analitically for single delta-scatterers [23, 60, 61, 24, 57, 59, 62,

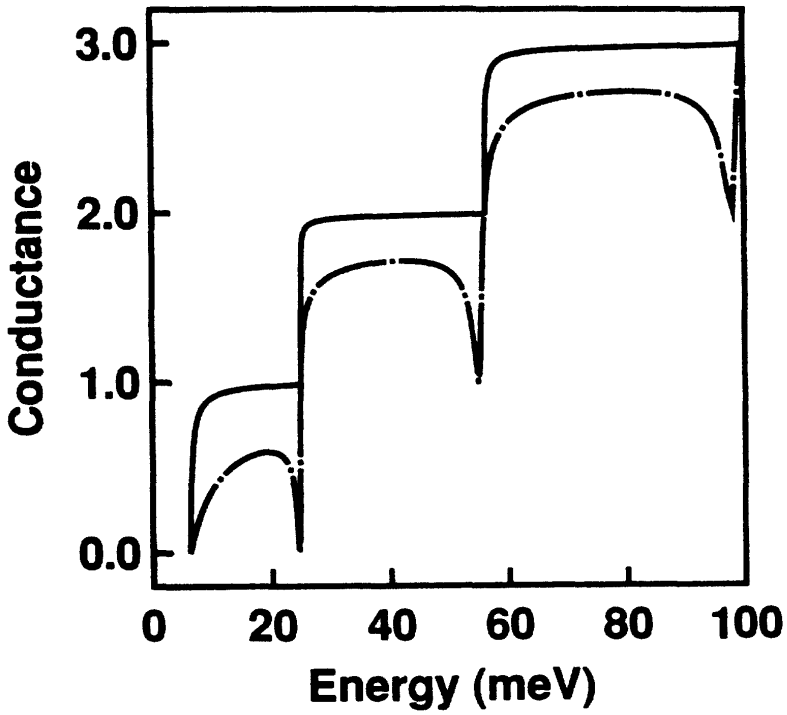

Figure 2.3: Conductance through a delta-impurity in the quasi-1D nanowire in units of $2e^2/h$. For the attractive scatterer $v_0 < 0$ (dashed line), the conductance at the threshold energy is the ballistic conductance and below these threshold energies conductance dips appear in the corresponding to *quasi-bound states* present in the nanowire. For the repusive scatterer $v_0 > 0$ (solid line), the resonant dip is not present. This figure taken from [23].

63, 64, 65], double-delta scatterers[66], finite-size scatterers [67, 68, 69], and even in for magnetic impurities [70], in the presence of an eternal magnetic field [71] and for time-dependent potentials [72, 73, 68]. In all these works, the resonant characteristics of the transmission were discussed in relation to the presence of quasi-bound states in the system. However, to our knowledge the scattering from an impurity in the nanowire in the presence of Rashba spin-orbit coupling remains unexplored.

2.2 Conclusion

In this chapter we introduce the Lippmann-Schwinger equation which we will use for the theoretical description of quantum scattering for a semiconducting nanowire. In particular we describe how the electronic transport is affected by the presence of the impurity in the nanowire. We first describe the approach in a general system and later focus on scattering on a delta-potential in a purely 1D system, discussing the limitations of the Born approximation. Finally we focus on a more realistic nanowire described by a transverse confining potential, discussing the emergence of resonant behaviour in the transmission as a consequence of quasi-bound states present in the nanowire. This effect arises from the localized impurity coupling the evanescent and propagating modes of the nanowire.

Our interest is in the possible effects arising from the interplay between the Rashba interaction and quasi-bound states. For this reason, Chapter 3 introduces the key ingredient in our study, namely the Rashba spin-orbit interaction in quantum nanowires.

Chapter 3

Spin Orbit Coupling in semiconductors

The field of spintronics aims to create devices that take advantages of both, the spin and charge degrees-of-freedom of electrons. In particular, semiconducting spintronics facilitate the study of the fundamental concepts in the field thanks to the easy integration with nowadays semiconductor electronics. One of the key ingredients garnering attention in this field is the spin-orbit coupling, specially some forms of symmetry-dependent spin-orbit coupling realized in semiconducting heterostructures hosting a two-dimensional electron gas (2DEG). Such is the case of the Rashba spin-orbit interaction.

In this Chapter we provide a brief introduction to spin-orbit interaction of the Rashba type. We discuss the spectral properties of low dimensional strcutures with Rashba spin-orbit coupling and provide a brief overview of two possible applications of materials with Rashba spin-orbit coupling, namely the Datta-Das spin-transistor and the detection of Majorana Bound States. Our interest in Rashba spin-orbit coupling is related to spin-dependent transport in quantum nanowires. For this reason, we first introduce the Hamiltonian model for a 2DEG and discuss its spectrum and symmetries. By further confining the 2DEG, one can creates a quasi one dimensional guide, or *quantum nanowire* . The confinement potential add complexity to the problem, and the Hamiltonian is no longer analitically solvable without approximations. Indeed, the subbands are deformed and avoided crossings appear in the energy dispersion, as we describe in this chapter. Later, in Chapter 5, we will treat Rashba spin-orbit interaction in

a perturbative way. Therefore in the present chapter we present the exact solution for the momentum in the energy dispersion where the subbands cross (the only point that presents spin degeneracy) which we will use as the unperturbed solution.

3.1 Introduction to Spin-Orbit Coupling

The spin-orbit coupling (SOC) is a widely studied effect that describes the interaction between the spin of a particle with its motion in the presence of an electric field. And it can be described by following Hamiltonian [56],

$$\mathcal{H}_{SO} = \frac{\hbar}{4m^2c^2}\hat{\vec{\sigma}}\left(\nabla V \times \mathbf{p}\right) \ , \tag{3.1}$$

where $\hat{\vec{\sigma}} = (\hat{\sigma}_x, \hat{\sigma}_y, \hat{\sigma}_z)$ is the vector of Pauli matrices, m is the rest mass of the electron, $V(\mathbf{r})$ is the electrostatic potential in which the electron propagates with momentum $\mathbf{p}$. For example, in atomic physics $V(\mathbf{r})$ is the Coulomb potential of the atomic core.

In semiconductor physics $V(\mathbf{r})$ is the potential of a crystalline lattice that arises from the hybridization of the electron orbitals of neighboring atoms. The spectral properties of these electrons are characterized by the band energy $E_n(k)$ and affected by the spin-orbit coupling. The effects of spin-orbit coupling in InAs, GaAs, InSb or other materials that are commonly used in the realization of nanowires, where the energy of the top valence band is strongly splitted in subbands depending on spin. [74, 75, 76].

Furthermore, the lack of centro-symmetry in the zinc-blende structure of III-V crystals and the confinement of 2DEGs allows for significant inversion asymmetry spin-orbit coupling effects in the lattice potential, lifting the spin degeneracy by splitting the energy bands in the absence of a magnetic field. The effects of this type of spin-orbit coupling can be better understood by exploring the relation between symmetry and band splitting, specifically time-reversal symmetry (TRS) and spatial inversion symmetry (SIS).

Spatial Inversion and Time Reversal Symmetries

The relation between symmetry and the splitting of the bands is fundamental for the understanding of some types of spin-orbit coupling

Reversed	**Preserved**
$p \to -p$	$q \to q$
$B \to -B$	$E \to E$
$\sigma \to -\sigma$	$p^2/2m \to p^2/2m$

Table 3.1: Observables preserved and reversed under the time reversal transformation.

[77]. The first symmetry of relevance is the time reversal symmetry. When a system undergoes a time reversal transformation $T : t \to -t$ characterized by the time reversal operator T, some observables are preserved while others are reversed. Some of these observables are presented in table 3.1. Then,under the reversal of time: because the angular momentum is reversed $\mathbb{L} \to -\mathbb{L}$ and the so is the spin $\sigma \to -\sigma$, the spin-orbit is preserved $\mathbb{L} \cdot \sigma \to \mathbb{L} \cdot \sigma$ and the momentum $\mathbb{k} \to -\mathbb{k}$. If a system is symmetric under time reversal (and the spin is half-integer), the Kramers theorem implies

$$E_n(\sigma, \mathbf{k}) = E_n(-\sigma, -\mathbf{k}) \tag{3.2}$$

for any band energy for a given spin σ and for a given momentum $\mathbb{k}$, corresponds a energy degenerate band with opposite spin $-\sigma$ and opposite momentum $-\mathbb{k}$.

The other important symmetry is the spatial inversion symmetry. Under space reversal $R : \mathbb{r} \to -\mathbb{r}$, while $\mathbb{L} \to \mathbb{L}$ and $\sigma \to -\sigma$ and consequently the spin-orbit $\mathbb{L} \cdot \sigma \to -\mathbb{L} \cdot \sigma$ and momentum $\mathbb{k} \to -\mathbb{k}$. Then, in the case of a system with spatial inversion symmetry,

$$E_n(\sigma, \mathbf{k}) = E_n(\sigma, -\mathbf{k}) \tag{3.3}$$

meaning that for any band with given spin σ and momentum $\mathbb{k}$, there is another degenerate band with same spin σ and opposite momentum $-\mathbb{k}$.

And if the system presents both time reversal and spatial inversion symmetries, then

$$E_n(\sigma, \mathbf{k}) = E_n(-\sigma, \mathbf{k}) \ . \tag{3.4}$$

Thus, in a system with two spin eigenstates $\uparrow$ and $\downarrow$ that presents both space inversion symmetry (SIS) and time reversal symmetry (TRS) the energy dispersion for the two subbands overlaps. However, for systems with TRS

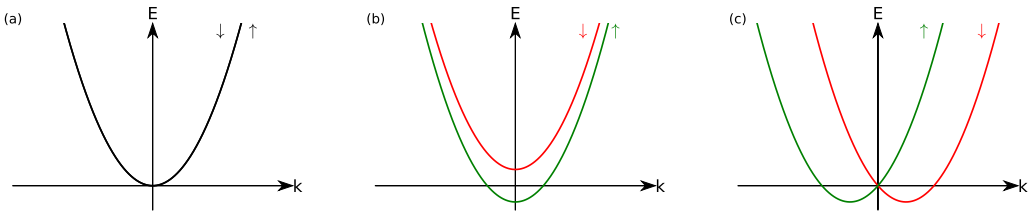

Figure 3.1: (a) Degenerate energy dispersion for a system with TRS and SIS.(b) Gaped spectrum for a system where TRS is broken.(c) Shifted energy dispersion for a system where SIS is broken and spin-degeneracy is lifted.

but broken SIS the spin-↑ and spin-↓ subbands have different energy at a given momentum $\mathbf{k}$ for the same spin so that,

$$E_n(\sigma, \mathbf{k}) \neq E_n(-\sigma, \mathbf{k}) \tag{3.5}$$

as is the case for systems with spin-orbit coupling in non-centrosymmetric materials (see Fig.3.1(c)). Furthermore, if time reversal symmetry is broken the Kramers degeneracy in Eq.(3.2) is lifted and

$$E_n(\sigma, \mathbf{k}) \neq E_n(-\sigma, -\mathbf{k}) \tag{3.6}$$

case when an external magnetic field is applied to the system (see Fig.3.1(b)).

Thus a potential that breaks spatial inversion symmetry lifts spin-degeneracy as stated in Eq.(3.5) while a potential that breaks time reversal symmetry lifts spin-degeneracy and Kramers degeneracy as seen in Eq.(3.6).

Symmetry dependent spin-orbit coupling

As described by Eq.(3.1) the main sources of SOC are electric fields, originating from asymmetries of the crystalline potential through its gradient ∇V. Therefore, it is an intrinsic effect, strongly depending on the material and its structure. As we already discussed in the case of zincblende III-V heterostructures such as GaAs, AlGaAs, InAs, etc., these asymmetries break down the spatial inversion spin-splitting the spectrum with two possible origins,

1. The first one is bulk inversion asymmetry (BIA), i.e., contrary to other crystalline structures such as that of silicon, the zinblende structure

lacks an inversion center. This asymmetry is fixed for a given sample, is intrinsic of the system and it is not possible to manipulate it externally. The spin-orbit coupling caused by this inversion asymmetry is known as Dresselhaus interaction [78].

2. The second one is only possible in low dimensional systems where the motion of electrons is confined to two dimension (2DEG), for example in quantum wells, where there is a lack of inversion symmetry in the growth direction. This is the structural inversion asymmetry (SIA), and the importance of this mechanism lies in the fact that the asymmetry in the confinement potential can be varied by electrostatic means, allowing to tune the SOC strength by an external gate voltage. The spin-orbit interaction corresponding to this asymmetry is called Rashba spin-orbit coupling (RSOC)[79].

The relative importance between both spin-orbit interactions, Dresselhaus and Rashba, varies depending on the band structure of the material, the electron density and the geometry of the sample under investigation. In narrow-gap III-V quantum wells, however, the Rashba SOC is generally much larger than the Dresselhaus,as well as being more interesting due to its tunability. As a consequence, in this thesis the focus will be on the Rashba interaction, neglecting the Dresselhaus term.

3.2 Applications of Rashba Spin-Orbit Coupling

In 1990 the first application of RSOC was proposed as what is known as the Datta-Das transistor or spin-Field Effect Transistor (spin-FET)[15] but it was not realized until later [80, 81]. This toy-model was developed as an analog to the electro-optic modulator and is based on the spin precession induced by the Rashba effect.

It follows from the general expression for the spin-orbit coupling in Eq.(3.1), that the Rashba SOC gives rise to an internal magnetic field $\mathbf{B}_{RSOC}$ and it can be written as $\mathbf{B}_{RSOC} = \alpha\left(E_z\right)\left(\mathbf{k}\times\mathbf{z}\right)$, i.e., the magnitude of the field is proportional to the momentum $\mathbf{k}$ and a voltage-dependent parameter α, and it is pointing in the direction

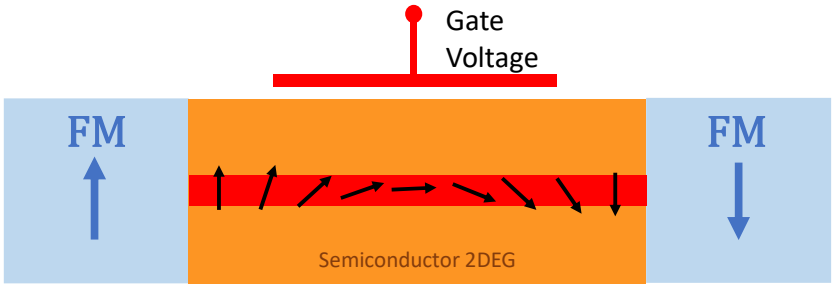

Figure 3.2: Skech of a Datta-Das spin transistor, with 2DEG sandwiched in between two ferromagnets. The injected spin can be controled by tuning the RSOC, which in turned is controlled by a gate voltage. If the alignment of the electron spins, as they reach the drain, is parallel to this ferromagnet, then the transistor will register a non-zero current. On the contrary, if like in this figure the magnetization of the drain ferromagnet is antiparallel to the electron spins, the transistor will register a zero-current.

perpendicular to both **k** and **z** (with **z** being the growth direction of the quantum well).

In the absence of an externally applied magnetic field, the spin will precess around this effective magnetic field B_{RSOC} in a similar way as the Larmor-precession around an external magnetic field. The precession frequency depends on the magnitude of the internal magnetic field $|B_{RSOC}|$, and hence can be tuned by applying a gate voltage [82, 83, 84, 85, 86]. This property has led to the proposal of a Datta-Das "toy-model" [15], also known as the Datta-Das spin-transistor.

Datta and Das consider a ballistic transport channel with Rashba SO coupling in-between ferromagnetic leads acting as spin polarizers(see Fig. 3.2). When a spin is injected from one of the leads, it precesses around the Rashba field B_{RSOC} until the spin arrives at the other ferromagnetic lead (the drain). The electron transmission probability into the drain depends on the relative alignment of its spin with the magnetization of the drain (this being fixed). Since the frequency of the precession of the spin during the travel to the drain can be controlled via gate voltage, so can the source-to-drain current (or conductance). The importance of this toy-model for the field of spintronics consists not on its physical realization but on the scientific discussion sparked around it about the role of Rashba SOC in the spin dynamics of 2DEG, its interplay with Dresselhaus SOC and Zeeman. In

return, this research has lead to the discovery of new spin-related phenomena and their applicability in new devices.

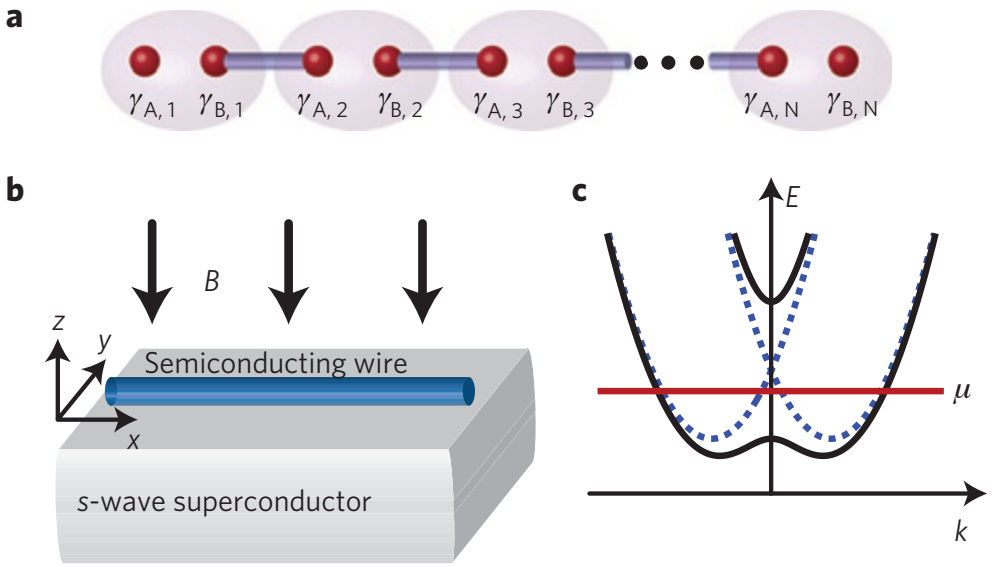

Figure 3.3: (a) Sketch of Majorana Fermions appearing at the ends of a nanowire. Each spinless fermion in the chain is formed by the overlap of two Majorana fermions $\gamma_{A,x}$ and $\gamma_{B,x}$. Majoranas $\gamma_{B,x}$ and $\gamma_{A,x+1}$ form an ordinary fermion with finite energy, leaving two uncombined Majorana Fermions at the ends of the nanowire. (b) Set-up for the observation of MF: a semiconducting nanowire with spin-orbit coupling sits on top of a s-wave superconductor while an external magnetic field B is applied. (c) In the absence of a magnetic field (dashed lines), the energy spectrum is spin-split, but if an external magnetic field is applied perpendicular to the H_{SO} a helical gap opens (solid lines) and superconductivity by proximity can drive the nanowire to a topological state. Figure taken from [87].

More recently there has been a revival of interest in studying SOC in semiconducting hybrid structures due to the possibility of finding Majorana zero modes hosted in Rashba nanowires in contact with superconducting electrodes, which are possible candidates for topological quantum computation due to their non-Abelian statistics [88, 89, 90, 87]. The basic idea is that such a structure can become a topological superconductor

under the right circumstances and support two non-local Majorana Bound States at the ends of the nanowire (see Fig. 3.3(a)). The strong SOC present in the nanowire shifts the two parabolic bands depending on their spin polarization and applying an external magnetic field perpendicular to the SO field breaks the TRS of the system opening a gap at the crossing point of the parabolas ($k = 0$), as seen in Fig. 3.3(c). If the Fermi energy μ is inside the opened gap the degeneracy is two-fold instead of four-fold. The proximity of a s-wave superconductor induces pairing in the nanowire between electron states of opposite momentum and opposite spins and induces a superconducting gap, Δ. Combining this two-fold degeneracy with an induced gap creates a topological superconducting phase for $B_Z > \sqrt{\Delta^2 + \mu^2}$ lifting electron-hole symmetry and Majoranas arise as zero-energy (i.e. mid-gap) bound states, one at each end of the wire [1, 2, 3, 4, 5, 6]. A visualization of such a set-up can be seen in Fig. 3.3(b).

3.3 The Rashba model for 2DEG

In this section we focus on how Rashba spin-orbit coupling affects the spectral properties of a free electron in a 2DEG, before going into a description of a quantum nanowire where further confinement is applied to the 2D system to obtain a quasi-1D system [91].

The effective Hamiltonian for an electron moving in a 2DEG system in the $(x, y)-$plane in the presence of the Rashba spin-orbit coupling and with effective electron mass m_e is given by,

$$\mathcal{H}_0 = \frac{\mathbf{p}^2}{2m^*} + \frac{\alpha}{\hbar} \left(\sigma \times \mathbf{p}\right)_z \ , \tag{3.7}$$

with eigenvalues

$$\mathcal{E}_{\pm} \left(\mathbf{k}\right) = \frac{\hbar^2 k^2}{2m^*} \pm \alpha k = \frac{\hbar^2}{2m^*} \left(k \pm k_R\right)^2 - \Delta_R \ , \tag{3.8}$$

where $k = \sqrt{k_x^2 + k_y^2}$ is the momentum, $k_R = \frac{\alpha m^*}{\hbar^2}$ is the Rashba spin-orbit coupling constant with momentum dimensions and $\Delta_R = \left(\frac{\alpha m^*}{\hbar}\right)^2$. The last term of Eq.(3.8) results in a downward shift of the bands that renormalizes the chemical potential, altough it is often neglected as it is second order in α.

The eigenspinor for the Hamiltonian in Eq. (3.7) with eigenvalues given by Eq.(3.8) are plane waves:

$$\Psi_{\pm}(\mathbf{r}) = \frac{e^{i\mathbf{k}\cdot\mathbf{r}}}{\sqrt{2}} \begin{pmatrix} 1 \\ \pm \mathrm{i}\, e^{-\mathrm{i}\theta} \end{pmatrix} , \tag{3.9}$$

where $\theta = \arctan(k_y/k_x)$ is the angle between the momentum vector and the k_x direction. Notice that the spinor direction is always perpendicular to the propagation direction according to Eq.(3.9). If an electron propagates along x, then the angle for the momentum is $\theta = 0$ and the spinors become $(1, \pm\mathrm{i})$. This implies that the spin is aligned along the $y-$axis. On the other hand, if the electron propagates along the $y-$axis with $\theta = \pi/2$, the spinors are given by $(1, \pm 1)$. This means that the spin is aligned in the $x-$axis, see Fig.3.4(b). This phenomenon is often referred to as spin-locking. In

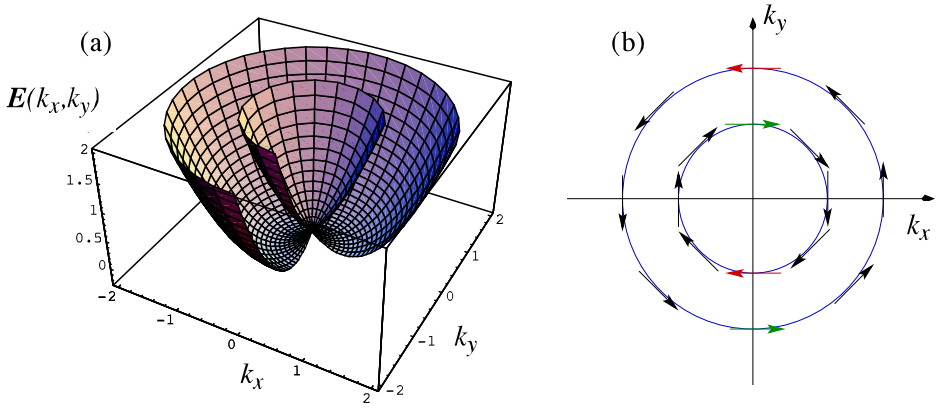

Figure 3.4: (a)Rashba parabola: 2D representation of the energy spectrum. (b) Cross-section of the parabola shows spin-locking for both spin-species, where the spin is perpendicular to k_x and k_y. Figure from [91].

Fig.3.1 we compare the energy spectrum as a function of k_x in the 2DEG for different situations. First, for a free electron in the 2DEG where both time reversal and spatial inversion symmetries are preserved: the subbands of the spectrum overlap as due to spin degeneracy. However, if we applied an external magnetic field the spin degeneracy would be lifted by breaking the time reversal symmetry opening a gap between the spin-up and spin-down species. But as we already discussed in the previous section, this lifting

of spin degeneracy is very different that the one that occurs for the Rashba spin-orbit coupling. In this case, the spin degeneracy is lifted by breaking the spatial inversion symmetry everywhere but for $k_x = 0$ where the subbands cross.

The semiclassical electron velocities are given by

$$\mathbf{v}_{\pm}(\mathbf{k}) = \frac{1}{\hbar}\frac{\partial \mathcal{E}_{\pm}(\mathbf{k})}{\partial \mathbf{k}} = \frac{\hbar \mathbf{k}}{m^*} \pm \alpha \mathbf{k} = \frac{\hbar}{m^*}(k \pm k_{SO})\ .\mathbf{k} \tag{3.10}$$

It is clear then, that the velocity of the electrons is no longer just the momentum divided by the effective mass as a consequence of the Rashba spin-orbit coupling. As a result, the parabola splits into two parabolas with spin and momentum locked to each other so that electrons with opposite spin travel in opposite directions (see Fig. 3.4).

3.4 RSOC in quantum wires: subband mixing

As discussed in Chapter 2, a quasi-1D nanowire can be realized by further confinement of the 2DEG along one direction (in this case the y direction). As a result it is not possible to solve analytically the system Hamiltonian, as in the previous section for the simple case of a 2DEG. However, different theoretical models have been used to account for the confinement effects [19, 21, 22]. Here we present one of these approaches. Assuming the electron propagates freely along the $x-$direction and the transversal confinement potential is applied in the $y-$direction, the Hamiltonian reads

$$\mathcal{H} = \mathcal{H}_{\parallel} + \mathcal{H}_{\perp} + \mathcal{H}_{mix} \tag{3.11}$$

with the following terms

$$\mathcal{H}_{\parallel} = \frac{p_x^2}{2m^*} - \frac{\hbar k_R}{m^*}\sigma_y p_x\ , \tag{3.12a}$$

$$\mathcal{H}_{\perp} = \frac{p_y^2}{2m^*} + V_{conf}(y)\ , \tag{3.12b}$$

$$\mathcal{H}_{mix} = \frac{\alpha}{\hbar}\sigma_x p_y\ . \tag{3.12c}$$

Where $V_{conf}(y) = \frac{1}{2}m^*\omega^2 y^2$ is a harmonic confinement potential characterized by the length $\lambda_y = \sqrt{\hbar/m^*\omega}$. Neglecting $\mathcal{H}_{mix}$ in Eq.(3.11), the terms from

Eq.(3.12a) and Eq.(3.12b) make for a solvable Hamiltonian with eigenvalues and eigenspinors:

$$E_{\parallel+\perp}(n,\sigma_y,k_x) = \frac{\hbar^2 k_x^2}{2m^*} + \hbar\omega\left(n+\frac{1}{2}\right) - \frac{\hbar^2 k_R k_x}{m^*}\langle\sigma_y\rangle \ , \quad (3.13)$$

$$\psi_{n\sigma_y k_x}(x,y) = \Phi(y)\,\psi_{k_x}(x)\,|\sigma_y\rangle \ , \quad (3.14)$$

where $\Phi_n(y)$ are the n-th eigenfunctions of the harmonic confinement potential $V_{conf}(y)$ as given by Eq.(2.30) and $\psi_{k_x}(x)$ are plane waves shifted by the RSOC, here $\langle\sigma_y\rangle$ can get the values ± 1. The term $\mathcal{H}_{mix}$ in Eq.(3.12c) mixes these eigenstates and leading to a deformation of the subbands and the appearance of anti-crossings in the energy spectrum, and is usually treated as a perturbation to the system. These anti-crossings occur between sub-bands corresponding to eigenstates with different band index n and opposite spin (see Fig. 3.5).

For 1D models there is a strict spin-momentum locking where the spin is aligned in-plane but perpendicular to the direction of propagating along the wire given by the momentum. On the other hand, for multi-band models it is well known that only far away from the anti-crossings is the spin locked perpendicular to the momentum. This means that the spin cannot be considered as a good quantum number. This can be seen in Fig.3.6a, where the expectation value for the spin along the $y-$direction $\langle S_y\rangle$ goes from $-1/2$ to $1/2$ as the momentum k_x goes from negative to positive values. Eq.(3.11) cannot be diagonalized exactly, but several works attempt a partial analytical/numerical solution by truncating the Hilbert space and considering a limited amount of lateral modes N. This produces great accurate results up to the band $N-1$. In addition to this truncation affecting the spectrum, it also affects the the effects polarization of the system. The effects of such a truncation are very well illustrated in the Fig. 3.6. In Fig. 3.6(a), the polarization of the first subband for a two-band model (dashed lines) and a $N = 50$ band model(solid lines) is compared and result in a reasonable agreement. However, in Fig.3.6(b), the second subband polarization presents a strong deviation from the behavior of a two-band model showing opposite values at large energies. The role of the number of bands in the calculations is of great relevance and is independent of the geometry of the confinement potential $V_{conf}(y)$. Bottom line here is that for a correct interpretation of the problem, enough subbands must be considered in the calculation.

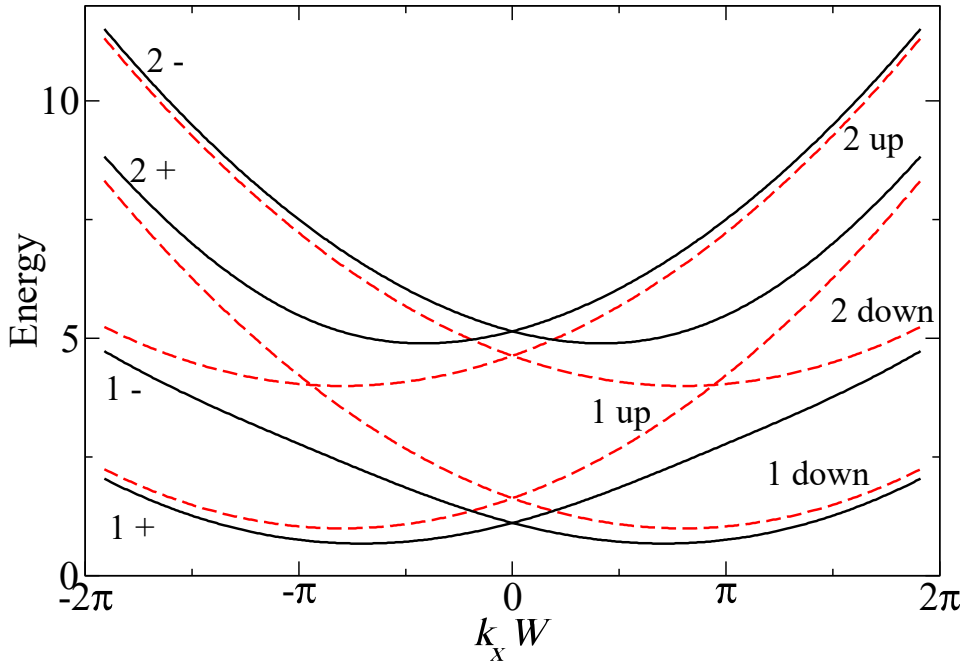

Figure 3.5: For a system with intermixing of subbands, spin is no longer a good quantum number. As a consequence, the 1st subband with spin down and the second subband with spin-up (both in black) avoid the crossing that would naturally occur in the absence of $\mathcal{H}_{mix}$(red dashed lines). This figure corresponds to diagonalization of a two-band model in a square well of width W. Figure from [22].

Furthermore, it has been observed that subband hybridization can also strongly influence results in the transmission of the nanowire which is the topic of interest in this thesis. Subband mixing has been shown to give rise to dips in the conductance of nanowires with Rashba spin-orbit coupling as shown in some works, both analytical and numerical [22, 92].

The authors of Ref.[92] provided a simple argument that shows that a local Rashba interaction in the 1D limit forms bound states for negative energies in a similar way to the case of nanowire with an impurity potential in Chapter 2. Consider the strict 1D limit of a ballistic quantum wire with

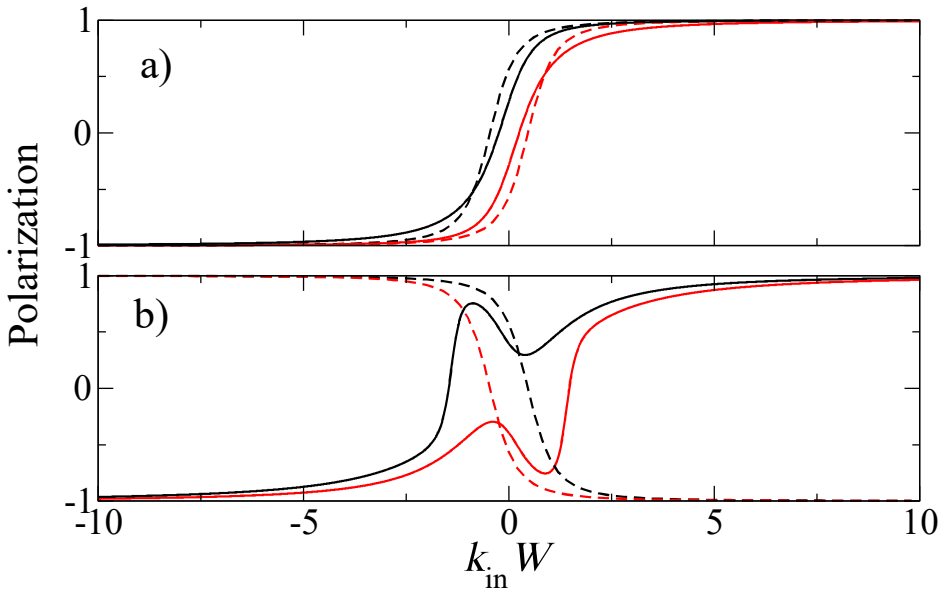

Figure 3.6: (a) Polarization for the first two subbands as a function of the injection energy, for the two-band model (dashed line) and for a 50-band model(solid line). (b) Polarization for the second subbands for the 50-band model (solid line) strongly deviates from the two-band model (dashed line). Figure from [22].

local Rashba interaction

$$\mathcal{H}_{1D} = \frac{p_x^2}{2m^*} + \frac{\alpha}{\hbar} p_x \hat{\sigma}_y \ , \tag{3.15}$$

and the electron wave function may be expanded,

$$\psi(x) = \psi_1(x) |\sigma_y\rangle_+ + \psi_2(x) |\sigma_y\rangle_- \ , \tag{3.16}$$

where $|\sigma_y\rangle_\pm$ are the spinor eigenstates.

By performing the gauge transformation $\psi_{1,2} \rightarrow \psi_{1,2}(x) \rightarrow \mathrm{e}^{\pm \mathrm{i} k_R x}$ the Schrödinger equation becomes

$$-\frac{\hbar^2}{2m^*} \psi''_{1,2}(x) = \left[E + \frac{\hbar^2 k_R^2}{2m^*} \right] \psi_{1,2}(x) \ , \tag{3.17}$$

which corresponds to a square-well impurity of strength $v_0 = -m^* \alpha^2 / \hbar^2$. This is a very similar problem to the delta-like impurity potential solved in

subsection **??**. Therefore, in a quasi-1D system one can expected the term $\mathcal{H}_{mix}$ to couple propagating states through the bound state in Eq.(**??**). As they point out in Ref. [92], with a quasi-1D system as described by the Hamiltonian in Eq.(3.11) the Rashba spin-orbit coupling plays both the role of an attractive potential and of the coupling to the continuum of evanescent modes generated by the confinement potential.

Our interest in going one step further in this system by studying the interplay between Rashba SOC, confinement and an actual physical impurity potential. This discussion is a good starting point for the effects of Rashba in the scattering impurity that will follow in Chaper 6. In our work we avoid the truncation of the Hilbert space (and its limitations and systematic mistakes), described in this section and commonly used [19, 21, 22].

Our approach to dealing analytically with the problems exposed in this section in order to solve Eq.(3.11) relies in gauge transformations and perturbation theory (see Chapter 5). For this reason, we think it is of interest to solve in the following subsections some limiting cases of the above mentioned Hamiltonian making use of these techniques. First, we do so for $k_x = 0$ and then we extend this result to the proximities of this point $k_x \approx 0$ by adding the term $\alpha p_x \hat{\sigma}_y$ as a perturbation for the $k_x = 0$ problem.

3.4.1 Exact solution for $k_x = 0$

The case $k_x = 0$ is special, because only the matrix $\hat{\sigma}$ is present in the problem and spin along x becomes a good quantum number again. At $k_x = 0$, we have

$$\mathcal{H}^{1\mathrm{D}} = \frac{p_y^2}{2m_e^*} + \frac{m_e^* \omega_0^2}{2} y^2 - \alpha p_y \sigma_x \,. \tag{3.18}$$

The term $-\alpha p_y \sigma_x$ in Eq.(3.18) can be treated exactly. It suffices to choose the spin basis such that σ_x becomes ± 1,

$$\sigma_x \left|\chi_\pm\right\rangle = \pm \left|\chi_\pm\right\rangle , \tag{3.19}$$

where we may choose

$$\chi_+ = \frac{1}{\sqrt{2}} \begin{pmatrix} 1 \\ 1 \end{pmatrix} \quad \text{and} \quad \chi_- = \frac{1}{\sqrt{2}} \begin{pmatrix} -1 \\ 1 \end{pmatrix} . \tag{3.20}$$

In the spin basis of Eq.(3.20), the problem separates into two blocks,

$$H_\pm^{1\mathrm{D}} = \frac{p_y^2}{2m_e^*} + \frac{m_e^* \omega_0^2}{2} y^2 \mp \alpha p_y . \tag{3.21}$$

Each block can be solved by shifting p_y as follows,

$$\psi_{\pm}(y) = e^{\pm \mathrm{i}y/\lambda_{SO}} \Phi_n(y) \ , \tag{3.22}$$

where $\Phi_n(y)$ can be shown to satisfy the equation for the quantum harmonic oscillator in Eq.(2.26) and $\lambda_{SO} = \hbar/m_e^*\alpha$.

Both blocks have identical eigenvalues and their wave functions are related to each other by a gauge transform. The solution to the initial problem becomes

$$\psi_{n,\pm}(y,s) = e^{\pm \mathrm{i}y/\lambda_{SO}} \Phi_n(y)\chi_{\pm}(s) \ , \tag{3.23}$$

with degenerate eigenvalues

$$E_{n,\pm} \equiv E_n = \hbar\omega_0 \left(n + \frac{1}{2}\right) - \frac{m_e^*\alpha^2}{2} \ . \tag{3.24}$$

Note that the states $\psi_{n\sigma}$ in Eq.(3.23) obey the orthonormalization condition $\langle \psi_{n'\sigma'} |\ \psi_{n\sigma} \rangle = \delta_{n'n}\delta_{\sigma'\sigma}$ where the scalar product is taken in both the y-coordinate and the spin spaces,

$$\langle \psi_{n'\sigma'} |\ \psi_{n\sigma} \rangle := \sum_s \int_{-\infty}^{+\infty} dy \psi^*_{n'\sigma'}(y,s)\psi_{n\sigma}(y,s) \ . \tag{3.25}$$

However, without summation over the spin degree of freedom the states $\psi_{n'\sigma'}$ and $\psi_{n\sigma}$ for $n' \neq n$ are orthogonal only provided $\sigma' = \sigma$,

$$\int_{-\infty}^{+\infty} dy \psi^*_{n'\sigma}(y,s')\psi_{n\sigma}(y,s) \propto \delta_{n'n} \ . \tag{3.26}$$

This is due to the phase factor $e^{\pm \mathrm{i}y/\lambda_{SO}}$ dropping out only when same spin states are involved. To emphasize that the wave function in Eq.(3.23) does not separate into a product of a y-coordinate component and a spin component, we write the states as

$$\psi_{n\sigma}(y,s) = e^{\mathrm{i}\hat{\sigma}_x y/\lambda_{SO}} \Phi_n(y)\chi_{\sigma}(s). \tag{3.27}$$

A product of two states without summation over the spin indices reduces to the direct product of the operators $e^{\mathrm{i}\hat{\sigma}_x y/\lambda_{SO}}$ taken from each of the states

in Eq.(3.27). It is convenient to represent such a direct product simply by supplying an index to the Pauli matrix,

$$e^{-\mathrm{i}\hat{\sigma}_x y/\lambda_{SO}} \otimes e^{\mathrm{i}\hat{\sigma}_x y/\lambda_{SO}} \rightarrow e^{\mathrm{i}(\hat{\sigma}^a - \hat{\sigma}^b)y/\lambda_{SO}} \ , \tag{3.28}$$

where $\hat{\sigma}_x^a$ and $\hat{\sigma}_x^b$ have separate Hilbert spaces for the time being, until we contract the spin indices. The quantity of interest is, therefore,

$$\int_{-\infty}^{+\infty} dy \Phi_{n'}^*(y)\Phi_n(y)e^{\mathrm{i}(\hat{\sigma}_x^a - \hat{\sigma}_x^b)y/\lambda_{SO}} \ , \tag{3.29}$$

which reduces to the following Fourier transform

$$\mathcal{F}_{n'n}(q) = \int_{-\infty}^{+\infty} dy \Phi_{n'}^*(y)\Phi_n(y)e^{iqy}. \tag{3.30}$$

Note that $\mathcal{F}_{n'n}(q) = [\mathcal{F}_{nn'}(-q)]^*$ and also that $\mathcal{F}_{n'n}(0) = \delta_{n'n}$. Actually, we will need $\mathcal{F}_{n'n}(q)$ evaluated at $q = \pm 2/\lambda_{SO}$.

The form-factor $\mathcal{F}_{n'n}(q)$ can be calculated for the case of harmonic confinement with the functions $\Phi_n(y)$ as given above. Since $\Phi_n(y)$ are chosen to be real, we have $\mathcal{F}_{n'n}(q) = \mathcal{F}_{nn'}(q)$, which subsequently leads to the relation $\mathcal{F}_{n'n}(-q) = [\mathcal{F}_{n'n}(q)]^*$. Then, without loss of generality, we take $n' \geq n$ and obtain

$$\begin{aligned} \mathcal{F}_{n'n}(q) &= \sqrt{\frac{2^{n'}n!}{2^n n'!}} L_n^{n'-n}\left(\frac{q^2\lambda_y^2}{2}\right) \\ &\quad \times \left(\frac{iq\lambda_y}{2}\right)^{n'-n} \exp\left(-\frac{q^2\lambda_y^2}{4}\right), \end{aligned} \tag{3.31}$$

where $L_n^\alpha(\xi)$ is the Laguerre polynomial,

$$L_n^\alpha(\xi) = \frac{1}{n!}e^\xi \xi^{-\alpha}\frac{\partial^n}{\partial \xi^n}(e^{-\xi}\xi^{n+\alpha}). \tag{3.32}$$

This limit case for $k_x = 0$ serves as the unperturbed solution to build upon for the following subsection.

3.4.2 Perturbative solution around $k_x \approx 0$

In order to build a solution around $k_x = 0$ we take the unperturbed Hamiltonian to be that of Eq.(3.18) so that the perturbed system is given by

$$\mathcal{H} = \mathcal{H}_0 + \alpha\hbar k_x \ . \tag{3.33}$$

where the terms proportional to αk_x can be treated by perturbation theory. Let us consider values of k_x which are small enough, such that the following regime holds

$$\alpha\hbar k_x \mathcal{F}_{nn'}(q_0) \ll E_n - E_{n'}, \qquad n \neq n'. \tag{3.34}$$

This condition roughly refers to "staying away from the avoided crossings" and is equivalent to $\lambda_y/\lambda_{SO} \ll 1$. This small parameter is very important as it appears again in Chapter 5 in the context of perturbation theory but for the Schrieffer-Wolff transformation. In this case, we treat the term $\alpha\hbar k_x\sigma_y$ as perturbation, whereas the term $-\alpha p_y\sigma_x$ is treated exactly. However, in Chapter 5 the opposite is true:$\alpha\hbar k_x\sigma_y$ is treated exactly, while the term $-\alpha p_y\sigma_x$ is considered a perturbation. The interest in the calculation presented in the current subsection is to find possible contributions of order α^2 arising from the term $-\alpha p_y\sigma_x$ alone. The reason behing this is because they may present corrections to the second order (α^2) in our calculation in Chapter 5.

One could expect that in order to determine this, it is sufficient to consider the point $k_x = 0$, which is exactly solvable. However, that point is degenerate and we have to consider its vicinity to understand how the states propagate and what are their transport properties when scattering off an impurity.

For this reason, we consider the zeroth-order of perturbation theory in the small parameter in Eq. (3.34). This corresponds to the degenerate perturbation theory around the point $k_x = 0$ for each subband n separately. While this approach is valid for a strong spin-orbit interaction and a very small k_x, we are interested here in answering the question about the role of the second-order corrections due to $-\alpha p_y\sigma_x$. In matrix form, the diagonal $(n' = n)$ part of the Hamiltonian of the system is given by,

$$\hat{H}_n^{\mathrm{1D}} = \begin{pmatrix} E_n & -i\alpha_n\hbar k_x \\ i\alpha_n\hbar k_x & E_n \end{pmatrix}, \tag{3.35}$$

where the basis is given as before by the states in Eq. (3.23). We denoted $\alpha_n = \alpha F_n(q_0)$ with $q_0 = 2/\lambda_{\mathrm{SO}}$.The form-factor $\mathcal{F}_n(q) \equiv \mathcal{F}_{nn}(q)$ is real and simplifies to

$$\mathcal{F}_n(q) \;=\; L_n\left(\frac{q^2\lambda^2}{2}\right)\exp\left(-\frac{q^2\lambda^2}{4}\right). \tag{3.36}$$

Any correction arising from the form factor is is $q_0^2 \propto \alpha^2$ and by multiplying it by the $\alpha\hbar k_x$ of the perturbation theory in Eq.(3.35) it goes with α^3 and

hence is beyond the accuracy of any calculation done in this work. However, we care about any α^2 correction arising from the states and there is also an α^2 overall energy shift, see Eq. (3.24).

The eigenstate of Eq. (3.35) corresponding to the energy

$$E_{n,+} = E_n + \hbar k_x \alpha_n, \tag{3.37}$$

is constructed out of the states in Eq. (3.23)

$$\chi_+ = \frac{1}{2}\begin{pmatrix} 1 \\ 1 \end{pmatrix} e^{iy/\lambda_{\rm SO}} + \frac{i}{2}\begin{pmatrix} -1 \\ 1 \end{pmatrix} e^{-iy/\lambda_{\rm SO}}. \tag{3.38}$$

And the eigenstate corresponding to the energy

$$E_{n,-} = E_n - \hbar k_x \alpha_n, \tag{3.39}$$

is constructed as

$$\chi_+ = \frac{1}{2}\begin{pmatrix} 1 \\ 1 \end{pmatrix} e^{iy/\lambda_{\rm SO}} - \frac{i}{2}\begin{pmatrix} -1 \\ 1 \end{pmatrix} e^{-iy/\lambda_{\rm SO}}. \tag{3.40}$$

They both are further multiplied by the same $\Phi_n(y)$ and by $e^{ik_x x}$, since these orbital components of the wave function are in common for the subband n. As expected, to this zeroth order of perturbation theory in $\alpha\hbar k_x$, the states are not affected at all by the parameter α_n. It enters only in the energy and together with the constant term $\hbar k_x^2/2m_e^*$ will determine the division into left and right movers.

The eigenstates of Eq. (3.35) can also be written in a compact form. If we multiply both states by a phase factor $e^{i\pi/4}$, then we obtain

$$\begin{aligned} \chi_+ &= \begin{pmatrix} \cos\left(\frac{\pi}{4} + \frac{y}{\lambda_{\rm SO}}\right) \\ i\sin\left(\frac{\pi}{4} + \frac{y}{\lambda_{\rm SO}}\right) \end{pmatrix}, \\ \chi_- &= \begin{pmatrix} i\sin\left(\frac{\pi}{4} + \frac{y}{\lambda_{\rm SO}}\right) \\ \cos\left(\frac{\pi}{4} + \frac{y}{\lambda_{\rm SO}}\right) \end{pmatrix}. \end{aligned} \tag{3.41}$$

These states reduce at $y = 0$ to

$$\chi_+ = \frac{1}{\sqrt{2}}\begin{pmatrix} 1 \\ i \end{pmatrix}, \qquad \chi_- = \frac{1}{\sqrt{2}}\begin{pmatrix} i \\ 1 \end{pmatrix}, \tag{3.42}$$

which are eigenstates of σ_y. However, at $y \neq 0$, they are no longer eigenstates of σ_y.

One can verify that the two states in Eq. (3.41) originate from the non-abelian gauge factor

$$e^{i\sigma_x\left(\frac{\pi}{4}+\frac{y}{\lambda_{\mathrm{SO}}}\right)}, \tag{3.43}$$

which multiplies the usual up and down states of the σ_z Pauli matrix. As a result of this, the corrections to the states of order α^2 are not affecting the scattering potential, because the above gauge factor commutes with the scattering potential. This is a relevant result for all analytical calculations done in this thesis, as we now can ensure the accuracy of the calculation for the perturbative methods, up to the second order α^2, use in subsequent chapters.

3.5 Conclusions

In summary, in this chapter we introduce the Rashba spin-orbit coupling going over some of its applications in the field of spintronics and in the detection of Majorana Bound States. We briefly discuss the spectral properties of a 2DEG with Rashba spin-orbit coupling before reviewing the complexities involved in the analytical solution of the model Hamiltonian for a quantum nanowire where the 2DEG is further confined. As a result of this confinement, not only is the energy spectrum of the system strongly affected but also the polarization of the spin. The combined effect of RSOC and confinement gives raise to anti-crossings between branches of opposite spin, deforming the spectrum. Moreover, we discussed the subbband mixing at the origin of this phenomena which leads to coupling between propagating and evanescent states in the quantum nanowire. As a result, a proper calculation needs to take into account enough subbands. Finally, we present an exact solution for the $k_x = 0$ that we use as the result for the unperturbed problem to obtain the solution of the problem in the vicinity of the point $k_x \approx 0$. This calculation allows us to ensure the accuracy of our perturbative approach up to α^2 in Chapter 5.

Chapter 4

The Landauer-Buttiker description of Transport

The Landauer-Büttiker formalism is widely used as a method to study charge transport in mesoscopic systems [93, 94, 95]. It provides a very intuitive description of macroscopic effects in terms of scattering properties, that may be related to microscopic details of a system. In this chapter we generalize the Landauer-Büttiker formalism to include the effects of Rashba spin-orbit coupling. Besides the importance of such generalization, our results will help us to derive our results on transport properties of a nanowire with Rashba spin-orbit coupling and a single point-like impurity in the next chapters.

In the next sections we present the Landauer-Büttiker formalism to describe both the charge and spin conductance. In this way we provide a simple description of spin-dependent transport that allows us to separate the spin-bias and voltage-bias contributions to the spin current. The Landauer-Büttiker formalism approach to deal with spin currents has been treated numerically or discussed in some models in the presence of Rashba spin-orbit coupling for either the Sin Hall Effect or three-terminal spin-filters [96, 97, 98, 99, 100, 101, 102, 103, 104, 105, 106]. Very recently an extension of the formalism was developed to better understand the origin and symmetries involved in spin currents in magnetic multi-layered systems [107]. In this chapter we derive an analytical expression for the spin current in terms of the spin-dependent transmission coefficients and discuss further the implications of scattering at an impurity on the transport. We identify a spin-torque as a consequence of spin-flip transmission mechanism mediated by such an impurity (see subsection

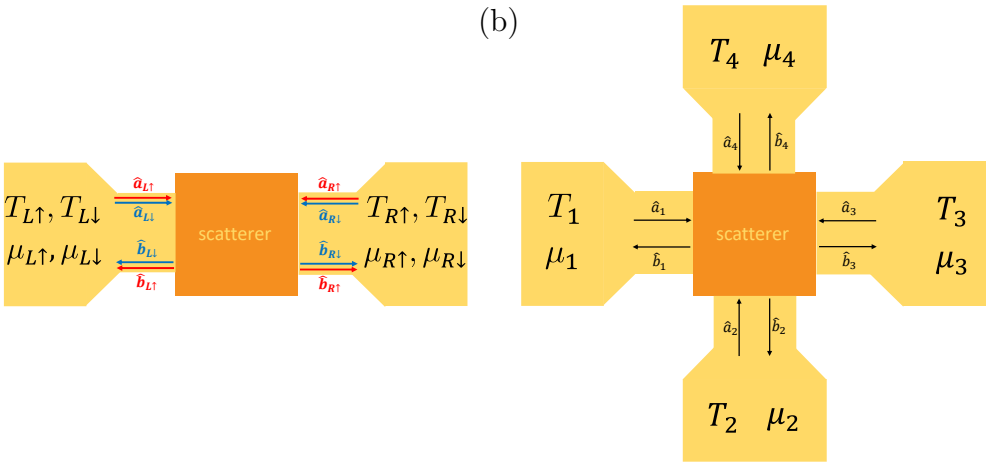

Figure 4.1: (a) Two-terminal spin-dependent geometry. (b) Four-terminal geometry.

4.3.1). In addition, we find a conection between our results and the concept of the spin-mixing conductance introduced in Ref.[108].

4.1 The Landauer-Büttiker approach for quantum transport

The goal of the Landauer-Büttiker approach is to write expressions for the current in terms of transmission probabilities between different terminals connected by a scattering region. Here we follow we Reference [109], and generalize the derivation of the formalism for the case of spin-dependent transport. Indeed, we are considering wires with Rashba spin-orbit interaction and therefore the scattering amplitudes depends on the spin.

In Fig.4.1 (a) we show the typical two-terminal system. The scattering region, in our case a nanowire, is connected to two ideal leads that we refer as left (L) and right (R). We treat each spin species as independent channels labeled by the index $\sigma =\uparrow,\downarrow$, see sketch in Fig.4.1 (a). The leads are characterized by temperature $T_{\alpha\sigma}$ and chemical potential $\mu_{\alpha\sigma}$, with $\alpha = L, R$.

It is worth noticing that the two-terminal spin-dependent geometry is equivalent to the four-terminal geometry sketched in 4.1 (b), where the temperatures for the terminals are $T_{1,2} = T_{L\uparrow,L\downarrow}$ and chemical potentials

$\mu_{1,2} = \mu_{L\uparrow,L\downarrow}$, and similarly $T_{3,4} = T_{R\uparrow,R\downarrow}$ and $\mu_{3,4} = \mu_{R\uparrow,R\downarrow}$. Thus, our analysis of 2-terminal setup for spin-dependent channels can be mapped to a 4-terminal situation with independent channels.

It is assumed that the leads are at local equilibrium and therefore the electronic distribution functions in each lead is given by the Fermi distribution function:

$$f_{\alpha,\sigma}(E) = \left[\mathrm{e}^{(E-\mu_\alpha)/k_B T_\alpha} + 1\right]^{-1}, \quad \alpha = L, R\,; \sigma = \uparrow, \downarrow \tag{4.1}$$

(see Fig.4.1). It is important to note that we are considering the contact leads to be wide compared to the crosssection of the quasi-1D nanowire, so that as far as the reservoirs are concerned, the nanowire represents only a small perturbation, and thus it is valid to describe the local properties in terms of an equilibrium state. Even though the dynamics of the scattering problem are described in terms of a Hamiltonian, the problem considered is irreversible[109]. This means that the processes for a particle entering or exiting the nanowire are uncorrrelated events; the reservoirs are fully determined by their respective Fermi distributions, and act as perfect sources and sinks for the particles independently of the energy of the particle entering or leaving the nanowire.

Between the leads we consider a ballistic nanowire with Rashba spin-orbit coupling and a local impurity potential that will act as a source of scattering inside the nanowire. Far from the impurity we assume that transverse motion longitudinal motion of particles are separable. As described in Section 2.1.3 the motion from left to right contact (longitudinal motion) is not-confined and the system is characterized by the conserved wave-vector k_n, where n denotes the index number of transverse channels introduced by the quantization across the leads in the transverse direction corresponding to transverse energies $E_{L,R;n,\sigma}$, which can be different for the left and right leads. We denote with $N_{L,R}(E)$ the number of incoming channels in the left and right lead, respectively.

We now introduce the creation and annihilation operators denoted by α, n and σ.The operators $\hat{a}^\dagger_{\alpha n\sigma}(E)$ and $\hat{a}_{\alpha n\sigma}(E)$ create and annihilate electrons respectively, with total energy E in the transverse channel n in the α lead, which are incident upon the sample. Similarly, the creation $\hat{b}^\dagger_{\alpha n\sigma}(E)$ and annihilation $\hat{b}_{\alpha n\sigma}(E)$ operators refer to electrons in the outgoing states. They

obey anticommutation relations:

$$\hat{a}^{\dagger}_{Ln\sigma}(E)\,\hat{a}_{\alpha n'\sigma'}(E') + \hat{a}_{\alpha n'\sigma'}(E')\,\hat{a}^{\dagger}_{\alpha n\sigma}(E) = \delta_{\alpha\beta}\delta_{nn'}\delta_{\sigma\sigma'}\delta(E-E')\ , \quad (4.2a)$$

$$\hat{a}_{\alpha n\sigma}(E)\,\hat{a}_{\alpha n'\sigma'}(E') + \hat{a}_{\alpha n'\sigma'}(E')\,\hat{a}_{\alpha n\sigma}(E) = 0\ , \quad (4.2b)$$

$$\hat{a}^{\dagger}_{\alpha n\sigma}(E)\,\hat{a}^{\dagger}_{\alpha n'\sigma'}(E') + \hat{a}^{\dagger}_{\alpha n'\sigma'}(E')\,\hat{a}^{\dagger}_{\alpha n\sigma}(E) = 0\ . \quad (4.2c)$$

We introduce creation and annihilation operators, $\hat{b}^{\dagger}_{\alpha n\sigma}(E)$ and $\hat{b}^{\dagger}_{\alpha n\sigma}(E)$, and their anticommutation relations in outgoing states in the same way as incoming states in eqs. (4.2a) to (4.2c).

The operators $\hat{a}_{\alpha n\sigma}(E)$ and $\hat{b}_{\alpha n\sigma}(E)$ are related trough the scattering matrix S as follows,

$$\begin{pmatrix} \hat{b}_{L1\uparrow} \\ \hat{b}_{L1\downarrow} \\ \dots \\ \hat{b}_{LN\uparrow} \\ \hat{b}_{LN\downarrow} \\ \hat{b}_{R1\uparrow} \\ \hat{b}_{R1\downarrow} \\ \dots \\ \hat{b}_{RN\uparrow} \\ \hat{b}_{RN\downarrow} \end{pmatrix} = S \begin{pmatrix} \hat{a}_{L1\uparrow} \\ \hat{a}_{L1\downarrow} \\ \dots \\ \hat{a}_{LN\uparrow} \\ \hat{a}_{LN\downarrow} \\ \hat{a}_{R1\uparrow} \\ \hat{a}_{R1\downarrow} \\ \dots \\ \hat{a}_{RN\uparrow} \\ \hat{a}_{RN\downarrow} \end{pmatrix} . \quad (4.3)$$

We can write a similar equation to Eq. (4.3) for the hermitian conjugated matrix $S^{\dagger}$ relating the creation operators $\hat{a}^{\dagger}_{\alpha n\sigma}(E)$ and $\hat{b}^{\dagger}_{\alpha n\sigma}(E)$.

The matrix S has dimensions $(N_L + N_R) \times (N_L + N_R)$. Its elements are energy-dependent, and it has the following block structure

$$S = \begin{pmatrix} r_{\sigma\sigma'} & t'_{\sigma\sigma'} \\ t_{\sigma\sigma'} & r'_{\sigma\sigma'} \end{pmatrix} . \quad (4.4)$$

Here the diagonal blocks $r_{\sigma\sigma'}$ and $r'_{\sigma\sigma'}$ describe electron reflection to the left and to the right reservoir, respectively. The off-diagonal blocks $t_{\sigma\sigma'}$ and $t'_{\sigma\sigma'}$ correspond to the electron transmission through the sample from the left to the right reservoir and from the right to the left reservoir, respectively. As discussed in Section 2.1.3, the flux conservation in the scattering process implies the unitarity of matrix S. In addition, in the presence of time-reversal symmetry as discussed in Section **??** the scattering matrix is also symmetric.

Our goal in the following sections is to describe the transport through a nanowire with an impurity. Specifically, we derive an expression for the total

current operator $\hat{I}_L(\mathbf{r},t)$ in the left lead far away from the localized impurity, and obtain an expression for the charge and spin-dependent conductances. In the Landauer-Bütiker formalism the current operator is expressed in terms of the creation and annihilation operators.

4.2 Charge conductance

The conservation of charge implies the continuity equation in quantum mechanics for the charge density $\rho = \mathrm{e}\hat{\Psi}^\dagger\hat{\Psi}$

$$\frac{d\rho}{dt} + \nabla\cdot\mathbf{j} = 0\ . \tag{4.5}$$

From this expression and teh Schrödinger equation we can derive an expression for the charge current density $\mathbf{j}$. To do so we start by differentiating with respect to time the expression for the charge density

$$\frac{d\rho}{dt} = \mathrm{e}\left[\frac{d\hat{\Psi}^\dagger}{dt}\hat{\Psi} + \hat{\Psi}^\dagger\frac{d\hat{\Psi}}{dt}\right]\ , \tag{4.6}$$

where $\hat{\Psi} = \left(\hat{\Psi}_1, \hat{\Psi}_2\right)^T$ is a two-component spinor and $\hat{\Psi}^\dagger$ its hermitian conjugate. We now make use of the Shrödinger equation $\mathrm{i}\hbar\frac{d\hat{\Psi}}{dt} = H\hat{\Psi}$ and its adjoint, where the Hamiltonian of the system is given by,

$$H = -\frac{\hbar^2\nabla^2}{2m_e^*} - \mathrm{i}\hbar\alpha\left(\partial_x\hat{\sigma}_y - \partial_y\hat{\sigma}_x\right) + V_{conf}\left(y\right)\ . \tag{4.7}$$

On the one hand, the kinetic term and the confinement potential in Eq.4.7 leads us to write the kinetic contribution for the evolution of the charge density in Eq.(4.6) as

$$\begin{aligned}\frac{d\rho_K}{dt} &= \frac{\mathrm{e}}{\mathrm{i}\hbar}\left[\hat{\Psi}^\dagger\left(-\frac{-\hbar^2}{2m}\nabla^2\hat{\Psi}\right) - \left(-\frac{-\hbar^2}{2m}\nabla^2\hat{\Psi}^\dagger\right)\hat{\Psi} + \hat{\Psi}^\dagger V_{conf}\hat{\Psi} - V_{conf}\hat{\Psi}^\dagger\hat{\Psi}\right] \\ &= -\frac{\mathrm{e}\hbar}{2m\mathrm{i}}\nabla\left[\hat{\Psi}^\dagger(\nabla\hat{\Psi}) - (\nabla\hat{\Psi}^\dagger)\hat{\Psi}\right]\ ,\end{aligned} \tag{4.8}$$

whereas the contribution from the spin-orbit coupling of the Hamiltonian to Eq.(4.6), usually referred as the anomalous term of the current, leads on the

other hand to

$$\begin{aligned}\frac{d\rho_{SO}}{dt} =& \frac{\mathrm{e}}{\mathrm{i}\hbar}\left[\hat{\Psi}^\dagger\left(H_{SO}\hat{\Psi}\right) - \left(H_{SO}\hat{\Psi}\right)^\dagger\hat{\Psi}\right] \\ =& \frac{\mathrm{e}}{\mathrm{i}\hbar}\left[(\hat{\Psi}_1^*,\hat{\Psi}_2^*)\alpha\hbar\begin{pmatrix}-\partial_x\hat{\Psi}_2\\ \partial_x\hat{\Psi}_1\end{pmatrix} - \alpha\hbar(-\partial_x\hat{\Psi}_2^*,\partial_x\hat{\Psi}_1^*)\begin{pmatrix}\hat{\Psi}_1\\ \hat{\Psi}_2\end{pmatrix}\right] \\ &+ \frac{\mathrm{e}}{\mathrm{i}\hbar}\left[(\hat{\Psi}_1^*,\hat{\Psi}_2^*)\alpha\hbar\begin{pmatrix}\partial_y\hat{\Psi}_2\\ \partial_y\hat{\Psi}_1\end{pmatrix} - \alpha\hbar(\partial_y\hat{\Psi}_2^*,\partial_y\hat{\Psi}_1^*)\begin{pmatrix}\hat{\Psi}_1\\ \hat{\Psi}_2\end{pmatrix}\right] \\ =& \frac{\mathrm{e}\alpha}{\mathrm{i}}\left[-\hat{\Psi}_1^*(\partial_x\hat{\Psi}_2) + \hat{\Psi}_2^*(\partial_x\hat{\Psi}_1) + (\partial_x\hat{\Psi}_2^*)\hat{\Psi}_1 - (\partial_x\hat{\Psi}_1^*)\hat{\Psi}_2\right] \\ &+ \frac{\mathrm{e}\alpha}{\mathrm{i}}\left[\hat{\Psi}_1^*(\partial_y\hat{\Psi}_2) + \hat{\Psi}_2^*(\partial_y\hat{\Psi}_1) + (\partial_y\hat{\Psi}_2^*)\hat{\Psi}_1 + (\partial_y\hat{\Psi}_1^*)\hat{\Psi}_2\right] .\end{aligned} \tag{4.9}$$

In Eq.(4.9) the previous expression we made use of the fact that

$$-\mathrm{i}\alpha\hbar\hat{\sigma}_y\hat{\Psi} = -\mathrm{i}\alpha_x\hbar\begin{pmatrix}0 & -\mathrm{i}\\ \mathrm{i} & 0\end{pmatrix}\begin{pmatrix}\partial_x\hat{\Psi}_1\\ \partial_x\hat{\Psi}_2\end{pmatrix} = \alpha\hbar\begin{pmatrix}-\partial_x\hat{\Psi}_2\\ \partial_x\hat{\Psi}_1\end{pmatrix} ,$$

and

$$\mathrm{i}\alpha\hbar\hat{\sigma}_x\partial_y\hat{\Psi} = \mathrm{i}\alpha\hbar\begin{pmatrix}0 & 1\\ 1 & 0\end{pmatrix}\begin{pmatrix}\partial_y\hat{\Psi}_1\\ \partial_y\hat{\Psi}_2\end{pmatrix} = \alpha\hbar\begin{pmatrix}\partial_y\hat{\Psi}_2\\ \partial_y\hat{\Psi}_1\end{pmatrix} ,$$

while their complex conjugated results in $(-\mathrm{i}\alpha\hbar\hat{\sigma}_y\hat{\Psi})^\dagger = \alpha_x\hbar(-\partial_x\hat{\Psi}_2^*,\partial_x\hat{\Psi}_1^*)$ and $(\mathrm{i}\alpha\hbar\hat{\sigma}_x\partial_y\hat{\Psi})^\dagger = \alpha_x\hbar(\partial_y\hat{\Psi}_2^*,\partial_x\hat{\Psi}_1^*)$. Notice also that $\hat{\Psi}^\dagger\hat{\sigma}_y\hat{\Psi} = -\mathrm{i}(\hat{\Psi}_1^*\hat{\Psi}_2 - \hat{\Psi}_2^*\hat{\Psi}_1)$ and $\hat{\Psi}^\dagger\hat{\sigma}_x\hat{\Psi} = +\mathrm{i}(\hat{\Psi}_1^*\hat{\Psi}_2 + \hat{\Psi}_2^*\hat{\Psi}_1)$ Taking into account both the kinetic contribution in Eq. (4.8) and the spin-orbit contribution in Eq. (4.9), we can write Eq.(4.6) as

$$\frac{d\rho}{dt} = -\frac{\mathrm{e}\hbar}{2m\mathrm{i}}\nabla\left[\hat{\Psi}^\dagger(\partial_x\hat{\Psi}) - (\nabla\hat{\Psi}^\dagger)\hat{\Psi}\right] - \mathrm{e}\alpha\partial_x\left(\hat{\Psi}^\dagger\hat{\sigma}_y\hat{\Psi}\right) + \mathrm{e}\alpha\partial_y\left(\hat{\Psi}^\dagger\hat{\sigma}_x\hat{\Psi}\right) . \tag{4.10}$$

From this expression and Eq.(4.5) we identify the total current density along the x-direction as a sum of a kinetic $(j_x)_K$ and a spin-orbit $(j_x)_{SO}$ term:

$$\begin{aligned} j_x &= (j_x)_K + (j_x)_{SO} \\ &= \frac{\mathrm{e}\hbar}{2m\mathrm{i}}\left[\hat{\Psi}^\dagger(\partial_x\hat{\Psi}) - (\partial_x\hat{\Psi}^\dagger)\hat{\Psi}\right] - \mathrm{e}\alpha\left(\hat{\Psi}^\dagger\hat{\sigma}_y\hat{\Psi}\right) ,\end{aligned} \tag{4.11}$$

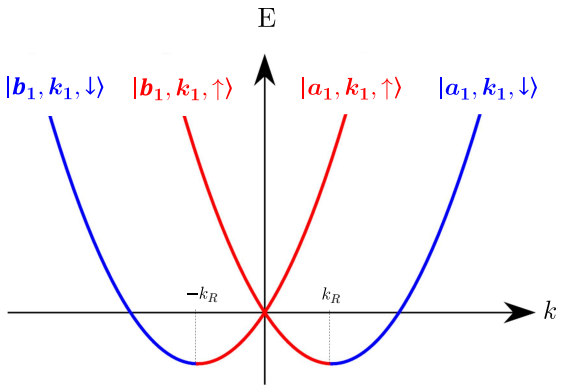

Figure 4.2: Energy dispersion spectrum with Rashba spin-orbit coupling where $\hat{a}$ states are incoming and $\hat{b}$ states outgoing.

and the total current density along the y-direction is given by

$$\begin{aligned} j_y &= (j_y)_K + (j_y)_{SO} \\ &= \frac{\mathrm{e}\hbar}{2m\mathrm{i}} \left[\hat{\Psi}^\dagger(\partial_y\hat{\Psi}) - (\partial_y\hat{\Psi}^\dagger)\hat{\Psi}\right] + \mathrm{e}\alpha\left(\hat{\Psi}^\dagger\hat{\sigma}_x\hat{\Psi}\right) . \end{aligned} \tag{4.12}$$

In the framework of the second quantization one can write the current operator as an integral of Eq.(4.11) in terms of the field operators $\hat{\Psi}$. The contribution to the current operator from the normal kinetic term in the left lead (far from the impurity) is then given by

$$\hat{I}_L^K(x,t) = \frac{\mathrm{e}\hbar}{2m\mathrm{i}} \int d\mathbf{r}_\perp \left[\hat{\Psi}_L^\dagger(\mathbf{r},t)(\partial_x\hat{\Psi}_L(\mathbf{r},t)) - (\partial_x\hat{\Psi}_L^\dagger(\mathbf{r},t))\hat{\Psi}_L(\mathbf{r},t)\right] . \tag{4.13}$$

Here $\mathbf{r} = (x, \mathbf{r}_\perp)$, $\mathbf{r}_\perp$ is the transverse coordinate and x is the coordinate along the wire. The field operators for the problem described in Eq. (4.7) will be obtained in Chapter 5 via gauge transformation that reduces the Hamiltonian problem to,

$$H = -\frac{\hbar^2\nabla^2}{2m_e^*} - \mathrm{i}\hbar\alpha\partial_x\hat{\sigma}_y + V_{conf}(y) - m_e^*\frac{\alpha^2}{2} . \tag{4.14}$$

Without getting into details about the solution of Hamiltonian in Eq. (4.7), it is possible to study dynamic properties of such a system because they remain unchanged under gauge transformations. Furthermore, it is possible to write the egienfunctions for a problem described by the Hamiltonian in Eq. (4.14) if one gauges away the term $-\mathrm{i}\hbar\alpha\partial_x\hat{\sigma}_y$ with the following transformation

$$\hat{\Psi} = \mathrm{e}^{-\mathrm{i}\left(\frac{m\alpha}{\hbar}\right)\hat{\sigma}_y x}\hat{\tilde{\Psi}} \ . \tag{4.15}$$

Where the field operators in this transformed problem are typically expanded in terms of the creation operator in the second quantization: $\hat{\tilde{\Psi}} = \sum_n \mathrm{e}^{\mathrm{i}k_n x}\hat{c}_{\alpha n\sigma}$, where α is the lead index and $\hat{c}_{\alpha n\sigma}$ can take the value $\hat{a}_{\alpha n\sigma}$ the incoming states and $\hat{b}_{\alpha n\sigma}$ for the outgoing ones. The gauge transformation adds a spin index σ. Hence the field operators of the original problem in the left lead $\hat{\Psi}_L(\mathbf{r},t)$ and $\hat{\Psi}^\dagger_L(\mathbf{r},t)$ can be expressed in terms of the operators defined in Refs. (4.2a-4.2c) as a superposition of incoming and outgoing states (see Fig. 4.2):

$$\begin{aligned}\hat{\Psi}_L(\mathbf{r},t) = &\int dE' \mathrm{e}^{-\mathrm{i}E't/\hbar}\sum_{n',\sigma'}\frac{\Phi_{Ln'\sigma'}(\mathbf{r}_\perp)}{\sqrt{2\pi v_{Ln'\sigma'(E')}}} \\ &\times\left\{\hat{a}_{Ln'\sigma'}(E')\mathrm{e}^{\mathrm{i}(k_{n'}(E')-\sigma' k_R)x} + \hat{b}_{Ln'\sigma'}(E')\mathrm{e}^{-\mathrm{i}(k_{n'}(E')+\sigma' k_R)x}\right\} \ , \end{aligned} \tag{4.16}$$

$$\begin{aligned}\hat{\Psi}^\dagger_L(\mathbf{r},t) = &\int dE \mathrm{e}^{\mathrm{i}Et/\hbar}\sum_{n,\sigma}\frac{\Phi^*_{Ln\sigma}(\mathbf{r}_\perp)}{\sqrt{2\pi v_{Ln\sigma(E)}}} \\ &\times\left\{\hat{a}^\dagger_{Ln\sigma}(E)\mathrm{e}^{-\mathrm{i}(k_n(E)-\sigma k_R)x} + \hat{b}^\dagger_{Ln\sigma}(E)\mathrm{e}^{\mathrm{i}(k_n(E)+\sigma k_R)x}\right\} \ , \end{aligned} \tag{4.17}$$

where $\Phi_{Ln\sigma}(\mathbf{r}_\perp)$ are the orthonormal transverse wave functions so that $\int d\mathbf{r}_\perp \Phi^*_{Ln\sigma}\Phi_{Ln'\sigma'}(\mathbf{r}_\perp) = \delta_{nn'}\delta_{\sigma\sigma'}$, $k_n = \hbar^{-1}\sqrt{2m(E-E_n+m\alpha^2)}$ is the momentum with $\alpha = \hbar k_R/m^*_e$ and the velocity of carriers is $v_{Ln\sigma} = \hbar k_n/m$.

Then, taking into account Eqs.(4.16)-(4.17) the expression in Eq.(4.13)

for the average of the kinetic current becomes

$$\begin{aligned}\hat{I}_L^K(\mathbf{x},t) = \frac{\mathrm{e}\hbar}{2m}\int dEdE' \sum_{n\sigma} \frac{\mathrm{e}^{\mathrm{i}(E-E')t/\hbar}}{2\pi\hbar\sqrt{v_{Ln'\sigma'}v_{Ln\sigma}}} \\ \times\Big\{(k_n(E)+k_{n'}(E')-2\sigma k_R)\,\hat{a}^\dagger_{Ln\sigma}(E)\hat{a}_{Ln\sigma}(E')\mathrm{e}^{-\mathrm{i}(k_n(E)-k_{n'}(E'))x} \\ -(k_n(E)+k_{n'}(E')+2\sigma k_R)\,\hat{b}^\dagger_{Ln\sigma}(E)\hat{b}_{Ln\sigma}(E')\mathrm{e}^{\mathrm{i}(k_n(E)-k_{n'}(E'))x} \\ +(k_n(E)-k_{n'}(E')-2\sigma k_R)\,\hat{a}^\dagger_{Ln\sigma}(E)\hat{b}_{Ln\sigma}(E')\mathrm{e}^{-\mathrm{i}(k_n(E)+k_{n'}(E'))x} \\ -(k_n(E)-k_{n'}(E')+2\sigma k_R)\,\hat{b}^\dagger_{Ln\sigma}(E)\hat{a}_{Ln\sigma}(E')\mathrm{e}^{\mathrm{i}(k_n(E)+k_{n'}(E'))x}\Big\}\,.\end{aligned} \tag{4.18}$$

The expression in Eq.(4.18) can be significantly simplified by taking into account that values of E and E' are close to each other and that the wave vectors $k_n(E)$ and velocities vary slowly with energy around the Fermi energy [109, 110]. This simplification leads to:

$$\begin{aligned}\hat{I}_L^K(\mathbf{x},t) = \frac{\mathrm{e}}{4\pi m}\int dEdE' \sum_{n\sigma} \frac{\mathrm{e}^{\mathrm{i}(E-E')t/\hbar}}{v_{Ln'\sigma'}} \\ \times 2\Big\{(k_n(E)-\sigma k_R)\,\hat{a}^\dagger_{Ln\sigma}(E)\hat{a}_{Ln\sigma}(E') - (k_n(E)+\sigma k_R)\,\hat{b}^\dagger_{Ln\sigma}(E)\hat{b}_{Ln\sigma}(E') \\ -\sigma k_R\left(\hat{a}^\dagger_{Ln\sigma}(E)\hat{b}_{Ln\sigma}(E')\mathrm{e}^{-2\mathrm{i}k_n(E)x} + \hat{b}^\dagger_{Ln\sigma}(E)\hat{a}_{Ln\sigma}(E')\mathrm{e}^{2\mathrm{i}k_n(E)x}\right)\Big\}\,.\end{aligned} \tag{4.19}$$

Following the same procedure we obtain the contribution to the current operator stemming from the anomalous velocity related to the spin-orbit coupling term in Eq.(4.11),

$$\begin{aligned}\hat{I}_L^{SO}(\mathbf{x},t) = \frac{\mathrm{e}\alpha_x}{2\pi\hbar}\int dEdE' \sum_{n\sigma} \frac{\mathrm{e}^{\mathrm{i}(E-E')t/\hbar}}{v_{Ln'\sigma'}} \\ \sigma\Big\{\hat{a}^\dagger_{Ln\sigma}(E)\hat{a}_{Ln\sigma}(E') + \hat{b}^\dagger_{Ln\sigma}(E)\hat{b}_{Ln\sigma}(E') \\ +\hat{a}^\dagger_{Ln\sigma}(E)\hat{b}_{Ln\sigma}(E')\mathrm{e}^{-2\mathrm{i}k_n(E)x} + \hat{b}^\dagger_{Ln\sigma}(E)\hat{a}_{Ln\sigma}(E')\mathrm{e}^{2\mathrm{i}k_n(E)x}\Big\}\,.\end{aligned} \tag{4.20}$$

Considering that $k_R = m\alpha_x/\hbar$, we can see that the terms linear in σk_R from Eq. (4.19) and Eq. (4.20) balance each other out (in agreement with

Ref.[111])and the velocity in the denominator cancels with $\hbar k_n/m$ in the numerator. Consequently,

$$\begin{aligned}\hat{I}_L(\mathbf{t}) &= \hat{I}_L^K + \hat{I}_L^{SO} \\ &= \frac{\mathrm{e}}{2\pi\hbar}\int dEdE'\mathrm{e}^{\mathrm{i}(E-E')t/\hbar}\sum_{n\sigma}\left\{\hat{a}^\dagger_{Ln\sigma}(E)\hat{a}_{Ln\sigma}(E') - \hat{b}^\dagger_{Ln\sigma}(E)\hat{b}_{Ln\sigma}(E')\right\} .\end{aligned} \tag{4.21}$$

Now, we focus on the term within brackets in Eq. (4.21), namely $\hat{a}^\dagger_{Ln\sigma}(E)\hat{a}_{Ln\sigma}(E') - \hat{b}^\dagger_{Ln\sigma}(E)\hat{b}_{Ln\sigma}(E')$. The creation and annihilation operators $\hat{a}_{Ln\sigma}$, $\hat{a}^\dagger_{Ln\sigma}$,$\hat{b}_{Ln\sigma}$ and $\hat{b}^\dagger_{Ln\sigma}$ are related through the scattering matrix S defined in the previous section by Eq.(4.3), so that

$$\hat{b}_{Ln\sigma} = \sum_{\beta ms} S_{Ln\sigma,\beta ms}\hat{a}_{\beta ms}, \tag{4.22}$$

$$\hat{b}^\dagger_{Ln\sigma} = \sum_{\alpha m's'} \hat{a}^\dagger_{\alpha m's'}S^\dagger_{\alpha m's',Ln\sigma} . \tag{4.23}$$

These expressions relate the outgoing states on the left lead for a fixed channel n and spin σ to all the possible incoming states from the leads ($\beta = L, R$) Notice that the spin indices from the leads are denoted by s and s' With the help of these expressions for the outgoing scattering states in Eq. (4.22)-(4.23) we can write Eq. (4.21) in terms of the incoming state creation and anhilation operatora, $\hat{a}$ and $\hat{a}^\dagger$,

$$\hat{I}_L(\mathbf{t}) = \frac{\mathrm{e}}{2\pi\hbar}\sum_{\alpha\beta}\sum_{m'm}\sum_{s's}\int dEdE'\mathrm{e}^{\mathrm{i}(E-E')t/\hbar}\hat{a}^\dagger_{\alpha ms'}(E)\mathcal{A}^{m's',ms}_{\alpha\beta}(L;E,E')\hat{a}_{\beta ms}(E') . \tag{4.24}$$

Here α and β take the reservoir values L or R and we define $\mathcal{A}^{m's',ms}_{\alpha\beta}(L;E,E') = \delta_{m'm}\delta_{s's}\delta_{\alpha L}\delta_{\beta L} - \sum_{n\sigma} S^\dagger_{\alpha m's',Ln\sigma}(E)S_{Ln\sigma,\beta ms}(E')$. This result for the charge current operator, agrees with the results of Rashba interaction in the coherent scattering formalism in Ref. [111]. In the next section we follow an analog procedure to obtain the expression for the spin-current operator.

In order to derive the average current from Eq. (4.24), we need to compute the average of the product between creation and annihilation operators for an electron gas at thermal equilibrium. This reads:

$$\left\langle \hat{a}^\dagger_{\alpha m's'}(E)\hat{a}_{\beta ms}(E')\right\rangle = \delta_{m'm}\delta_{s's}\delta_{\alpha\beta}\delta\left(E-E'\right)f_\alpha\left(E\right) . \tag{4.25}$$

In the averaging process only terms with $\alpha = \beta$ survive. The corresponding scattering matrix elements are $S_{Ln\sigma,Lms} = r_{n\sigma,ms}$ and $S_{Ln\sigma,Rms} = t'_{n\sigma,ms}$. Then it is possible to write the average of Eq. (4.24) as

$$\begin{aligned}
&\sum_{\alpha\beta}\sum_{m'm}\sum_{s's}\left\langle \hat{a}^{\dagger}_{\alpha ms'}(E)\mathcal{A}^{m's',ms}_{\alpha\beta}(L;E,E')\hat{a}_{\beta ms}(E')\right\rangle = \\
&= \sum_{ms}\left[1-\sum_{n\sigma} r^{\dagger}_{ms,n\sigma}r_{n\sigma,ms}\right] f_L\left(E\right)\delta\left(E-E'\right) \\
&- \sum_{ms}\sum_{n\sigma} t'^{\dagger}_{ms,n\sigma}t'_{n\sigma,ms} f_R\left(E\right)\delta\left(E-E'\right)\ . \qquad (4.26)
\end{aligned}$$

The unitarity condition $S^{\dagger}S = SS^{\dagger} = 1$, implies, among others, the following identities:

$$\begin{aligned}
t'^{\dagger}r &= -r'^{\dagger}t \rightarrow t'^{\dagger} = -r'^{\dagger}tr^{-1}, \\
rt^{\dagger} &= -t'r'^{\dagger} \rightarrow t' = -rt^{\dagger}(r'^{\dagger})^{-1}\ ,
\end{aligned}$$

resulting in $t'^{\dagger}t' = r'^{\dagger}tr^{-1}rt^{\dagger}(r'^{\dagger})^{-1} = r'^{\dagger}tt^{\dagger}(r'^{\dagger})^{-1}$. Then we can prove that for the scattering coefficients in Eq.(4.26),

$$\begin{aligned}
\sum_{ms}\sum_{n\sigma} t'^{\dagger}_{ms,n\sigma}t'_{n\sigma,ms} &= Tr\left(t'^{\dagger}t'\right) = Tr\left(r'^{\dagger}tt^{\dagger}(r'^{\dagger})^{-1}\right) = Tr\left((r'^{\dagger})^{-1}r'^{\dagger}tt^{\dagger}\right) \\
&= Tr\left(tt^{\dagger}\right) = Tr\left(t^{\dagger}t\right)\ . \qquad (4.27)
\end{aligned}$$

On the other hand $r^{\dagger}r + t^{\dagger}t = 1$, hence

$$\sum_{ms}\sum_{n\sigma}\left[1 - r^{\dagger}_{ms,n\sigma}r_{n\sigma,ms}\right] = \sum_{ms}\sum_{n\sigma} t^{\dagger}_{ms,n\sigma}t_{n\sigma,ms} = Tr\left(t^{\dagger}t\right)\ . \qquad (4.28)$$

Substitution of Eq. (4.28) and Eq. (4.27) into Eq. (4.26), and the latter into Eq. (4.24), we finally obtain for the average current :

$$\begin{aligned}
\left\langle \hat{I}_L(\mathbf{t})\right\rangle &= \frac{\mathrm{e}}{2\pi\hbar}\int dEdE'\mathrm{e}^{\mathrm{i}(E-E')t/\hbar}\ Tr\left(t^{\dagger}t\right)\left[f_L\left(E\right) - f_R\left(E\right)\right]\delta\left(E-E'\right) \\
&= \frac{\mathrm{e}}{2\pi\hbar}\int dE\ Tr\left(t^{\dagger}t\right)\left[f_L\left(E\right) - f_R\left(E\right)\right]\ . \qquad (4.29)
\end{aligned}$$

If we now consider a voltage bias situation, with different chemical potentials in the left and right leads, such that $\mu_L - \mu_R = eV$, we can calculate the

conductance as $\mathcal{G} = I/V$ with current I given by Eq.(4.29), resulting in

$$\begin{aligned}\mathcal{G} &= \frac{1}{V}\frac{e}{2\pi\hbar}\int dE\ Tr\left(t^{\dagger}t\right)\left[f\left(E-\mu_L\right)-f\left(E-\mu_R\right)\right] \\ &= \frac{1}{V}\frac{e}{2\pi\hbar}\int dE\ Tr\left(t^{\dagger}t\right)\left[-(\mu_L-\mu_R)f'\left(E\right)\right] \\ &= \frac{e^2}{2\pi\hbar}\int dE\ Tr\left(t^{\dagger}t\right)\delta\left(E-E_F\right)\ .\end{aligned}$$

In the last step in Eq.(**??**) we assume in the zero-temperature limit the Fermi distribution function is a step function whose derivative becomes a delta in energy $-f'(E) = \delta\left(E - E_F\right)$. Finally we obtain:

$$\mathcal{G} = \frac{e^2}{2\pi\hbar}Tr\left(t^{\dagger}(E_F)t(E_F)\right)\ . \tag{4.30}$$

Eq. (4.30) is the well-known Landauer-Büttiker expression. It establishes the connection between the scattering matrix and the conductance of the system. We must notice that independently of the choice of basis, the conductance can be expressed in terms of transmission probabilities T_n for each channel, as the expression $t^{\dagger}(E_F)t(E_F)$ is diagonalizable and hence $Tr\left(t^{\dagger}t\right) = \sum_n T_n$. Furthermore, another version of Eq. (4.30) allows us to write the conductance in terms of the transmission probabilities for electrons leaving the left lead L from a channel n and with spin σ to arrive to the m channel in the right lead R with spin σ',

$$\mathcal{G} = \frac{e^2}{2\pi\hbar}\sum_{m\sigma',n\sigma}\left|t_{m\sigma',n\sigma}\right|^2\ . \tag{4.31}$$

Once we have reviewed the way to write the charge conductance in the Landauer-Büttiker formalism we will generalize it in the next section for the case of spin-dependent observables such as the spin-current and spin-polarized conductance.

4.3 Spin current along the nanowire

As we mention in the previous section, in Chapter 5 we obtain the solutions for the Hamiltonian described by Eq.(4.7) via a gauge transfromation that preserves the dynamics of the system. In this transformed system, effectively described by the Hamiltonian in Eq. (4.14) we can define a spin-density (not

equivalent to the "true spin") the y-component. Since we expect that away from the impurity of the spin to be conserved we can use the continuity equation. This way, we are able to derive expressions for the spin currents in both leads.

In analogy to previous subsection, we start first deriving the corresponding conservation equation from the spin density $S_y = \mathrm{e}\hat{\Psi}^\dagger\hat{\sigma}_y\hat{\Psi}$ by differentiating with respect to time,

$$\frac{dS_y}{dt} = \mathrm{e}\left[\frac{d\hat{\Psi}^\dagger}{dt}\hat{\sigma}_y\hat{\Psi} + \hat{\Psi}^\dagger\hat{\sigma}_y\frac{d\hat{\Psi}}{dt}\right] . \tag{4.32}$$

For the kinetic term and confinement described by our problem Hamiltonian in Eq.(4.14) we can write

$$\begin{aligned}\frac{(dS_y)_K}{dt} &= \frac{\mathrm{e}}{\mathrm{i}\hbar}\left[\hat{\Psi}^\dagger\hat{\sigma}_y\left(-\frac{-\hbar^2}{2m}\nabla^2\hat{\Psi}\right) - \left(-\frac{-\hbar^2}{2m}\nabla^2\hat{\Psi}^\dagger\right)\hat{\sigma}_y\hat{\Psi}\right.\\ &\left. + \hat{\Psi}^\dagger\hat{\sigma}_y\left(V_{conf}\hat{\Psi}\right) - \left(V_{conf}\hat{\Psi}^\dagger\right)\hat{\sigma}_y\hat{\Psi}\right]\\ &= -\frac{\mathrm{e}\hbar}{2m\mathrm{i}}\nabla\left[\hat{\Psi}^\dagger\hat{\sigma}_y(\nabla\hat{\Psi}) - (\nabla\hat{\Psi}^\dagger)\hat{\sigma}_y\hat{\Psi}\right] .\end{aligned} \tag{4.33}$$

And for the additional spin-orbit or anomalous term the contribution is given by,

$$\begin{aligned}\frac{d(S_y)_{SO}}{dt} &= \frac{\mathrm{e}}{\mathrm{i}\hbar}\left[\hat{\Psi}^\dagger\hat{\sigma}_y\left(H_{SO}\hat{\Psi}\right) - \left(H_{SO}\hat{\Psi}\right)^\dagger\hat{\sigma}_y\hat{\Psi}\right]\\ &= \frac{\mathrm{e}}{\mathrm{i}\hbar}\left[(\hat{\Psi}_1^*, \hat{\Psi}_2^*)\hat{\sigma}_y\alpha_x\hbar\begin{pmatrix}-\partial_x\hat{\Psi}_2\\ \partial_x\hat{\Psi}_1\end{pmatrix} - \alpha_x\hbar(-\partial_x\hat{\Psi}_2^*, \partial_x\hat{\Psi}_1^*)\hat{\sigma}_y\begin{pmatrix}\hat{\Psi}_1\\ \hat{\Psi}_2\end{pmatrix}\right]\\ &= \frac{\mathrm{e}\alpha_x}{\mathrm{i}}\left[(\hat{\Psi}_1^*, \hat{\Psi}_2^*)\begin{pmatrix}-\mathrm{i}\partial_x\hat{\Psi}_1\\ -\mathrm{i}\partial_x\hat{\Psi}_2\end{pmatrix} - (-\partial_x\hat{\Psi}_2^*, \partial_x\hat{\Psi}_1^*)\begin{pmatrix}-\mathrm{i}\hat{\Psi}_2\\ \mathrm{i}\hat{\Psi}_1\end{pmatrix}\right]\\ &= -\alpha\mathrm{e}\partial_x\left[\hat{\Psi}^\dagger\hat{\Psi}\right] .\end{aligned} \tag{4.34}$$

Taking into account both kinetic and spin-orbit contributions in Eq.(4.33) and Eq.(4.34) respectively, we can write the total evolution for the spin-density polarized along y-axis as follows

$$\frac{dS_y}{dt} = -\frac{\mathrm{e}\hbar}{2m\mathrm{i}}\partial_x\left[\hat{\Psi}^\dagger\hat{\sigma}_y(\partial_x\hat{\Psi}) - (\partial_x\hat{\Psi}^\dagger)\hat{\sigma}_y\hat{\Psi}\right] - \mathrm{e}\alpha_x\partial_x\left(\hat{\Psi}^\dagger\hat{\Psi}\right) . \tag{4.35}$$

All the terms in Eq.(4.35) can be gathered under the same partial derivative ∂_x and therefore written in the form of $\frac{dS_y}{dt} + \partial_x j_x^y = 0$, that is to say we can define a conserved spin current along x with spin-polarization along y such that,

$$\begin{aligned} j_x^y &= (j_x^y)_K + (j_x^y)_{SO} \\ &= \frac{\mathrm{e}\hbar}{2m\mathrm{i}} \left[\hat{\Psi}^\dagger \hat{\sigma}_y (\partial_x \hat{\Psi}) - (\partial_x \hat{\sigma}_y \hat{\Psi}^\dagger) \hat{\Psi} \right] - \mathrm{e}\alpha_x \left(\hat{\Psi}^\dagger \hat{\Psi} \right) . \end{aligned} \tag{4.36}$$

Then, in the framework of the second quantization one can write the current operator as an integral of Eq.(4.36) in terms of the field operators $\hat{\Psi}$ with a kinetic contribution given by

$$\begin{aligned} (\hat{I}_L^y)^K(\mathbf{x},t) = \frac{\mathrm{e}\hbar}{2m} \int dE dE' \sum_{n\sigma} \frac{\mathrm{e}^{\mathrm{i}(E-E')t/\hbar}}{2\pi\hbar\sqrt{v_{Ln'\sigma'} v_{Ln\sigma}}} \\ \times \Big\{ \hat{a}^\dagger_{Ln\sigma}(E) \left(k_n(E)\sigma + \sigma k_{n'}(E') - 2k_R \right) \hat{a}_{Ln\sigma}(E') \mathrm{e}^{-\mathrm{i}(k_n(E) - k_{n'}(E'))x} \\ - \hat{b}^\dagger_{Ln\sigma}(E) \left(k_n(E)\sigma + \sigma k_{n'}(E') + 2k_R \right) \hat{b}_{Ln\sigma}(E') \mathrm{e}^{\mathrm{i}(k_n(E) - k_{n'}(E'))x} \\ + \hat{a}^\dagger_{Ln\sigma}(E) \left(k_n(E)\sigma - \sigma k_{n'}(E') - 2k_R \right) \hat{b}_{Ln\sigma}(E') \mathrm{e}^{-\mathrm{i}(k_n(E) + k_{n'}(E'))x} \\ - \hat{b}^\dagger_{Ln\sigma}(E) \left(k_n(E)\sigma - \sigma k_{n'}(E') + 2k_R \right) \hat{a}_{Ln\sigma}(E') \mathrm{e}^{\mathrm{i}(k_n(E) + k_{n'}(E'))x} \Big\} . \end{aligned}$$

Again, the expression in Eq.(4.37) can be significantly simplified by taking into account that values of E and E' are close to each other and that the wave vectors $k_n(E)$ and velocities vary slowly with energy around the Fermi energy. This way,

$$\begin{aligned} (\hat{I}_L^y)^K(\mathbf{x},t) = \frac{\mathrm{e}}{4\pi m} \int dE dE' \sum_{n\sigma} \frac{\mathrm{e}^{\mathrm{i}(E-E')t/\hbar}}{v_{Ln'\sigma'}} \\ \times 2 \Big\{ \hat{a}^\dagger_{Ln\sigma}(E) \left(k_n(E)\sigma - k_R \right) \hat{a}_{Ln\sigma}(E') - \hat{b}^\dagger_{Ln\sigma}(E) \left(k_n(E)\sigma + k_R \right) \hat{b}_{Ln\sigma}(E') \\ - 2k_R \left(\hat{a}^\dagger_{Ln\sigma}(E) \hat{b}_{Ln\sigma}(E') \mathrm{e}^{-2\mathrm{i}k_n(E)x} + \hat{b}^\dagger_{Ln\sigma}(E) \hat{a}_{Ln\sigma}(E') \mathrm{e}^{2\mathrm{i}k_n(E)x} \right) \Big\} . \end{aligned} \tag{4.37}$$

And for the spin-orbit contribution Eq.(4.36),

$$(\hat{I}_L^y)^{SO}(\mathbf{x},t) = \frac{\mathrm{e}\alpha_x}{2\pi\hbar}\int dEdE' \sum_{n\sigma} \frac{\mathrm{e}^{\mathrm{i}(E-E')t/\hbar}}{v_{Ln'\sigma'}} \times \Big\{ \hat{a}^\dagger_{Ln\sigma}(E)\hat{a}_{Ln\sigma}(E') + \hat{b}^\dagger_{Ln\sigma}(E)\hat{b}_{Ln\sigma}(E') + \hat{a}^\dagger_{Ln\sigma}(E)\hat{b}_{Ln\sigma}(E')\mathrm{e}^{-2\mathrm{i}k_n(E)x} + \hat{b}^\dagger_{Ln\sigma}(E)\hat{a}_{Ln\sigma}(E')\mathrm{e}^{2\mathrm{i}k_n(E)x} \Big\} \ . \tag{4.38}$$

Finally the expression for the spin current polarized along the y-axis in the left lead is given by the sum of both kinetic Eq. (**??**) and spin-orbit contributions Eq. (4.38), so that

$$\begin{aligned}\hat{I}_L^y(\mathbf{t}) &= \hat{I}_L^K + \hat{I}_L^{SO} \\ &= \frac{\mathrm{e}}{2\pi\hbar}\int dEdE'\mathrm{e}^{\mathrm{i}(E-E')t/\hbar}\sum_{n\sigma}\Big\{\hat{a}^\dagger_{Ln\sigma}(E)\sigma\hat{a}_{Ln\sigma}(E') - \hat{b}^\dagger_{Ln\sigma}(E)\sigma\hat{b}_{Ln\sigma}(E')\Big\} \ .\end{aligned} \tag{4.39}$$

Now we will focus on the term in between the brackets where the sum over the σ index is going to influence the final result as we will see. Reorganizing a bit the different sums it is possible to rewrite the expression for the spin-polarized current in Eq. (4.39) as given by the following expression only in terms of the creation and annihilation operators of the incoming basis,

$$\hat{I}_L^y(\mathbf{t}) = \frac{\mathrm{e}}{2\pi\hbar}\sum_{\alpha\beta}\sum_{m'm}\sum_{s's}\int dEdE'\mathrm{e}^{\mathrm{i}(E-E')t/\hbar}\hat{a}^\dagger_{\alpha n\sigma}(E)\mathcal{B}^{m's',ms}_{\alpha\beta}(L;E,E')\hat{a}_{\beta n\sigma}(E') \ , \tag{4.40}$$

here again, α and β take the reservoir values L or R and $\mathcal{B}^{m's',ms}_{\alpha\beta}(L;E,E') = \delta_{m'm}\delta_{s's}\delta_{\alpha L}\delta_{\beta L}\ s - \sum_{n\sigma} S^\dagger_{\alpha m's',Ln\sigma}(E)\sigma S_{Ln\sigma,\beta ms}(E')$. In order to derive the average spin-polarized current, we need to know that the product of the creation and annihilation operators of a electron Fermi gas at thermal equilibrium is

$$\left\langle \hat{a}^\dagger_{\alpha m's'}(E)\hat{a}_{\beta ms}(E')\right\rangle = \delta_{m'm}\delta_{s's}\delta_{\alpha\beta}\delta\left(E-E'\right)f_{\alpha s'}\left(E\right) \ . \tag{4.41}$$

We have added a spin index in the Fermi distribution, $f_{\alpha s'}\left(E\right) = \left[\mathrm{e}^{(E-\mu_{\alpha s'})/k_BT_{\alpha s'}}+1\right]^{-1}$, to describe eventually different spin

chemical potential and spin temperature in each lead. This means we have an additional index with respect to Eq.(4.25). Similarly, in the averaging process we notice that only $\alpha = \beta$ terms are going to survive and that $S_{Ln\sigma,Lms} = r_{n\sigma,ms}$ and $S_{Ln\sigma,Rms} = t'_{n\sigma,ms}$. Then, using the previously derived unitary identities and this other one $\sum_s \left[r^\dagger_{s,\sigma} r_{\sigma s} + t^\dagger_{s,\sigma} t_{\sigma s}\right] = 1$ we can rewrite the integrand in Eq. (4.39) using the Eq.(4.41),as follows

$$\begin{aligned}
&\sum_{\alpha\beta}\sum_{m'm}\sum_{s's}\left\langle \hat{a}^\dagger_{\alpha ms}(E)\mathcal{B}^{m's',ms}_{\alpha\beta}(L;E,E')\hat{a}_{\beta ms}(E')\right\rangle \\
&= \sum_{m'\sigma'}\left(\sigma' - \sum_{m\sigma} r^\dagger_{m'\sigma',m\sigma}\sigma r_{m\sigma,m's'}\right) f_{L\sigma'}(E)\,\delta(E-E') \\
&+ \sum_{m'\sigma'}\sum_{m\sigma}\left(t'^\dagger_{m'\sigma',m\sigma}\sigma t'_{m\sigma,m'\sigma'}\right) f_{R\sigma'}(E)\,\delta(E-E')\ . \qquad (4.42)
\end{aligned}$$

Substituing Eq. (4.42) into Eq. (4.39) we obtain the expression for the average spin-current :

$$\begin{aligned}
\left\langle \hat{I}^y_L(\mathbf{t})\right\rangle = \frac{\mathrm{e}}{2\pi\hbar}\int dE \Bigg[&\sum_{m'\sigma'}\left(\sigma' - \sum_{m\sigma} r^\dagger_{m'\sigma',m\sigma}\sigma r_{m\sigma,m's'}\right) f_{L\sigma'}(E) \\
&+ \sum_{m'\sigma'}\sum_{m\sigma}\left(t'^\dagger_{m'\sigma',m\sigma}\sigma t'_{m\sigma,m'\sigma'}\right) f_{R\sigma'}(E)\Bigg]\ . \qquad (4.43)
\end{aligned}$$

Due to the spin-dependence of the Fermi distribution we can write explicitly the spin current of Eq. (4.43) as follows

$$\begin{aligned}
\left\langle \hat{I}^y_L(\mathbf{t})\right\rangle = \frac{\mathrm{e}}{2\pi\hbar}\int dE \Big[&T_\uparrow f_{L\uparrow}(E) - T_\downarrow f_{L\downarrow}(E) - T'_\uparrow f_{R\uparrow}(E) + T'_\downarrow f_{R\downarrow}(E) \\
&+ \left(r^\dagger_{\downarrow\uparrow} r_{\uparrow\downarrow} + r^\dagger_{\uparrow\downarrow} r_{\downarrow\uparrow}\right)\left(f_{L\uparrow}(E) - f_{L\downarrow}(E)\right) \\
&+ \left(t'^\dagger_{\downarrow\uparrow} t'_{\uparrow\downarrow} + t'^\dagger_{\uparrow\downarrow} t'_{\downarrow\uparrow}\right)\left(f_{R\uparrow}(E) - f_{R\downarrow}(E)\right)\Big]\ . \qquad (4.44)
\end{aligned}$$

where $T_\uparrow = t^\dagger_{\uparrow\uparrow} t_{\uparrow\uparrow} + t^\dagger_{\downarrow\uparrow} t_{\uparrow\downarrow}$ is the transmission amplitude with spin-up on the left lead. Similarly, $T_\downarrow = t^\dagger_{\downarrow\downarrow} t_{\downarrow\downarrow} + t^\dagger_{\uparrow\downarrow} t_{\downarrow\uparrow}$ for the transmission amplitude with spin-down. In order to keep track of the origin of each transmission amplitudes we work with $T'_{\uparrow,\downarrow} = t'^\dagger_{\uparrow\uparrow} t'_{\uparrow\uparrow} + t'^\dagger_{\downarrow\uparrow} t'_{\uparrow\downarrow}$, that is to say, the transmission amplitudein the left lead for electrons incident from the right, although due

to the unitarity of the scattering matrix they are equivalent to $T_{\uparrow,\downarrow}$. In the absence of spin bias, i.e.($f_{L,R\uparrow} = f_{L,R\downarrow}$), Eq. (4.44) is reduced to:

$$\left\langle \hat{I}_L^y(\mathbf{t}) \right\rangle = \frac{\mathrm{e}}{2\pi\hbar} \int dE \left[T_\uparrow - T_\downarrow \right] \left(f_L(E) - f_R(E) \right) \ ,$$

where we used $T_{\uparrow,\downarrow} = T'_{\uparrow,\downarrow}$.

In a general case, when no assumption is made regarding the chemical potentials, we can write in linear response

$$\begin{aligned} \int dE T_\uparrow(E) \left(f_{L\uparrow}(E) - f_{R\uparrow}(E) \right) &= T_\uparrow \left(\mu_L^\uparrow - \mu_R^\uparrow \right), \\ \int dE T_\downarrow(E) \left(f_{L\downarrow}(E) - f_{R\downarrow}(E) \right) &= T_\downarrow \left(\mu_L^\downarrow - \mu_R^\downarrow \right) \ . \end{aligned} \tag{4.45}$$

and similarly,

$$\begin{aligned} \int dE \left(r_{\downarrow\uparrow}^\dagger r_{\uparrow\downarrow} + r_{\uparrow\downarrow}^\dagger r_{\downarrow\uparrow} \right) \left(f_{L\uparrow}(E) - f_{L\downarrow}(E) \right) &= \left(r_{\downarrow\uparrow}^\dagger r_{\uparrow\downarrow} + r_{\uparrow\downarrow}^\dagger r_{\downarrow\uparrow} \right) \left(\mu_L^\uparrow - \mu_L^\downarrow \right), \\ \int dE \left(t_{\downarrow\uparrow}'^\dagger t'_{\uparrow\downarrow} + t_{\uparrow\downarrow}'^\dagger t'_{\downarrow\uparrow} \right) \left(f_{R\uparrow}(E) - f_{R\downarrow}(E) \right) &= \left(t_{\downarrow\uparrow}'^\dagger t'_{\uparrow\downarrow} + t_{\uparrow\downarrow}'^\dagger t'_{\downarrow\uparrow} \right) \left(\mu_R^\uparrow - \mu_R^\downarrow \right) \ . \end{aligned} \tag{4.46}$$

These differences in chemical potential are $\left(\mu_L^{\uparrow,\downarrow} - \mu_R \uparrow, \downarrow \right) = eV_{L\to R}^{\uparrow,\downarrow}$ and for the spin-biases $\left(\mu_{L,R}^\uparrow - \mu_{L,R}^\downarrow \right) = \mathrm{e} V_{L,R}^y$ as we polarize the spin along the y-direction. Substituting Eqs.(**??**)-(4.46) into Eq.(4.44) that finally we can express the spin current polarized alon y-direction in the left lead as

$$\langle I_L^s \rangle = \frac{e^2}{2\pi\hbar} \left[T_\uparrow V_{L\to R}^\uparrow - T_\downarrow V_{L\to R}^\downarrow + \left(r_{\downarrow\uparrow}^\dagger r_{\uparrow\downarrow} + r_{\uparrow\downarrow}^\dagger r_{\downarrow\uparrow} \right) V_L^y + \left(t_{\downarrow\uparrow}'^\dagger t'_{\uparrow\downarrow} + t_{\uparrow\downarrow}'^\dagger t'_{\downarrow\uparrow} \right) V_R^y \right] \ . \tag{4.47}$$

With this expression we close the subsection giving a way to probe the spin current in the left lead in order to find the spin-dependent conductance for different spin and charge biases applied. The same calculation for the right lead is straightforward and is used in the next subsection as we discuss the appearance of the spin torque related to the spin-flip processes in transport calculations.

4.3.1 Spin Torque in the nanowire

In the previous section we derived the spin current on the left lead, far away from the impurity, due to the presence of Rashba spin-orbit coupling. However, close to the impurity we can no longer assume continuity of the spin-density and Eq.(4.32) presents a source term,

$$\frac{\partial S^y}{\partial t} + \partial_x j_x^y = T\left(x\right) \ . \tag{4.48}$$

the right hand side is a torque term $T\left(x\right) = T_0\delta\left(x - x_{imp}\right)$ due to the presence of the impurity. By integrating the expression for the spin-current for the static problem ($\frac{\partial S^y}{\partial t} = 0$) around the position of the impurity,

$$T_0 = \int_{x_{imp}-\epsilon}^{x_{imp}+\epsilon} \left(\partial_x j_x^y\right) dx = -\left\langle I_R^y\right\rangle - \left\langle I_L^y\right\rangle \ . \tag{4.49}$$

the expression for the spin current on the right side of the impurity $x_{imp} + \epsilon$ corresponds to a current traveling from left to right, implying a negative sign.

Then, we need to calculate the expression for the average of the spin-current on the right lead from Eq.(4.40) where the indexes for the L lead have been substituted with L indexes. This implies a change of the scattering coefficients involved (t instead of t' and r' instead of r),

$$\left\langle I_R^s\right\rangle = \frac{\mathrm{e}^2}{2\pi\hbar}\left[T_\uparrow V_{R\to L}^{\uparrow} - T_\downarrow V_{R\to L}^{\downarrow} + \left(r_{\downarrow\uparrow}'^{\dagger} r_{\uparrow\downarrow}' + r_{\uparrow\downarrow}'^{\dagger} r_{\downarrow\uparrow}'\right) V_R^y + \left(t_{\downarrow\uparrow}^{\dagger} t_{\uparrow\downarrow} + t_{\uparrow\downarrow}^{\dagger} t_{\downarrow\uparrow}\right) V_L^y\right] \ , \tag{4.50}$$

where $V_{R\to L}^{\uparrow,\downarrow} = -V_{L\to R}^{\uparrow,\downarrow}$. So that the Eq.(4.49) for the torque in combination with the results of Eq.(4.47) and Eq.(4.50) becomes,

$$\begin{aligned} T_0 = -\frac{\mathrm{e}^2}{2\pi\hbar}\Big[&\left(t_{\downarrow\uparrow}^{\dagger} t_{\uparrow\downarrow} + t_{\uparrow\downarrow}^{\dagger} t_{\downarrow\uparrow} + r_{\downarrow\uparrow}^{\dagger} r_{\uparrow\downarrow} + r_{\uparrow\downarrow}^{\dagger} r_{\downarrow\uparrow}\right) V_L^y \\ &+ \left(t_{\downarrow\uparrow}'^{\dagger} t_{\uparrow\downarrow}' + t_{\uparrow\downarrow}'^{\dagger} t_{\downarrow\uparrow}' + r_{\downarrow\uparrow}'^{\dagger} r_{\uparrow\downarrow}' + r_{\uparrow\downarrow}'^{\dagger} r_{\downarrow\uparrow}'\right) V_R^y\Big] \ . \end{aligned} \tag{4.51}$$

As a result evidence by Eq.(4.51), applying a spin-bias on either the right or left lead generates a spin-orbit torque expressed here as a function of the scattering coefficients related to spin-flip processes mediated by the impurity. In the result section of Chapter 6 we discuss fully the importance of this result.

4.3.2 Relation the spin-mixing conductance

The mixing conductance is a concept of great importance for transport between noncollinear ferromagnets and is responsible for the spin rotation around the magnetization axis of the ferromagnet [108]. This quantity is itnroduced as a way to highlight the fact that scattering mixes the two components in a spinor and one must not see spin species as independent. In order to show this, they propose a toy model where an electron incides in the scatterer from the right, $\psi_i \mathrm{e}^{-ii k_x x}$ and is reflected onto the right side of the scatterer as $\psi_f \mathrm{e}^{-ii k_x x}$. Both the incident and the final state are related through the scattering matrix and contribute to the spin current as shown in the Landauer-Bütiker expression of Eq.(4.39),

$$j_\alpha^{(S)} = \frac{\hbar}{2} v_x \left(\psi_i^* \hat{\sigma}_\alpha \psi_i - \psi_f^* \hat{\sigma}_\alpha \psi_f \right) \ , \tag{4.52}$$

with final states given by

$$\psi_f = \begin{pmatrix} r_\odot & 0 \\ 0 & r_\otimes \end{pmatrix} \psi_i \ , \tag{4.53}$$

substituting the spinors polarized in the x, y-directions and integrating over energy we obtain the spin currents:

$$I_x^S \approx (\mathrm{Re}\, G_{\uparrow\downarrow} V_R^x + \mathrm{Im}\, G_{\uparrow\downarrow} V_R^y) \tag{4.54}$$

$$I_y^S \approx (\mathrm{Re}\, G_{\uparrow\downarrow} V_R^y + \mathrm{Im}\, G_{\uparrow\downarrow} V_R^x) \ , \tag{4.55}$$

where the complex conductance $G_{\uparrow\downarrow}$ is given by,

$$G_{\uparrow\downarrow} = G_0 \left(1 - r_\odot r_\otimes^* \right) \ . \tag{4.56}$$

We want to establish a comparison between the y-component of the spin current in Eq.(4.55) to our previous result for the spin current on the right side of the scatterer as described by Eq.(4.50). First, in this toy model there appears to be spin bias only on the right side of the scatterer, hence $V_L^y = 0$ in Eq.(4.50). In the toy model the only process considered is the reflection, resultin in $T_\uparrow = T_\downarrow = 0$, one must remember that these transmission amplitudes include both spin-conserved and spin-flip transmission processes. By this account, the expression in Eq.(4.50)

becomes for the toy-model where a spin bias is applied on the right side of the scatterer

$$\langle I_R^s \rangle = \frac{\mathrm{e}^2}{2\pi\hbar}\left(r'^{\dagger}_{\downarrow\uparrow} r'_{\uparrow\downarrow} + r'^{\dagger}_{\uparrow\downarrow} r'_{\downarrow\uparrow}\right) V_R^y \,. \tag{4.57}$$

Nazaroz writes his scattering matrix in the basis of the $\hat{\sigma}_z$ matrix,

$$\hat{S} = |\uparrow_z\rangle\langle\uparrow_z|\hat{S}_{\odot} + |\downarrow_z\rangle\langle\downarrow_z|\hat{S}_{\otimes} \,, \tag{4.58}$$

but when we calculate our S-matrix in Chapter 5 it will be in the basis of $\hat{\sigma}_y$. So, by writing the scattering matrix in Eq.(4.58) in our basis,

$$\hat{S} = \frac{1}{2}\left[(\hat{S}_{\odot} + \hat{S}_{\otimes})(|\uparrow_y\rangle\langle\uparrow_y| + |\downarrow_y\rangle\langle\downarrow_y|) + (\hat{S}_{\odot} - \hat{S}_{\otimes})(|\uparrow_y\rangle\langle\downarrow_y| + |\downarrow_y\rangle\langle\uparrow_y|)\right] \,. \tag{4.59}$$

From Eq.4.59 we can write the reflexion matrix as,

$$\hat{r}' = \frac{1}{2}\left(\begin{array}{c|c} r_{\odot} + r_{\otimes} & r_{\odot} - r_{\otimes} \\ r_{\odot} - r_{\otimes} & r_{\odot} + r_{\otimes} \end{array}\right) \,. \tag{4.60}$$

The out-of-diagonal elements in Eq.(4.60) are the $r'_{\uparrow\downarrow}$ and $r'_{\downarrow\uparrow}$ in Eq. (4.57). This equation written in the language of $r_{\odot}$ and $r_{\otimes}$ becomes,

$$\begin{aligned}
\langle I_R^s \rangle &= \frac{\mathrm{e}^2}{2\pi\hbar}\frac{1}{4}\left[2(r_{\odot} - r_{\otimes})^{\dagger}(r_{\odot} - r_{\otimes})\right] V_R^y \\
&= \frac{\mathrm{e}^2}{2\pi\hbar}\frac{1}{2}\left[r_{\odot}^{\dagger} r_{\odot} + r_{\otimes}^{\dagger} r_{\otimes} - r_{\odot}^{\dagger} r_{\otimes} - r_{\otimes}^{\dagger} r_{\odot}\right] V_R^y \\
&= \frac{\mathrm{e}^2}{2\pi\hbar}\frac{1}{4}\left[2 - 2\,\mathrm{Re}(r_{\otimes}^{\dagger} r_{\odot})\right] V_R^y \\
&= \frac{\mathrm{e}^2}{2\pi\hbar}\,\mathrm{Re}(1 - r_{\otimes}^{\dagger} r_{\odot}) V_R^y \,.
\end{aligned} \tag{4.61}$$

If we consider no spin-bias for the polarization along x-direction, $V_R^x = 0$, it is pretty clear that we recover Eq.(4.55) in Eq. (4.61). We see then that even in the absence of the traditional conductance $T_{\uparrow} = T_{\downarrow} = 0$, we recover some mixing conductance on the right side of the impurity. This means that the spin current flows even in the absence of charge transport.

4.4 Conclusions

In summary, in this chapter we extend the Landauer-Büttiker formalis to include the effect of the spin-orbit coupling for the description of the

transport properties of a nanowire. We derive an expression for the spin current polarized along y-direction in the left lead to be far away from the impurity. This expression, Eq.(4.47), is the highlight of this chapter. It allows us to express such a spin current as a function of the scattering coefficients of the S-matrix making it easy to track the contributions to the spin current from the different voltage and spin-biases. In combination with the expression for the spin current on the right lead, Eq.(4.50), allows us to describe a torque that arises at the impurity position, as a consequence of the spin-flip transport mechanisms resulting from the Rashba spin-orbit coupling. This mechanism will have important consequence on the conductance as it is discussed in subsequent chapters. Furthermore, we are able to make a connection between our expressions and those obtained in the context of the spin-mixing conductance in magnetic hybrid structures. So far we have expressed all transport properties in terms of the scattering coefficients. In the next chapter we determine such coefficients for the scattering from an impurity in a nanowire in the presence of Rashba spin-orbit coupling.

Chapter 5

Scattering Matrix Coefficients in a nanowire

In previous chapters we introduced all the necessary ingredients to address the transport properties of a nanowire with spin-orbit coupling in the presence of an impurity. In this chapter we determine the scattering coefficients from a short-range, delta- like impurity in a quasi-1D system, namely a Rashba nanowire where electrons propagate freely along x and are confined in the y direction. For this sake we use the Lippmann-Schwinger approach addressed in Chapter 2. From the knowledge of the scattering matrix coefficients we can analyse different aspects of the charge and spin transport in nanowires by using the Landauer-Büttiker formalism introduced in the previous chapter 4.

The main difficulty in dealing with a system with a confinement and spin-orbit coupling can be understand already from the model Hamiltonian for a wire parallel to the x-axis, and a finite Rashba spin-orbit interaction:

$$\begin{aligned} H^{\text{wire}} &= \frac{p_x^2 + p_y^2}{2m_e^*} + \frac{m_e^* \omega_0^2}{2} y^2 + H_{\text{SO}} \ , \\ H_{\text{SO}} &= \alpha \left(p_x \sigma_y - p_y \sigma_x \right) \ , \end{aligned} \tag{5.1}$$

As discussed in Chapter 3, the momentum p_x in Eq. (5.1) is a conserved quantity as the electron moves ballistically in the x-direction (and can be written as $p_x = \hbar k_x$). The term $p_x \sigma_y$ in H_{SO} leads to a splitting of the spectrum branches, by shifting them differently depending on the spin. In other words there is a lifting of the spin-degeneracy. In addition, the

harmonic confinement in Eq. (5.1) combined with the term $-p_y\sigma_x$ of the Rashba interaction deforms the branches of the spectrum so that subbands with opposite spin and different label avoid crossings (see Fig. 3.5). This phenomenon arises from subband mixing, breaking down the spin-momentum locking of in-plane spin in a way that makes the spin no longer a good quantum number. Also the term $-p_y\sigma_x$ of the Rashba interaction is a problem in the exact analytical treatment of the nanowire. Nevertheless the problem can be addressed in different limiting cases and in a number of ways. Usually the mixing of subbands is treated perturbatively [19, 21, 22] or included in a numerical treatment [20, 112]. Here we focus on the weak spin-orbit interaction case, and use perturbation theory. We already introduced the solutions for the $k_x = 0$ and surroundings in a perturbative way in subsections 3.4.1 and 3.4.2. In this approach we treated the mixing of subbands $\alpha p_y\hat{\sigma}_x$ exactly, while considering $\alpha p_x\hat{\sigma}_y$. The insight gained from this approach will be of help in the next section where we take a perturbative approach where $\alpha p_y\hat{\sigma}_x$ is considered as the perturbation instead. The starting point of our analysis is the Schrieffer-Wolff transformation [113], a unitary transformation which diagonalizes the Hamiltonian to first order in the Rashba interaction. In such a way we obtain an effective low-energy model Hamiltonian which simplifies considerably the problem, but nevertheless catches interesting physics.

5.1 The Schrieffer-Wolff transformation: effective model Hamiltonian

The Schrieffer-Wolff transformation, transforms a Hamiltonian $\mathcal{H} = H + V$, into a diagonal one, up to the desired order of perturbation in the V potential. If we denote with M the generator of the transformation, such that $\tilde{\mathcal{H}} = \mathrm{e}^{M}\mathcal{H}\mathrm{e}^{-M}$, we can expand the exponentials with help of the Baker-Campbell-Haussdorff formula such that the effective Hamiltonian can be formally be written as

$$\tilde{\mathcal{H}} = \mathcal{H} + [M, \mathcal{H}] + \frac{1}{2}[M, [M, \mathcal{H}]] + \dots . \tag{5.2}$$

One writes the Hamiltonian as $\mathcal{H} = H + V$, being V the perturbation potential, such that Eq. (5.2) reads,

$$\tilde{\mathcal{H}} = H + V + [M, H] + [M, V] + \frac{1}{2}[M, [M, H]] + \frac{1}{2}[M, [M, V]] + \dots , \tag{5.3}$$

The goal now is to find a transformation which removes the off-diagonal terms up to first order. For this the following condition needs to be satisfied,

$$V + [M, H] = 0 \, . \tag{5.4}$$

Using this condition Eq. (5.3) results in ,

$$\tilde{\mathcal{H}} = H + \frac{1}{2}[M, V] + \mathcal{O}\left(V^3\right) \, . \tag{5.5}$$

We now apply the above transformation to our Hamiltonian, Eq. (5.1). Taking into account the different effects and scales that are going to come in play it is convenient to rewrite the Hamiltonian as the sum of three contributions:

$$H^{\text{wire}} = H_0 + H_{\text{x}} + H_{\text{mix}} \, , \tag{5.6}$$

with

$$H_0 = \frac{p_x^2 + p_y^2}{2m_e^*} + \frac{m_e^* \omega_0^2}{2} y^2 \, , \tag{5.7}$$

$$H_{\text{x}} = \alpha_x p_x \sigma_y \, , \tag{5.8}$$

$$H_{\text{mix}} = -\alpha_y p_y \sigma_x \, . \tag{5.9}$$

In this way we separate the term responsible for the subbands mixing, Eq. (5.9), from the rest. This term is considered as the perturbation potential , i.e. $H_{\text{mix}} = V$ in Eq. (5.2). Thus, the condition Eq. (5.4) which needs to be satisfied when performing the Schrieffer-Wolff transformation is:

$$H_{\text{mix}} + [M, H_0 + H_{\text{x}}] = 0 \implies [H_0 + H_{\text{x}}, M] = H_{\text{mix}} \, . \tag{5.10}$$

In the next section we show how to find an explicit expression for the generator M. Once it is found, the Hamiltonian can then be projected to any subspace accurately as long as the strength of H_{mix} is much smaller than the energy difference between subspaces [114].

Transformation operator

In order to obtain the transformation operator M we will follow a similar method to the one described in Refs. [115, 116] for a quantum point contact with both Rashba and Dresselhaus spin-orbit coupling and a Zeeman field.

To satisfy the condition Eq. (5.10), the operator M can be formally written as

$$M = \frac{1}{L_0 + L_{\rm x}} H_{\rm mix} = \frac{1}{L_0} \sum_{m=0}^{\infty} \big(-L_{\rm x} \frac{1}{L_0}\big)^m H_{\rm mix} \ , \tag{5.11}$$

where L is the Liouville superoperator for a given Hamiltonian defined by $L\hat{A} \equiv [H, \hat{A}]$. For a harmonic confinement $V_{conf}(y) = \frac{1}{2} m_e^* \omega_0^2 y^2$, we have

$$\begin{aligned} \frac{1}{L_0} y &= \frac{-i}{\hbar m_e^* \omega_0^2} p_y \ , \\ \frac{1}{L_0} p_y &= \mathrm{i} \frac{m_e^*}{\hbar} y \ , \end{aligned} \tag{5.12}$$

which allows us to obtain the generator for the transformation M

$$M = -\mathrm{i}\alpha_y \frac{(\hbar\omega_0)^2}{(\hbar\omega_0)^2 - (2\alpha_x p_x)^2} \left[\frac{m_e^*}{\hbar} (y \cdot \hat{\sigma}_x) + \frac{2\alpha_x p_x}{(\hbar\omega_0)^2} (p_y \cdot \hat{\sigma}_z) \right] \ , \tag{5.13}$$

as long as $2\alpha_x p_x / \hbar\omega_0 < 1$. Moreover, besides this condition also $2\alpha_x p_x / \hbar\omega_0 \ll 1$ has to be fulfilled, as we are expanding in the small parameter

$$\frac{\lambda_y}{\lambda_{SO}} \ll 1,$$

with $\lambda_{SO} = \hbar / m_e^* \alpha_x$. This small parameter ensures that one focuse on energies away from the anticrossing points which ocurr between subbands of indices n and m at $2\alpha_x (\hbar k_x) = \pm \hbar\omega_0 |m - n|$. It is important to bear in mind that for the previous analysis we use the fact that translational symmetry in the x-direction, ensures $p_x = \hbar k_x$ to be good quantum number.

The energies that we are interested in are those close to the edge of the next subband, so $p_x \sim \hbar/\lambda_y$, then $2\alpha_x p_x / \hbar\omega_0 \sim \lambda_y / \lambda_{SO} \implies 2\alpha_x p_x \ll \hbar\omega_0$, and we can write the final expression for the Schrieffer-Wolff transformation matrix as:

$$M = -\mathrm{i}\alpha_y \left[\frac{m_e^*}{\hbar} (y \cdot \hat{\sigma}_x) + \frac{2\alpha_x p_x}{(\hbar\omega_0)^2} (p_y \cdot \hat{\sigma}_z) \right] \ . \tag{5.14}$$

We can now write the effective Hamiltonian of the system as follows:

$$\tilde{H} = \frac{p_x^2 + p_y^2}{2m_e^*} + \frac{1}{2} m_e^* \omega_0^2 y^2 + \alpha_x p_x \hat{\sigma}_y - \frac{m_e^* \alpha_y^2}{2} + \tilde{V}_{\rm imp} \ , \tag{5.15}$$

with a small shift down in the spectrum by an amount $m_e^*\alpha_y^2/2$. The transformed impurity potential reads:

$$\tilde{V}_{\rm imp} = V_{\rm imp} + [M, V_{\rm imp}] = V_{\rm imp} + 2{\rm i}\Big(\frac{\alpha_x\alpha_y}{\omega_0^2}\Big)[\partial_x\partial_y, V_{\rm imp}]\cdot\sigma_z \ , \tag{5.16}$$

since $[y, V_{\rm imp}] = 0$. As we see, after the transformation the impurity potential acquires a small contribution with a spin structure in the form of σ_z in spite of it being assumed as a non-magnetic impurity. The presence of the derivatives is on itself a complicated issue as they would act on the states of the Lippmann-Schwinger. We will address this problem in the next section of the chapter. Before this we focus on how the above transformation modifies the wave functions by performing a step by step analysis.

Transformation of the states

A way of undertanding the Schrieffer-Wolff transformation is to focus on the states. The states can be obtained in two consecutive unitary transformations: first, a standard gauge transformation along y, and then a rotation in spin space such that σ_y becomes diagonal.

Our starting point is our original Hamiltonian Eq. (5.1)

$$H^{\rm wire} = \frac{p_x^2 + p_y^2}{2m_e^*} + \frac{m_e^*\omega_0^2}{2}y^2 + \alpha_x p_x\sigma_y - \alpha_y p_y\sigma_x \ . \tag{5.17}$$

Clearly, we can write the states as

$$\Psi_{k_x n}(x,y) = \frac{1}{\sqrt{L}}e^{ik_x x}\psi_{k_x n}(y) \ , \tag{5.18}$$

where n is a subband index. The procedure by which bands are labeled is not clear from the beginning, and in the best case one hopes to map the problem onto a simple one with independent bands. However, this is not working when avoided crossing occur. In such a case, one obtains transcendental equations which set the rules for labelling bands. In other words, it can happen that the only quantum number is the energy and by solving for energy levels one introduces a band index (principal quantum number) through a procedure that is not analytic. This is exactly what we avoid by the transformation below that allows for a clean label band label.

For the state $\psi_{k_x n}(y)$ in Eq. (5.18) we write further

$$\psi_{k_x n}(y) = e^{i\sigma_x y/\lambda_{\rm SO}} \tilde{\psi}_{k_x n}(y) \ , \tag{5.19}$$

which is the gauge along y. Here, we define $\lambda_{\rm SO} = \hbar/m_e^* \alpha_y$. We can recognize this as the transformation discussed in subsection 3.4.2. In this subsection we realized that corrections to the states of order $\alpha_x \alpha_y$ are not affecting the scattering potential as this gauge factor commutes with said potential. Note that this second step is interchangeable with the first one, because the two exponential factors commute.

After these two steps, the effective Hamiltonian becomes

$$\begin{aligned} H^{\rm wire} &= \frac{p_y^2}{2m_e^*} + \frac{m_e^* \omega_0^2}{2} y^2 \\ &\quad + \alpha_x \hbar k_x \left[\sigma_y \cos\left(\frac{2y}{\lambda_{\rm SO}}\right) + \sigma_z \sin\left(\frac{2y}{\lambda_{\rm SO}}\right) \right] \qquad (5.20) \\ &\quad + \frac{\hbar^2 k_x^2}{2m_e^*} - \frac{m_e^* \alpha_y^2}{2} \ , \qquad (5.21) \end{aligned}$$

which can be written more compactly:

$$H^{\rm wire} = \frac{p_y^2}{2m_e^*} + \frac{m_e^* \omega_0^2}{2} y^2 + \alpha_x \hbar k_x \sigma_y e^{-i\frac{2y}{\lambda_{\rm SO}}\sigma_x} + \frac{\hbar^2 k_x^2}{2m_e^*} - \frac{m_e^* \alpha_y^2}{2} \ . \tag{5.22}$$

Next we rotate in the spin space such that σ_y transforms into σ_z. This is achieved by the transformation:

$$\tilde{\psi}_{k_x n}(y) = e^{i\sigma_x \pi/4} \bar{\psi}_{k_x n}(y) \ . \tag{5.23}$$

The effective Hamiltonian becomes

$$\begin{aligned} H^{\rm wire} &= \frac{p_y^2}{2m_e^*} + \frac{m_e^* \omega_0^2}{2} y^2 \\ &\quad + \alpha_x \hbar k_x \left[-\sigma_y \sin\left(\frac{2y}{\lambda_{\rm SO}}\right) + \sigma_z \cos\left(\frac{2y}{\lambda_{\rm SO}}\right) \right] \\ &\quad + \frac{\hbar^2 k_x^2}{2m_e^*} - \frac{m_e^* \alpha_y^2}{2}. \qquad (5.24) \end{aligned}$$

If further we take the diagonal matrix element $n = n'$, then we obtain the renormalized α_n by the form factor $\mathcal{F}_n$, which arises here from the cosine

term. At the same time, the sine term drops out, since it has only off-diagonal matrix elements, i.e. it admixes excited subbands. We expand that latter Hamiltonian up to order α^2,

$$\begin{aligned} H^{\text{wire}} &= \frac{p_y^2}{2m_e^*} + \frac{m_e^*\omega_0^2}{2}y^2 + \alpha_x\hbar k_x\sigma_z \\ &\quad -2m_e^*\alpha_x\alpha_y k_x\sigma_y y + \frac{\hbar^2 k_x^2}{2m_e^*} - \frac{m_e^*\alpha_y^2}{2} \ , \end{aligned} \tag{5.25}$$

and re-write it as follows

$$\begin{aligned} H^{\text{wire}} &= \frac{p_y^2}{2m_e^*} + \frac{m_e^*\omega_0^2}{2}\left(y - \frac{2\alpha_x\alpha_y}{\omega_0^2}k_x\sigma_y\right)^2 + \alpha_x\hbar k_x\sigma_z \\ &\quad +\frac{\hbar^2 k_x^2}{2m_e^*} - \frac{m_e^*\alpha_y^2}{2} - \frac{2m_e^*\alpha_x^2\alpha_y^2}{\omega_0^2}k_x^2 \ . \end{aligned} \tag{5.26}$$

The shift in the harmonic oscillator center can be gauged away in a similar way as the linear in momentum terms of the spin-orbit interaction, which also could be interpreted as a shift of the kinetic energy central position as a function of momentum. The next transformation has the form

$$\tilde{\psi}_{k_x n}(y) = e^{-i\sigma_y p_y y_0/\hbar}\bar{\psi}_{k_x n}(y) \ , \tag{5.27}$$

where $p_y = -i\hbar\partial_y$ and

$$y_0 = \frac{2\alpha_x\alpha_y}{\omega_0^2}k_x \ . \tag{5.28}$$

After this transformation the Hamiltonian reads

$$\begin{aligned} H^{\text{wire}} &= \frac{p_y^2}{2m_e^*} + \frac{m_e^*\omega_0^2}{2}y^2 \\ &\quad +\alpha_x\hbar k_x\left[\sigma_z\cos\left(\frac{2p_y y_0}{\hbar}\right) - \sigma_x\sin\left(\frac{2p_y y_0}{\hbar}\right)\right] \\ &\quad +\frac{\hbar^2 k_x^2}{2m_e^*} - \frac{m_e^*\alpha_y^2}{2} - \frac{2m_e^*\alpha_x^2\alpha_y^2}{\omega_0^2}k_x^2 \ . \end{aligned} \tag{5.29}$$

The last term is of fourth order in α and can be omitted, because we are accurate only to the second order. Similarly the cosine and sine contain y_0

which is proportional to α^2 and there is another α in front of the whole term. As a result, we obtain, up to order α^2, the final effective Hamiltonian

$$\begin{aligned} H^{\text{wire}} &= \frac{p_y^2}{2m_e^*} + \frac{m_e^*\omega_0^2}{2}y^2 + \alpha_x \hbar k_x \sigma_z \\ &\quad + \frac{\hbar^2 k_x^2}{2m_e^*} - \frac{m_e^*\alpha_y^2}{2} \ . \end{aligned} \tag{5.30}$$

This Hamiltonian is rather simple. It can be solved analytically and the corresponding Green's function can be written straightaway, as we will see in the next sections. The eigenfunctions can be the written by summarizing up the above transformations:

$$\Psi_{k_x n}(x,y) = e^{i\sigma_x\left(\frac{m_e^*\alpha_y}{\hbar}y+\frac{\pi}{4}\right)}\ e^{-i\sigma_y\frac{2\alpha_x\alpha_y}{\hbar^2\omega_0^2}p_x p_y}\frac{1}{\sqrt{L}}e^{ik_x x}\Phi_n(y)\ , \tag{5.31}$$

where we restored $\hbar k_x \to p_x$ in the second factor. We can also restore $\hbar k_x \to p_x$ in Eq. (5.30), since the Hamiltonian is diagonal in the quantum number k_x. The lateral wavefunctions $\Phi_n(y)$ for a harmonic confinement are given by Eq.(2.30) as discussed in Chapter 2.

5.2 Scattering states

We now follow the procedure described in Chapter 2 to obtain the scattering states for the effective system of a multiband quasi-1D nanowire in the presence of Rashba interaction. We focus first on the Green's functions corresponding to the effective Hamiltonian Eq.(5.30). The Green's function is a sum of Green's functions of the independent sub-bands,

$$G(\boldsymbol{r},\boldsymbol{r}') = \sum_n \Phi_n(y)\Phi_n^*(y')G_n(x,x')\ . \tag{5.32}$$

This expression implies separation of variables for the channel without impurity. In our case, we take out the spin degree of freedom into a matrix structure,

$$\hat{G}(\boldsymbol{r},\boldsymbol{r}') = \sum_{n\sigma} \Phi_n(y)\Phi_n^*(y')\left|\sigma\right\rangle\left\langle\sigma\right| G_{n\sigma}(x,x')\ . \tag{5.33}$$

The Green's function for each individual channel is given by

$$G_{n\sigma_y}(x,x') = \frac{2m_e^*}{\hbar^2}\frac{i}{2k_n}e^{ik_n|x-x'|}e^{-i\sigma_y\frac{m_e^*\alpha_x}{\hbar}(x-x')}\ , \tag{5.34}$$

where

$$k_n = \frac{1}{\hbar}\sqrt{2m_e^*\left[E - \epsilon_n + \frac{m_e^*\left(\alpha_x^2 + \alpha_y^2\right)}{2}\right]} \,. \tag{5.35}$$

For what follows it is convenient to write these Green's functions as follows,

$$G_{n\sigma_y}(x,x') = g_{n\sigma_y}\begin{cases} u_{n\sigma_y}(x)u^*_{n\sigma_y}(x') \,, & x > x' \,, \\ v_{n\sigma_y}(x)v^*_{n\sigma_y}(x') \,, & x < x' \,, \end{cases} \tag{5.36}$$

where

$$u_{n\sigma_y}(x) = \sqrt{\frac{m_e^*}{\hbar k_n}}e^{ik_n x}e^{-i\sigma_y\frac{m_e^*\alpha_x}{\hbar}x} \,, \tag{5.37}$$

$$v_{n\sigma_y}(x) = \sqrt{\frac{m_e^*}{\hbar k_n}}e^{-ik_n x}e^{-i\sigma_y\frac{m_e^*\alpha_x}{\hbar}x} \,. \tag{5.38}$$

These functions are normalized to carry unit flux density. With such a normalization, we have the common factor to be

$$g_{n\sigma_y} = \frac{i}{\hbar} \,. \tag{5.39}$$

The state $u_{n\sigma_y}(x)$ is the outgoing state on the right side of the impurity($x > x'$ or $x \to +\infty$). It is a right mover and we shall choose this state also as an incident state from the left, $\Phi_L(x) = u_{n\sigma_y}(x)$. Similarly, the state $v_{n\sigma_y}(x)$ is the outgoing state on the left side of the source ($x < x'$ or $x \to -\infty$). It is a left mover and we shall choose this state also as an incident state from the right, $\Phi_R(x) = v_{n\sigma_y}(x)$.

The Lippmann-Schwinger equation after the Schrieffer-Wolff transformation reads:

$$\Psi(\boldsymbol{r}) = \Phi(\boldsymbol{r}) - \int \hat{G}(\boldsymbol{r},\boldsymbol{r}')e^{M}V_{\rm imp}(\boldsymbol{r}')e^{-M}\Psi(\boldsymbol{r}')d^2r' \,, \tag{5.40}$$

where we explicitly write the transformed $\hat{V}_{\rm imp}(\boldsymbol{r}')$. Notice that in the basis Eq. (5.36), the incoming state $\Phi(\boldsymbol{r})$ can be written as

$$\Phi^L_{n\sigma}(x,y) = u_{n\sigma}(x)\Phi_n(y)\left|\sigma\right\rangle \,, \tag{5.41}$$

for incident from the left, and similarly

$$\Phi^R_{n\sigma}(x,y) = v_{n\sigma}(x)\Phi_n(y)\left|\sigma\right\rangle \,, \tag{5.42}$$

for incident from the right. Because of the small support of $V_{\rm imp}(\boldsymbol{r'})$, the exponents get projected on a state with $\boldsymbol{r'} = \boldsymbol{r}_0$, and effectively behaves as a delta-like function. After introducing the dimensionless projector

$$|\boldsymbol{r}_0\rangle \langle \boldsymbol{r}_0| \ , \tag{5.43}$$

we obtain from Eq. (5.40) in the limit of a point-like scatterer,

$$\Psi(\boldsymbol{r}) = \Phi(\boldsymbol{r}) - v_0 e^{M(\boldsymbol{r_0})} \hat{G}(\boldsymbol{r}, \boldsymbol{r}_0) \, |\boldsymbol{r}_0\rangle \langle \boldsymbol{r}_0| \, e^{-M(\boldsymbol{r_0})} \Psi(\boldsymbol{r}_0) \ . \tag{5.44}$$

By expanding the exponential functions and using Eq. (5.14) we obtain:

$$\begin{aligned} \Psi(\boldsymbol{r}) &= \Phi(\boldsymbol{r}) - v_0 \\ &\times \left\{ \hat{G}(\boldsymbol{r}, \boldsymbol{r}_0) + \frac{2i\alpha_x\alpha_y}{\omega_0^2} \left[\partial_{x_0} \partial_{y_0} \hat{G}(\boldsymbol{r}, \boldsymbol{r}_0) \right] \hat{\sigma}_z \right\} \\ &\times \left\{ \Psi(\boldsymbol{r}_0) - \frac{2i\alpha_x\alpha_y}{\omega_0^2} \hat{\sigma}_z \left[\partial_{x_0} \partial_{y_0} \Psi(\boldsymbol{r}_0) \right] \right\} \ . \end{aligned} \tag{5.45}$$

In order to determine the wave function $e^{-S}\Psi(\boldsymbol{r})$ at position $\boldsymbol{r} = \boldsymbol{r}_0$, we act with e^{-S} on the Lippmann-Schwinger equation

$$e^{-S}\Psi(\boldsymbol{r}) = e^{-S}\Phi(\boldsymbol{r}) - \int e^{-S} \hat{G}(\boldsymbol{r}, \boldsymbol{r'}) e^{S} V_{\rm imp}(\boldsymbol{r'}) e^{-S} \Psi(\boldsymbol{r'}) d^2 r' \ , \tag{5.46}$$

and set $\boldsymbol{r} = \boldsymbol{r}_0$:

$$\left[\mathbb{1} + \int e^{-S} \hat{G}(\boldsymbol{r}_0, \boldsymbol{r'}) e^{M} V_{\rm imp}(\boldsymbol{r'}) d^2 r' \right] e^{-S} \Psi(\boldsymbol{r}_0) = e^{-M} \Phi(\boldsymbol{r}_0) \ . \tag{5.47}$$

The contribution of evanescent states to the sum over n in the Green's function diverges if we simply set $\boldsymbol{r'} = \boldsymbol{r}_0$ for a δ-like $V_{\rm imp}(\boldsymbol{r'})$. However, we can do that for the propagating states and this is the reason why one can take the term $e^{-M}\Psi$ out of the integrand.

The bound states are determined by the condition:

$$\det \left[\mathbb{1} + \int e^{-S} \hat{G}(\boldsymbol{r}_0, \boldsymbol{r'}) e^{S} V_{\rm imp}(\boldsymbol{r'}) d^2 r' \right] = 0 \ . \tag{5.48}$$

The expression $e^{-S}\hat{G}(\boldsymbol{r}_0, \boldsymbol{r'})e^{S}$ represents the exact Green's function of the channel (without impurity). However our treatment is perturbative in the

spin-orbit interaction, and thefore:

$$\begin{aligned} e^{-S}\hat{G}(\boldsymbol{r},\boldsymbol{r}')e^{S} &\approx \hat{G}(\boldsymbol{r},\boldsymbol{r}') \\ &+\frac{2i\alpha_x\alpha_y}{\omega_0^2}\left[\partial_{x'}\partial_{y'}\hat{G}(\boldsymbol{r},\boldsymbol{r}')\right]\hat{\sigma}_z \\ &-\frac{2i\alpha_x\alpha_y}{\omega_0^2}\hat{\sigma}_z\left[\partial_x\partial_y\hat{G}(\boldsymbol{r},\boldsymbol{r}')\right]+\dots\ . \end{aligned} \tag{5.49}$$

To attain unitarity of the scattering matrix, additional (overcounting) terms might be necessary, as explained in the next section.

Notice that the Green's function is diagonal in the basis of σ_y,

$$\begin{aligned} |+\rangle &= \frac{1}{\sqrt{2}}\begin{pmatrix} 1 \\ i \end{pmatrix}, \\ |-\rangle &= \frac{1}{\sqrt{2}}\begin{pmatrix} 1 \\ -i \end{pmatrix}\ , \end{aligned} \tag{5.50}$$

and therefore σ_z reads.

$$\hat{\sigma}_z = |+\rangle\langle -| + |-\rangle\langle +|\ . \tag{5.51}$$

In this basis the Green's function is a diagonal 2×2 matrix

$$\hat{G}(\boldsymbol{r},\boldsymbol{r}') = \begin{pmatrix} G_{++} & 0 \\ 0 & G_{--} \end{pmatrix}\ , \tag{5.52}$$

where $G_{\pm\pm}$ is the Green's function projected onto the state with $\sigma_y = \pm 1$. We construct symmetric and antisymmetric combinations with respect to the change of sign of $x - x'$,

$$G_{\rm s} = \frac{G_{++}+G_{--}}{2} = \sum_{n\sigma}\Phi_n(y)\Phi_n^*(y')\frac{i\,m_e^*}{\hbar^2 k_n}e^{ik_n|x-x'|}\cos\left[\frac{m_e^*\alpha_x}{\hbar}(x-x')\right], \tag{5.53}$$

$$G_{\rm a} = \frac{G_{++}-G_{--}}{2} = \sum_{n\sigma}\Phi_n(y)\Phi_n^*(y')\frac{m_e^*}{\hbar^2 k_n}e^{ik_n|x-x'|}\sin\left[\frac{m_e^*\alpha_x}{\hbar}(x-x')\right] \tag{5.54}$$

Because of the translational invariance over x, the single band Green's function obeys

$$\partial_x G_{n\sigma}(x,x') = -\partial_{x'}G_{n\sigma}(x,x')\ . \tag{5.55}$$

This is also valid to the full Green's function $\hat{G}(\boldsymbol{r},\boldsymbol{r}')$, but only with respect to x and x'. Therefore, we can write Eq. 5.49 as

$$\begin{aligned} e^{-S}\hat{G}(\boldsymbol{r},\boldsymbol{r}')e^{S} &\approx \hat{G}(\boldsymbol{r},\boldsymbol{r}') \\ &\quad -\frac{2i\alpha_x\alpha_y}{\omega_0^2}\left[\partial_x\partial_{y'}\hat{G}(\boldsymbol{r},\boldsymbol{r}')\right]\hat{\sigma}_z \\ &\quad -\frac{2i\alpha_x\alpha_y}{\omega_0^2}\hat{\sigma}_z\left[\partial_x\partial_y\hat{G}(\boldsymbol{r},\boldsymbol{r}')\right] , \end{aligned} \tag{5.56}$$

or in a matrix form

$$e^{-S}\hat{G}(\boldsymbol{r},\boldsymbol{r}')e^{S} \approx \begin{pmatrix} G_{++} & -\frac{2i\alpha_x\alpha_y}{\omega_0^2}\partial_x\left(\partial_{y'}G_{++}+\partial_y G_{--}\right) \\ -\frac{2i\alpha_x\alpha_y}{\omega_0^2}\partial_x\left(\partial_{y'}G_{--}+\partial_y G_{++}\right) & G_{--} \end{pmatrix} . \tag{5.57}$$

The scatterer potential is assumed to be symmetric. In particular $V_{\rm imp}(\boldsymbol{r})$ has mirror symmetry with respect to $x\to -x$, where x is measured for this purpose with respect to x_0. Therefore, in Eq. (5.48) only the symmetric part of G contributes to integrals of the form

$$\int G_{++}(\boldsymbol{r}_0,\boldsymbol{r}')V_{\rm imp}(\boldsymbol{r}')d^2r' . \tag{5.58}$$

Notice that because G has a block structure in spin space, we can consider each block contribution to Eq. (5.48) independently. On the other hand he anti-symmetric part of G contributes to the integrals of the form

$$\int \left[\partial_x G_{++}(\boldsymbol{r},\boldsymbol{r}')\right]\big|_{\boldsymbol{r}=\boldsymbol{r}_0} V_{\rm imp}(\boldsymbol{r}')d^2r' , \tag{5.59}$$

only the anti-symmetric part of G enters. As a result, the matrix in Eq. (5.57) which enters in Eq. (5.48) can be written as

$$\begin{pmatrix} G_{\rm s} & -\frac{2i\alpha_x\alpha_y}{\omega_0^2}\partial_x\left(\partial_{y'}-\partial_y\right)G_{\rm a} \\ \frac{2i\alpha_x\alpha_y}{\omega_0^2}\partial_x\left(\partial_{y'}-\partial_y\right)G_{\rm a} & G_{\rm s} \end{pmatrix} . \tag{5.60}$$

We introduce the short notations:

$$\begin{aligned} \langle\!\langle G_{\rm s}\rangle\!\rangle &= \frac{1}{v_0}\int G_{\rm s}(\boldsymbol{r}_0,\boldsymbol{r}')V_{\rm imp}(\boldsymbol{r}')d^2r', \\ \left\langle\!\!\left\langle \partial^2 G_{\rm a}\right\rangle\!\!\right\rangle &= \frac{1}{v_0}\int \left[\partial_x\left(\partial_{y'}-\partial_y\right)G_{\rm a}(\boldsymbol{r},\boldsymbol{r}')\right]\big|_{\boldsymbol{r}=\boldsymbol{r}_0} V_{\rm imp}(\boldsymbol{r}')d^2r' . \end{aligned} \tag{5.61}$$

and rewrite Eq. (5.48) as

$$\det\left[\mathbb{1} + v_0 \left\langle\!\left\langle \hat{G} \right\rangle\!\right\rangle\right] = 0 \,, \tag{5.62}$$

where

$$\left\langle\!\left\langle \hat{G} \right\rangle\!\right\rangle = \begin{pmatrix} \langle\!\langle G_{\rm s} \rangle\!\rangle & -\frac{2i\alpha_x\alpha_y}{\omega_0^2} \langle\!\langle \partial^2 G_{\rm a} \rangle\!\rangle \\ \frac{2i\alpha_x\alpha_y}{\omega_0^2} \langle\!\langle \partial^2 G_{\rm a} \rangle\!\rangle & \langle\!\langle G_{\rm s} \rangle\!\rangle \end{pmatrix} \,. \tag{5.63}$$

Or explicitly

$$\left(1 + v_0 \langle\!\langle G_{\rm s} \rangle\!\rangle\right)^2 - \left(\frac{2\alpha_x\alpha_y v_0}{\omega_0^2}\right)^2 \left\langle\!\left\langle \partial^2 G_{\rm a} \right\rangle\!\right\rangle^2 = 0 \,. \tag{5.64}$$

This is the condition for bound states, which can be written also as

$$1 + v_0 \left(\langle\!\langle G_{\rm s} \rangle\!\rangle \pm \frac{2\alpha_x\alpha_y}{\omega_0^2} \left\langle\!\left\langle \partial^2 G_{\rm a} \right\rangle\!\right\rangle \right) = 0 \,. \tag{5.65}$$

According to the Kramers theorem, the two solutions obtained from this equation (for the $\pm$ sign) must be degenerate and therefore, $\langle\!\langle \partial^2 G_{\rm a} \rangle\!\rangle$ has to vanish at the leading order of our approximation (a rigorous proof is presented in Appendix A. Such that Eq. (5.47) results in

$$e^{-S}\Psi(\boldsymbol{r}_0) = \frac{1}{1 + v_0 \langle\!\langle G_{\rm s} \rangle\!\rangle} e^{-S}\Phi(\boldsymbol{r}_0) \,. \tag{5.66}$$

Inserting this result into Eq. (5.45) we finally obtain

$$\begin{aligned} \Psi(\boldsymbol{r}) &= \Phi(\boldsymbol{r}) - \frac{v_0}{1 + v_0 \langle\!\langle G_{\rm s} \rangle\!\rangle} \\ &\times \left\{ \hat{G}(\boldsymbol{r}, \boldsymbol{r}_0) + \frac{2i\alpha_x\alpha_y}{\omega_0^2} \left[\partial_{x_0}\partial_{y_0} \hat{G}(\boldsymbol{r}, \boldsymbol{r}_0) \right] \hat{\sigma}_z \right\} \\ &\times \left\{ \Phi(\boldsymbol{r}_0) - \frac{2i\alpha_x\alpha_y}{\omega_0^2} \hat{\sigma}_z \left[\partial_{x_0}\partial_{y_0} \Phi(\boldsymbol{r}_0) \right] \right\} \,. \end{aligned} \tag{5.67}$$

The scattering matrix

we can now calculate the scattering matrix. For this, we send a sate $\Phi^L_{n\sigma}(\boldsymbol{r})$ incident from the left and look at $x \to +\infty$. The Green's function at $x \to +\infty$ is

$$\hat{G}\left(\boldsymbol{r}, \boldsymbol{r}'\right) = \sum_{n\sigma} \Phi_n(y)\Phi^*_n(y') \left|\sigma\right\rangle \left\langle\sigma\right| g_{n\sigma} u_{n\sigma}(x) u^*_{n\sigma}(x') \,. \tag{5.68}$$

The transmission amplitude to scatter from left to right is found from

$$t^{RL}_{m\sigma',n\sigma} = \left.\frac{\delta\Psi(\boldsymbol{r})}{\delta\Phi^{L}_{m\sigma'}(\boldsymbol{r})}\right|_{\Phi(\boldsymbol{r})\to\Phi^{L}_{n\sigma}(\boldsymbol{r})} . \tag{5.69}$$

The final expression for the transmission is the obtained from Eqs(5.67-5.69). In the absence of scatterer, the transmission amplitude is unity

$$t^{RL}_{m\sigma',n\sigma} = \delta_{mn}\delta_{\sigma'\sigma} . \tag{5.70}$$

In the presence of a scatterer, an additional term appears

$$t^{RL}_{m\sigma',n\sigma} = \delta_{m\sigma',n\sigma} + A^{RL}_{m\sigma',n\sigma} , \tag{5.71}$$

where $A^{RL}_{m\sigma',n\sigma} \equiv A_{m\sigma',n\sigma}$ is the forward scattering amplitude. It is convenient to write $A_{m\sigma',n\sigma}$ as a 2×2 block-matrix in the spin space. In fact we can write

$$\hat{A}_{m,n} = -i\hat{\mathcal{A}}_m\hat{\mathcal{B}}_n , \tag{5.72}$$

with $\hat{\mathcal{A}}_m$ and $\hat{\mathcal{B}}_n$ given by

$$\begin{aligned}
\hat{\mathcal{A}}_m &= -iv_0\hat{g}_m\left[\Phi^{*}_{m}\hat{u}^{\dagger}_{m} + \frac{2i\alpha_x\alpha_y}{\omega_0^2}\Phi'^{*}_{m}\hat{u}'^{\dagger}_{m}\hat{\sigma}_z\right], \\
\hat{\mathcal{B}}_n &= \frac{1}{1+v_0\langle\!\langle G_{\rm s}\rangle\!\rangle}\left[\Phi_n\hat{u}_n - \frac{2i\alpha_x\alpha_y}{\omega_0^2}\hat{\sigma}_z\Phi'_n\hat{u}'_n\right] .
\end{aligned} \tag{5.73}$$

Here, all functions are evaluated at the position of the scatterer. We have also introduced such matrices:

$$\begin{aligned}
\hat{u}_n(x) &= \sqrt{\frac{m^*_e}{\hbar k_n}}e^{ik_nx}e^{-i\hat{\sigma}_y\frac{m^*_e\alpha_x}{\hbar}x}, \\
\hat{u}^{\dagger}_n(x) &= \sqrt{\frac{m^*_e}{\hbar k_n}}e^{-ik_nx}e^{i\hat{\sigma}_y\frac{m^*_e\alpha_x}{\hbar}x}, \\
\hat{v}_n(x) &= \sqrt{\frac{m^*_e}{\hbar k_n}}e^{-ik_nx}e^{-i\hat{\sigma}_y\frac{m^*_e\alpha_x}{\hbar}x}, \\
\hat{v}^{\dagger}_n(x) &= \sqrt{\frac{m^*_e}{\hbar k_n}}e^{ik_nx}e^{i\hat{\sigma}_y\frac{m^*_e\alpha_x}{\hbar}x} .
\end{aligned} \tag{5.74}$$

Similarly, to obtain the reflection amplitude we calculate

$$r^{RL}_{m\sigma',n\sigma} = \left.\frac{\delta\Psi(\boldsymbol{r})}{\delta\Phi^{R}_{m\sigma'}(\boldsymbol{r})}\right|_{\Phi(\boldsymbol{r})\to\Phi^{L}_{n\sigma}(\boldsymbol{r})} , \tag{5.75}$$

where we adopted the basis for the outgoing states on the left to be $\Phi^R_{m\sigma'}(\boldsymbol{r})$, *i.e.* to be the incident states from the right. It is important that the Green's function is now taken for $x \to -\infty$, which reads

$$\hat{G}\left(\boldsymbol{r},\boldsymbol{r}'\right) = \sum_{n\sigma} \Phi_n(y)\Phi^*_n(y')\left|\sigma\right\rangle\left\langle\sigma\right| g_{n\sigma} v_{n\sigma}(x) v^*_{n\sigma}(x') \ . \tag{5.76}$$

In a similar way we obtain

$$\hat{r}_{m,n} = -i\hat{\mathcal{C}}_m \hat{\mathcal{B}}_n \ , \tag{5.77}$$

where

$$\hat{\mathcal{C}}_m \ = \ -iv_0\hat{g}_m\left[\Phi^*_m \hat{v}^\dagger_m + \frac{2i\alpha_x\alpha_y}{\omega_0^2}\Phi'^*_m \hat{v}'^\dagger_m \hat{\sigma}_z\right] \ , \tag{5.78}$$

and $\hat{\mathcal{B}}_n$ is given by Eq. (5.73).

5.3 Brief discussion of the unitary of the S-matrix

The problem with our approach to obtain the scattering coefficients is that being a perturbative method the unitarity of the scattering matrix is affected and $\hat{S}^\dagger\hat{S} \neq 1$ but some other hermitian matrix $\hat{A}$, such that $\hat{S}^\dagger\hat{S} = \hat{A}$. One can device a method to recover unitarity. Being Hermitian, the matrix $\hat{A}$ has real eigenvalues and is diagonalizable via a unitary transformation,

$$\hat{A} = \hat{U}^\dagger \hat{A}_{\text{diag}} \hat{U} \ , \tag{5.79}$$

where the eigenvalues of $\hat{A}$ are the diagonal elements of $\hat{A}_{\text{diag}}$ and the eigenvectors of $\hat{A}$ are the colums of $\hat{U}$. Now this means

$$\hat{S}^\dagger\hat{S} = \hat{U}^\dagger\hat{A}_{\text{diag}}\hat{U} \implies \hat{U}\hat{S}^\dagger\hat{U}^\dagger\hat{U}\hat{S}\hat{U}^\dagger = \hat{A}_{\text{diag}} \ . \tag{5.80}$$

As the matrix $\hat{A}_{\text{diag}}$ is diagonal with real values, it is possible to write it as the square of $\sqrt{\hat{A}_{\text{diag}}}$ in order to invert them on the left hand side of Eq. (5.80) and rewrite the new unitary scattering matrix,

$$\hat{S}' = \hat{U}\hat{S}\hat{U}^\dagger\left(\hat{A}_{\text{diag}}\right)^{-1/2} \ . \tag{5.81}$$

This implies renormalization of the scattering coefficients which can be recalculated from the above expression. In the next chapter when we present the main results we impose unitarity for the calculation of all observables.

5.4 Conclusions

In this chapter we present a detail derivation of the scattering coefficients for a short-range, delta- like impurity in a nanowire with Rashba spin-orbit coupling where electrons motion is confined in the y direction. We do so by probing the scattering states at the extremes of the nanowire via the Lippmann-Schwinger equation. The intersubband mixing arising from the interplay between Rashba spin-orbit coupling and the harmonic confinement complicates the analytical solution of the Lippmann-Schwinger equation. Our way to deal with these difficulties is by performing a Schrieffer-Wolff transformation. In this manner, we gauge away the intersubband mixing, up to second order in perturbation theory. As a result, the Green's function in the Lippmann-Schwinger can be obtained straightforwardly. On the other hand the complexity is absorbed into the impurity potential or the eigenfunctions of the system. Consequently, the impurity, that is assumed from the beginning to be a scalar, acquires a spin-structure. From the form of the scattering coefficients we already understand that by scattering at the the impurity the electron spin may flip. Such spin-flip processes will have important consequence on the transport properties of the wire, as discussed in the next chapter, where we will use the results of the preset and previous chapters. We close the chapter describing a method to recover unitarity of the S-matrix, after the perturbative approach used in the calculation.

Chapter 6

Quasi-bound states in a nanowire: Effects of the Rashba spin-orbit coupling

In this chapter we derive the conductance for a nanowire with Rashba spin-orbit coupling in the presence of an impurity potential. The latter couples propagating and evanescent states. This coupling results in quasi-bound states (QBS) that strongly affect charge transport. Furthermore, the presence of Rashba spin-orbit coupling allows for different spin-dependent mechanisms for electronic transport. As a result, the conductance presents perfect ballistic transmission at the threshold energy of the opening of the next propagating channel, as well as a dip that strongly suppresses the conductance just below such threshold. In order to study the interplay between both, RSOC and the impurity potential, we make use of the scattering coefficients obtained in Chapter 5 via the S-matrix formalism and the expression for the charge conductance, Eq. (4.30) in Chapter 4. We present also a systematic study of the conductance dependence on the strength and lateral position of the impurity potential. We also make a comparison between an effective 1D model, derived in Appendix C, and the full quasi-1D situation analysed in Chapter 5. By using the results in Chapter 4 on the spin-dependent conductance and the the spin-orbit torque, Eq. (4.44), we provide an exhaustive study of the spin transport in the wire. We find the underlying relation between the spin-flip transmission and the $SU(2)$ field. At the resonant energy, the only transmission allowed is through spin-flip allowing

us to connect a physical quantity with the corresponding $SU(2)$ symmetry. We complete the presentation with systematic study of the spin-flip transmission as a function of the lateral position of the impurity, to maximize the spin-flip transmission, and in turn the spin torque per discussed in Chapter 4.

6.1 Electronic Transport: effect of Rashba spin-orbit coupling in the charge conductance

From Eqs.(5.69-5.73), derived in Chapter 5, it follows the transmission coefficient:

$$t^{RL}_{m\sigma',n\sigma} = \delta_{m\sigma',n\sigma} - \mathrm{i}\frac{\frac{m_e^*}{\hbar^2}v_0}{1+\mathrm{i}v_0\frac{m_e^*}{\hbar^2}\sum_n \frac{\Phi_n^2}{k_n}}\left[\Phi^*_m\Phi_n\frac{\mathrm{e}^{\mathrm{i}(k_n-k_m)x_{imp}}}{\sqrt{k_m k_n}}\right.$$
$$\left. + \frac{2\alpha_x\alpha_y}{\omega_0^2}\left(k_n\Phi^*_m\Phi'_n + k_m\Phi'^*_m\Phi_n\right)\frac{\mathrm{e}^{\mathrm{i}(k_n+k_m-2k_R)x_{imp}}}{\sqrt{k_m k_n}}\hat{\sigma}_z\right] . \quad (6.1)$$

This coefficient describes the transmission probability of an incident electron with spin σ from a channel n on the left side of the nanowire to a channel m on the right end with spin σ'. As in section 5.1, Φ_n are the lateral modes of the nanowire for a harmonic confinement described by Eq. (2.30) and evaluated at the impurity position y_{imp}. One should bear in mind that within our basis choice $\hat{\sigma}_z = \begin{pmatrix} 0 & 1 \\ 1 & 0 \end{pmatrix}$.

As discussed in Chapter 4, the total conductance of the nanowire can be expressed in terms of the transmission amplitudes

$$\mathcal{G} = \frac{e^2}{2\pi\hbar}\sum_{m\sigma',n\sigma}|t_{m\sigma',n\sigma}|^2 , \quad (6.2)$$

summed over all the spin and conduction channels. As a direct result of the presence of Rashba spin-orbit coupling the spin-degeneracy is lifted and consequently there are two possible scattering processes for an electron prepared in a spin-up state: The spin is either conseeved or flip to a spin-down state. From now on we will refer to the transmission probabilities associated to these mechanisms as spin-conserved transmission

and spin-flip transmission, respectively. In this section we explore the characteristics of the conductance and the effect that Rashba spin-orbit coupling has on them. We will do so by first introducing the resonant characteritics in the conductance in the absence of Rashba spin-orbit coupling and then focusing on the effects of RSOC is finite. As we see in the Subsection 6.1.2 the main result is the absence of the full suppression of the charge conductance at the resonant energy associated with the quasi-bound state.

6.1.1 Resonant characteristics of the conductance:perfect transmission and quasi-bound states

The effect of delta-like impurities in electron transmission though nanowires is well known in the absence of Rashba interaction. While for a clean nanowire the transport is ballistic and the conductance shows the typical $\frac{e^2}{2\pi\hbar}$ steps for every new opened channel, in the presence of an impurity potential the transmission amplitude, and hence the conductance, is detrmined by Eq. (6.1) for $\alpha_x = \alpha_y = 0$. Namely, the conductance for such a system is determined by the sum of transmission amplitudes of all the channels, $T = \sum_n T_n$ with $T_n = \sum_m |t_{m,n}|^2$. The latter can be written as

$$T = N - \frac{\mathrm{Im}^2\left(G\right)}{\left[\frac{\hbar^2}{m_e^* v_0} + \mathrm{Re}\left(G\right)\right]^2 + \mathrm{Im}^2\left(G\right)} \,, \tag{6.3}$$

where N is the number of opened channels and G is the Green's function for the clean nanowire at the impurity position $r_{imp} = (x_{\mathbf{imp}}, y_{imp})$, see Eq. (2.32). It is convenient to write it as:

$$\begin{aligned} G\left(r_{imp}, r_{imp}\right) &= \mathrm{Re}\left(G\right) + \mathrm{i}\,\mathrm{Im}\left(G\right) \\ &= \sum_n^{ev} \frac{\Phi_n^2}{\kappa_n} + \mathrm{i} \sum_n^{prop} \frac{\Phi_n^2}{k_n} \,. \end{aligned} \tag{6.4}$$

Energies for a propagating channel are denoted as threshold energies $\epsilon_n = \hbar\omega_0(n - 1/2)$ and are governed by the harmonic confinement. For energies below the threshold energies, the channels are evanescent with $\kappa_n = \sqrt{2m_e^*(\epsilon_n - E)/\hbar^2}$. The real part of the Green's function in Eq. (6.4)

corresponds to the sum over all the evanescent modes with energy below the threshold and similarly, the imaginary part of the Green's function corresponds to the sum over all the propagating states with energies above their corresponding threshold energies.

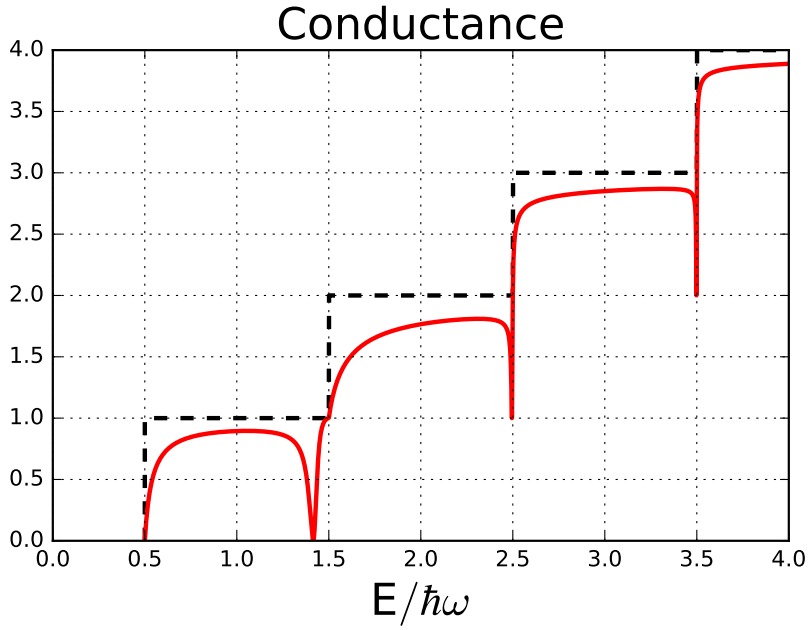

Figure 6.1: Conductance (in units of the quantum conductance $\mathcal{G}_0 = e^2/2\pi\hbar$) as a function of the Fermi energy (in units of the confinement energy $\hbar\omega_0$) for a nanowire with an impurity potential of strenghts $v_0 = 0.9$ (solid red line) and $v_0 = -0.9$ (dashed red line). The black dashed line indicates the ballistic conductance of a clean nanowire. Every time the Fermi energy reaches the bottom of a new subband a new propagaing state is allowed. In the absence of the impurity (black dashed lines) the transmission probability is 1 for each subband, hence the conductance is proportional to the number of propagating channels N. However, in the presence of an impurity, perfect transmission is only achieved at the threshold energies ϵ_n. In addition, for an attractive impurity (dashed red line) the conductance is further reduced and it presents a resonance just below the threshold energy effectively blocking a propagating channel reducing the conductance to $N - 1$.

In Fig. 6.1 we show the behaviour of the conductance as a function of the Fermi energy in units of the confinement energy, $\hbar\omega_0$, for both an attractive

(dashed red line) and a repulsive (solid red line) delta-like impurity of the same strength. This behaviour can be understood from Eqs. (6.3)- (6.4): whenever a new subband minima is reached at the threshold $E = \epsilon_n$, the momentum of this subband becomes $\kappa_n = 0$. As a consequence the real part of the Green's function $\mathrm{Re}\,(G) \to \infty$ outweight the rest of contributions in the denominator of Eq. (6.3). This occurs for both, repulsive (dashed red line) and repulsive (solid red line) impurities, while only attractive impurities exhibit the resonant feature. Close to the opening of the next subband with threshold energy given by ϵ_{ns}, Eq. (6.3) can be rewritten as,

$$\begin{aligned} T &= N - \frac{\mathrm{Im}^2(G)}{\left[\frac{\hbar^2}{m_e^* v_0} + \frac{\Phi_{ns}^2}{\kappa_{ns}} + \sum_{n=ns+1} \frac{\Phi_n^2}{\kappa_n}\right]^2 + \mathrm{Im}^2(G)} \\ &\sim N - \frac{\mathrm{Im}^2(G)}{\left[\frac{\hbar^2}{m_e^* \tilde{v}_0} + \frac{\Phi_{ns}^2}{\kappa_{ns}}\right]^2 + \mathrm{Im}^2(G)} \,. \end{aligned} \tag{6.5}$$

In the last equation we have renormalized the impurity strength in order to include the weight of all evanescent modes except the next subband, such that [1]

$$\frac{\hbar^2}{m_e^* \tilde{v}_0} = \frac{\hbar^2}{m_e^* v_0} + \sum_{n=ns+1} \frac{\Phi_n^2}{\kappa_n}. \tag{6.6}$$

This renormalization absorbs the relatively small contribution of the higher evanescent modes. To verify this, we plot in Fig.6.2 the real part of the Green's function with a solid red line and the individual contributions of each evanescent mode with dashed red lines . One can see that close to the first threshold (vertical black lines), the contribution from the next subband (dashed blue line)is much larger than that from the tails of the rest of evanescent modes. As a result of this renormalization we can write the resonant energy as

$$E = \epsilon_{ns} - \frac{\tilde{v}_0^2 \Phi_{ns}^4}{2}, \tag{6.7}$$

[1] It is important to note that in a full symmetric case, when the impurity is located in the center of the wire, $y = 0$, the evanescent weight vanishes for even modes, and hence the dip is suppressed. Therefore, in following plots we choose the position of the impurity such that $y_{imp} \neq 0$. A detailed analysis of the dependence of the conductance on the impurity position is given in next sections.

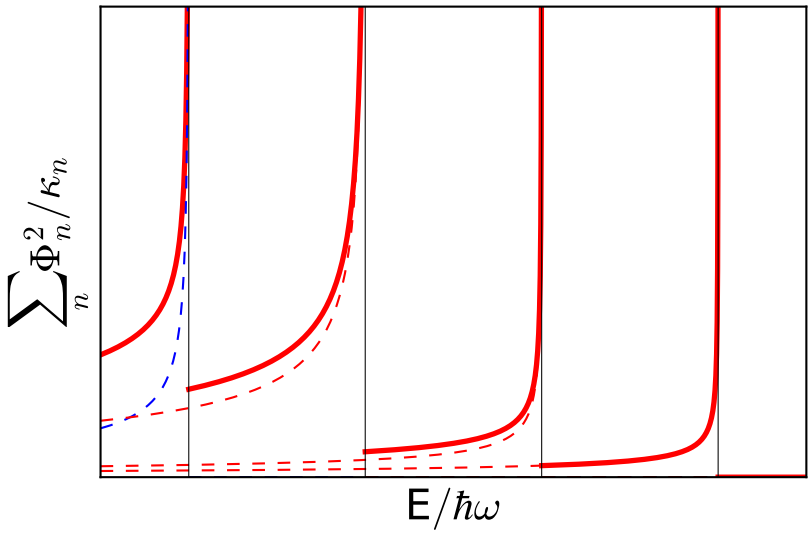

Figure 6.2: Real part of the Green's function as a function of the energy (red solid line). As the energy approaches a threshold $E \to \epsilon_n$ (black lines), the contribution of the next subband to become propagating (blue dashed line) is much larger than the sum of the individual contributions from the tails of the higher evanescent modes(dashed red lines).

from the resonant condition $\frac{\hbar^2}{m_e^* \tilde{v}_0} + \frac{\Phi_{ns}^2}{\kappa_{ns}} = 0$. This condition is only possible to fullfill for negative values of $\tilde{v}_0$, that is to say for attractive scatterers. Then, at these resonant energies Eq. (6.5) is reduced to

$$T \sim N - \frac{\mathrm{Im}^2(G)}{+\mathrm{Im}^2(G)} = N - 1\,, \tag{6.8}$$

as the attractive impurity compensates the contribution from the next evanescent mode, about to become propagating. If the energy is close, but smaller than the threshold energies a dip in the conductance shows up, as shown with a red dashed line in Fig. 6.1. For the particular case where there is only one propagating channel, Eq. (6.8) implies that all incoming electrons are reflected and no transport is allowed. These dips are associated to the formation of quasi-bound states splitting from the next subband and localized around the impurity . Description of quasi-bound states, as the poles of the transmission coefficient, requires the inclusion of the evanescent modes. As discussed in Chapter 2 this description of

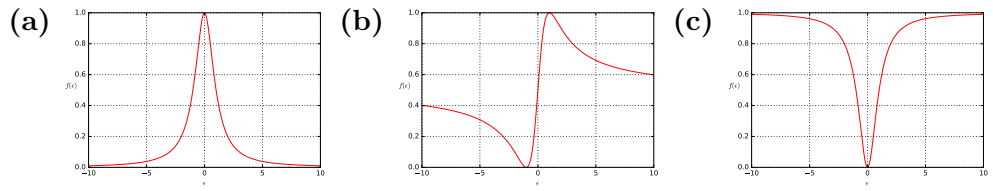

Figure 6.3: Fano line-shape $f(\epsilon)$ as a function of the dimensionless energy parameter ϵ for: (a) $q \to \infty$, where the transmission occurs through the discrete state, (b) $q = 1$ and the transition through the discrete the discrete and the continuum of states is of equal strength with minimum at $E_{min} = E_R - \Gamma/2q$ and maximum at $E_{max} = E_R + \Gamma/2q$, and (c) $q = 0$ for the resonant symmetric line-shape.

quasi-bound states was first introduced by Bagwell [23]. This discussion was later picked up by [24] and related to the sum over evanescent modes throught the Green's function. As the evanescent mode is associated with a decaying length(corresponding to the evanescent κ_n), these states are not properly bound as opposed to the stable bound-state of a delta-scatterer in Eq.(2.23)), as discussed by other authors [57, 58, 59].

At this point, it is worth emphasizing the advantages of using the Lipmann-Schwinger approach. As noted by Ref. [65], many other approach the system by solving the Schrödinger equation through matching the wavefunctions for the modes on both sides of the impurity potential and obtaining an infinite set of coupled equations[23, 117, 118]. In order to solve such a problem one needs to truncate the system of equations, and correspondingly rescale the coupling constants. In contrast, by using the Lippmann-Schwinger equation the system is analytically solvable, as all the information for the coupling is encoded in the Green's function of the bare nanowire.

Quasi-bound states as Fano resonances

As pointed out before, the presence of quasi-bound states is due to the coupling between a discrete state and the continuum of subbands available in the nanowire. This is nothing but a Fano resonance, described by the asymmetric Fano line-shape [119],

$$f(\epsilon) = \frac{(\epsilon + q)^2}{1 + \epsilon^2}, \tag{6.9}$$

where $\epsilon = (E - E_R)/\Gamma$ is the dimenssionless energy measured from the resonance, Γ is the resonance width and q is the asymmetry parameter introduced by Fano in his original paper[120]. By equation Eq.(6.9) we see that the minimum $f_{min} = 0$ occurs at $\epsilon = -q$ and the maximum $f_{max} = 1 + q^2$ at $\epsilon = 1/q$.

In the limit $|q| \to \infty$, the transition occurs through a discrete state as the transition trough the continuum becomes very weak. This results in a Lorentzian peak of the form $f(\epsilon) \to 1/(1+\epsilon^2)$ (see Fig. 6.3 (a)). If the asymmetry parameter is close to unity $q \to 1$, transition through both the discrete and the continuum and Eq.(6.9) leads to curves of the type shown in in 6.3 (b). Finally, for the case $q \to 0$ the Fano resonance becomes $f(\epsilon) \to q^2/(1+q^2)$ forming a dip at $E = E_R$ with a symmetrical lineshape (see Fig. 6.3 (c)). This last case is unique to Fano resonance and is sometimes referred in the literature as anti-resonance [119].

We can now fit our result for the conductance as expressed in Eq. (6.3) to Eq. (6.9) and obtain, the following expressions for the Fano parameters,

$$E_R = E_n - \left[\frac{v_0^2 \operatorname{Im}^2(G) - 1}{v_0^2 \operatorname{Im}^2(G) + 1}\right]^2 \frac{v_0^2 \Phi_n^4}{2}, \tag{6.10}$$

$$q = \pm \frac{2 v_0 \operatorname{Im}(G)}{|v_0^2 \operatorname{Im}^2(G) - 1|}, \tag{6.11}$$

$$\Gamma = \pm v_0^3 \operatorname{Im}(G) \Phi_n^4 \left[\frac{|v_0^2 \operatorname{Im}^2(G) - 1|}{v_0^2 \operatorname{Im}^2(G) + 1}\right]. \tag{6.12}$$

The resonance energy in Eq. (6.10) coincides, up to a correction factor, with Eq. (6.7). In the limit of weak impurity such factor equals unity and we recover that result. This is equivalent to a Lorentzian when $q \to \infty$.

The possibility of destructive interference leading to asymmetric lineshapes due to disorder has been widely studied in quasi-one-dimensional waveguides [72, 58, 67, 121, 122]. But the inclusion of RSOC as a source of Fano resonances is even more interesting, either in nanowires [92, 123, 124].

6.1.2 Effect of Rashba spin-orbit coupling in the conductance

So far we have described the effect of delta-like impurity in a simple nanowire. In this section we study how the Rashba spin-orbit coupling

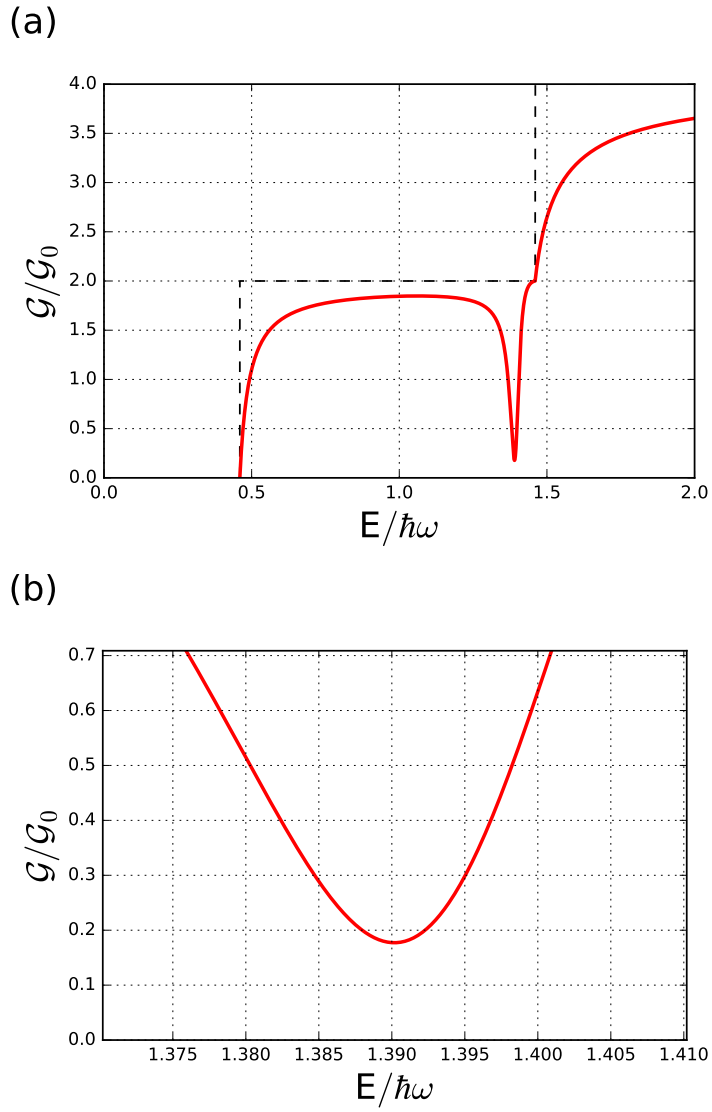

Figure 6.4: (a) Conductance in the presence of a scatterer of strenght $v_0 = -0.9$ and RSOC $\alpha_x = \alpha_y = 0.2$ (solid red line). The ballistic conductance is shown in black dashed lines. At the threshold energy below $1.5\hbar\omega$, the transmission is perfect. Close and below the threshold the conductance exhibits a dip related to the quasi-bound state forming in the nanowire as explained in the main text. (b) A zoom into the quasi-bound state resonance. One clearly see that the transmission is not fully suppressed.

affects the nanowire conductance. The expression for the conductance is no longer as simple as the one describe in Eq. (6.3). As mentioned in the introduction to this section, in the presence Rashba spin-orbit coupling transport properties are spin-dependent. The combination of the Rashba spin-orbit coupling with the delta-like impurity leads to striking transport properties, both in the charge and spin conductances, due to spin-flip events discussed below. At first glance, the charge conductance shown in Fig.6.4(a) shows similar resonant features as those in a wire without Rashba spin-orbit coupling (see previous section and Fig.6.1): a perfect ballistic transmission at the threshold and the dips just below the threshold. However, a closer look shows important differences. One is the shift to lower energies of threshold energy given by $\epsilon_n = \hbar\omega_0(n - 1/2) - m_e^*(\alpha_x^2 + \alpha_y^2)/2)$ as a consequence of the sinking in the subband energy dispersion. As mentioned in the introduction of this chapter, the presence of Rashba spin-orbit coupling allows for different transmission mechanisms mediated by the impurity embedded in the nanowire. As a result, tranmission of an incoming electron can occur conserving the spin-alignment with probability $|t_{\uparrow\uparrow}|^2$ for states prepared with spin-up ($|t_{\downarrow\downarrow}|^2$ for states prepared with spin-down) or with a flip in the alignment of the spin with probability $|t_{\uparrow\downarrow}|^2$ for states prepared with spin-up($|t_{\downarrow\uparrow}|^2$). Although spin-flip transmission is much smaller than spin-conserved transmission as it depends on $2\alpha_x\alpha_y/\omega_0^2$ as shown in Eq. (6.1), it is not negligible. The relevance of this factor will become clear in Section 6.2, where we study the spin transport and its relation with a SU(2) field. As in the case where Rashba spin-orbit coupling is absent, the resonant behaviour of the conductance is dictated by the denominator in Eq. (6.1). When the energy approaches the threshold for the opening of the next subband, the dominant nature of $\mathrm{Re}\,(G) \to \infty$ in the denominator results in a zero-probability of the spin-flip transmission. This is the same characteristic that responsible for the perfect transmission of the spin-conserved component. Consequently, the conductance at the threshold energy is $2N$ due to the lifting of spin-degeneracy (see Fig.6.4(a)).

The main effect of Rashba spin-orbit coupling is the absence of the full supression of the conductance at the resonant energy, as shown in detail in Fig.6.4(b). To clarify the origin of this, we refer again to Eq. (6.1) in order

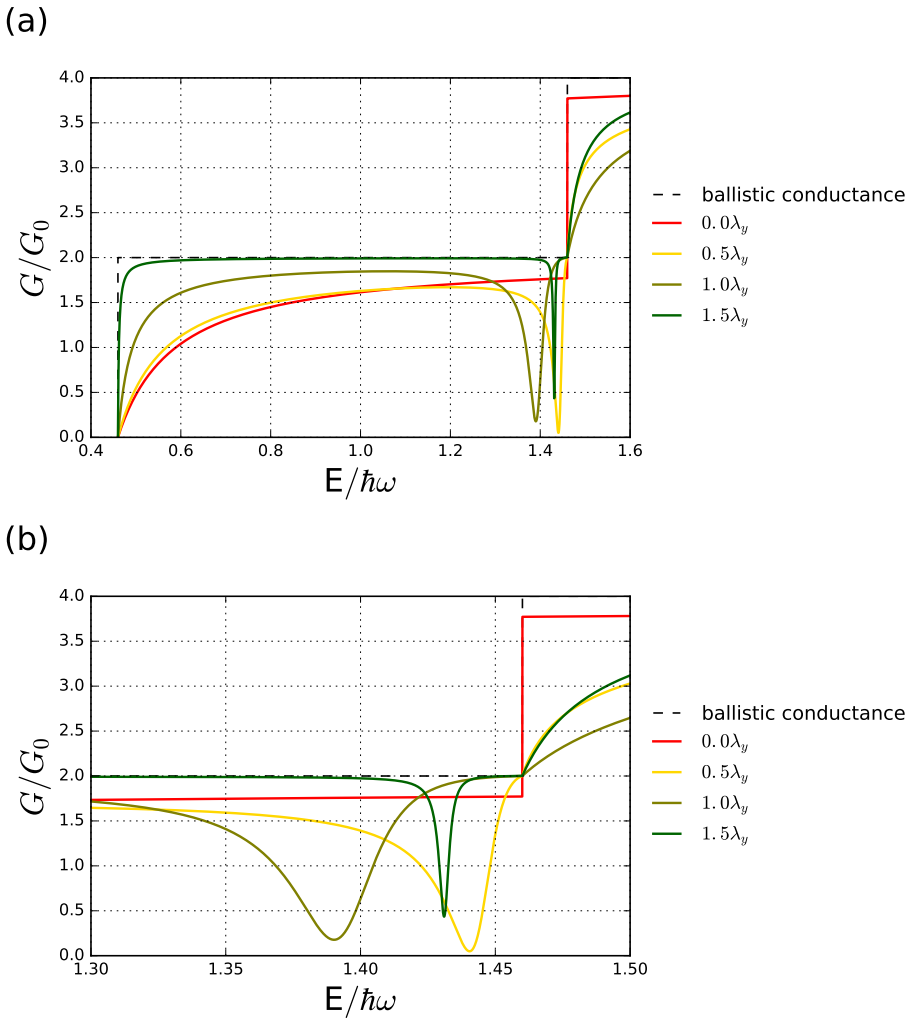

Figure 6.5: (a) Conductance for a scatterer of strenght $v_0 = -0.9$. The different colour correspond to different position of the impurity y_{imp}. The position is given in units of the confinement length $\lambda_y = \sqrt{\hbar/m_e^*\omega_0}$. The chosen RSOC is $\alpha_x = \alpha_y = 0.2$. (b) Zoom in of the resonance for the same plots.

to write the following expression for the transmission of a spin-up state,

$$T_{0\uparrow} \sim N - \frac{\mathrm{Im}^2(G)}{\mathrm{Im}^2(G)} + \left(\frac{2\alpha_x\alpha_y}{\omega_0^2}\right)^2 \frac{\left(2\Phi_0\Phi_0'\right)^2/k_0}{\mathrm{Im}^2(G)}\,, \tag{6.13}$$

It becomes clear from Eq. (6.13) that while the spin-conserved contribution to the transmission will be fully suppressed when there is only one propagating band, there is a finite contribution to the spin-flip transmission. We can conclude then, that the effect of the quasi-bound state in the charge conductance is strongly spin-dependent in the presence of RSOC interaction. Specifically , at the resonant energy only spin-flip transmission is allowed while spin-conserved transmission is completely suppressed. In a next section we discuss this in more detail and the consequences on the spin-dependent transport. But before that we present a systematic study of the charge conductance as a function of the impurity strength and lateral position.

Dependence on the impurity position and strength

As briefly mentioned above, due to the translational symmetry along x-axis, the impurity position x_{imp} is irrelevant. However, the lateral position y_{imp} is important. As the even lateral modes $\Phi_n(y_{imp})$ vanish at the center of the harmonic oscillator, resulting in the decoupling of the subbands as the imaginary part of the Green's function in the denominator of Eq. (6.1) vanishes $\mathrm{Re}\,(G) = \Phi_n^2(0)/\kappa_0 = 0$. This is a consequence of the symmetric states of the quantum harmonic oscillator for even modes, $n = 0, 2, 4, ...$ As a consequence there is no propagating weight for the impurity potential to compensate. The lack of coupling between subbands suppresses the dip resonance. In most of the plots, when not explicitly said, it is assumed that the impurity is located at $y_{imp} \neq 0$, in order to study the dip.

In Fig.6.5(a) we present the conductance as a function of different lateral positions for the impurity. One can see the suppression of the resonant dip for $y_{imp} = 0$, which only appears when the transverse position of the impurity breaks the mirror symmetry. We define the binding energy of the quasi-bound state as the energy difference between the threshold and the resonant energy $E_{QBS} = E_{th} - E_R$. Focusing into energies close to the resonance (see Fig. 6.5(b)), we can appreciate that first E_{QBS} increases with the distance from the centre up to a certain maximum value at around $y_{imp} = 1.0\lambda_y$, and then decreases for larger values.

It is also worth noticing that the further away the impurity is from the center, the higher conductance minima is, implying there is a higher spin-flip transmission probability. This becomes clear from Eq. (6.13), as the spin-flip transmission depends on the derivative of the wave-function at the impurity

position $\Phi_0'(y_{imp})$. Similarly, in Fig. 6.6(a) we study the dependence of the quasi-bound state resonant energy with the impurity strength for a fixed position, $y_{imp} = \lambda_y$. We can see in Fig. 6.6 (b) that while the binding energy of the quasi-bound state, E_{QBS}, strongly increases with the strength of the impurity potential v_0, the conductance minima weakly depends on v_0. This can be understood from Eq. (6.13) since both spin-conserved and spin-flip transmission probabilities depend on the impurity strength in the same way.

Effective 1D potential

We have also derived an effective one-dimensional model (see Appendix C for details). Within such effective model, the effect of all higher subbands is projected onto the a single band. This results in the following transmission coefficient,

$$t^{RL}_{00,\sigma'\sigma} = \delta_{\sigma'\sigma} - \mathrm{i}\frac{\frac{m_e^*}{\hbar^2}v_0}{1+\mathrm{i}v_0\frac{m_e^*}{\hbar^2}\frac{\Phi_0^2}{k_0}}\left[\frac{\Phi_0^*\Phi_0}{k_0} + \frac{2\alpha_x\alpha_y}{\omega_0^2}\left(2k_0\Phi_0^*\Phi_0'\right)\frac{\mathrm{e}^{\mathrm{i}2(k_0+k_R)x_{imp}}}{k_0}\hat{\sigma}_z\right] \quad (6.14)$$

Comparison between Eq. (6.14) and Eq. (6.1) reveals similarities. However, in the strict 1D situation the sum over all the evanescent modes is not taken into account. This sum, which appear in the denominator of Eq. (6.1) for the quasi 1D case, is absence in Eq. (6.14). As discussed in Section 6.1.1, evanescent modes are required to form a quasi-bound state. As for the numerator in Eq. (6.1), we recover the previous result of Eq. (6.14), but of course for a single propagating band per spin species ($m = n = 0$) and energy E_0.

The absence of the quasi-bound state in the 1D model prevent the resonant behaviour to be observed, blue curve in Fig.6.7. Thus the result for the conductance obtained from Eq. (6.1) is a good approximation for the energies close to the bottom of the propagating band. However, there is a way to recover the results obtained in the quasi 1D case from the pure 1D, by adding "by hand" in the denominator of the second term in Eq.(6.14), the contribution of the evanescent modes. By doing this one obtains an excellent agreement between the full solution and the one obtained from the 1D model, as shown in Fig.6.8.

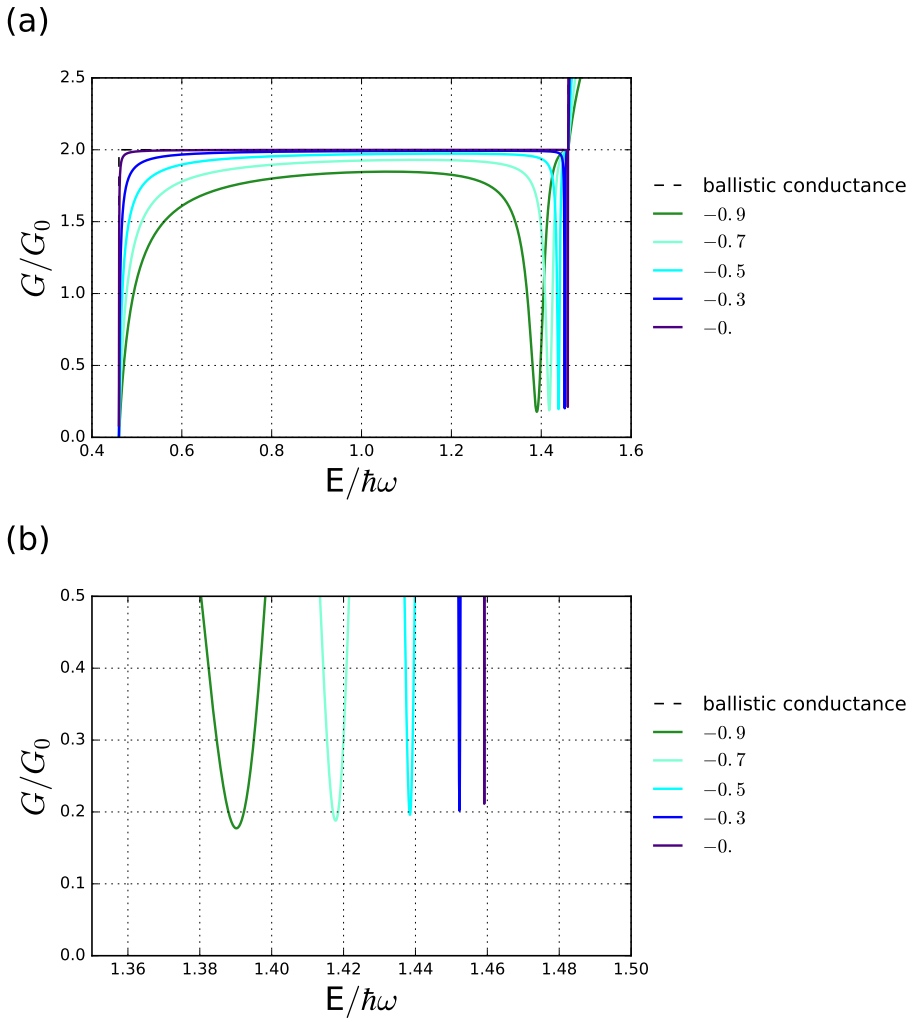

Figure 6.6: The dependence of the conductance on the impurity strength for a nanowire with RSOC: (a) Conductance for different strength v_0 of the attractive scatter. We have chosen RSOC $\alpha_x = \alpha_y = 0.2$, and $y_{imp} = 1.0\lambda_y$. (b) Zoom of the resonance for the same values.

6.2 Spin-dependent transport properties

We understand from previous sections the relevant role of Rashba spin-orbit coupling on the charge transport properties of a nanowire with an impurity. In previous sections, we identified two different scattering mechanisms

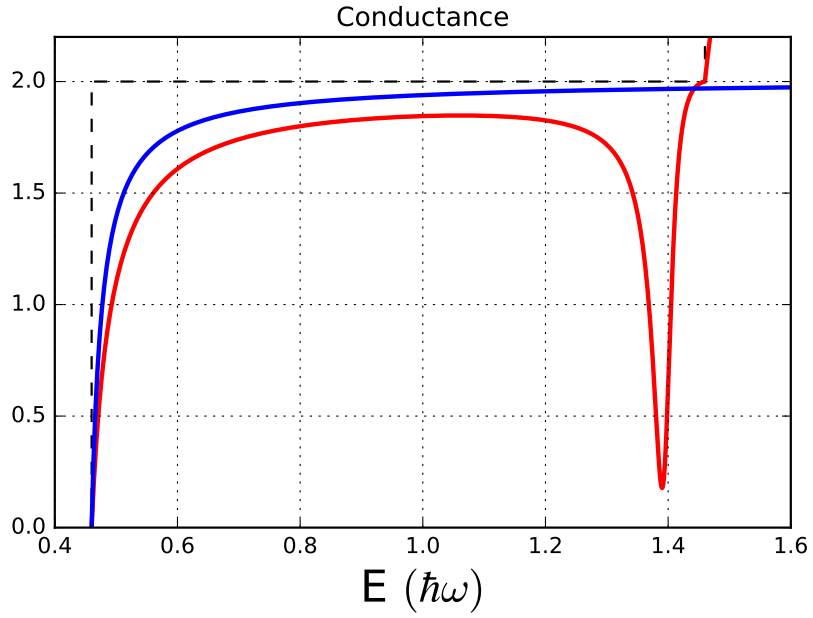

Figure 6.7: Conductance for an effective 1D model (blue) vs conductance for the full quasi-1D model (red) in units of $\mathcal{G}_0$ for an impurity potential of strength $v_0 = -0.9$ at position $y_{imp} = 1.0\lambda_y$ respect to the center of the nanowire with Rashba parameters $\alpha_x = \alpha_y = 0.2$.

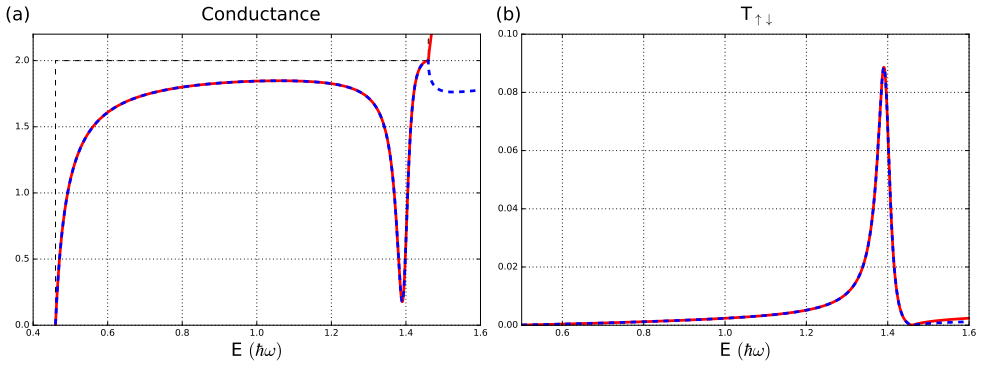

Figure 6.8: (a)Conductance and (b) spin-flip transmission for the quasi-1D model (solid red line) and for the effective 1D model (dashed blue line) after adding by hand the contribution from the evanescent modes.

mediated via the impurity potential, which are distinguished by whether the spin is conserved or flipped after scattering. The interplay between these two mechanism manifest on a modification of the quasi-bound states resonance in the charge conductance. Specifically, as shown in Fig. 6.4 and Eq. (6.13), at the resonant energy the dip in the conductance does not reach zero as was the case in for transport in the absence of Rashba spin-orbit interaction. Because this effect is due to spin-dependent processes, one expects that it has consequences on the spin transport itself. Therefore in this section we focus on the spin-dependent transport.

In Fig. 6.9(a) we plot the spin-flip transmission as a function of the injection (Fermi) energy. Even though it is small in comparison to the total conductance, spin-flip transport is not negligible. We can observe two features that are closely related to the resonant characteristics discussed in Section 6.1.2. To begin with, the spin-flip transmission is exactly zero at the threshold energy where the next propagating subband in opened. This is in agreement with our conclusions in Section from Eq. (6.1), namely: the dominant nature in the denominator of the real part of the Green's function $\mathrm{Re}\,(G) \to \infty$ at the threshold energy results in perfect transport for the spin-conserved transmission while the spin-flip transport is completely suppressed. On the other hand, below the threshold energy the spin-flip transmission presents a significant enhancement. In Fig.6.9(b) we plot the ratio between spin-flip transmission probability and total transmission probability $T_{\uparrow\downarrow}/(T_{\uparrow\uparrow} + T_{\uparrow\downarrow})$ for an incoming spin-up state. We can observe that at certain energy below the threshold the only transport allowed is spin-flip transport.

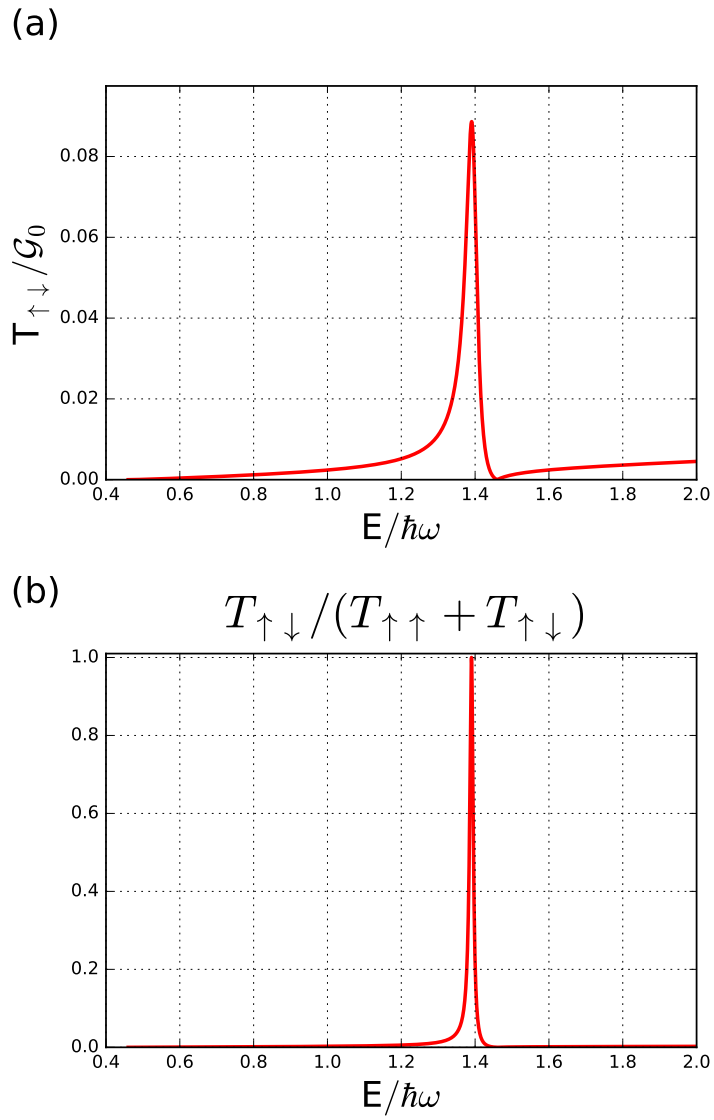

Figure 6.9: Spin-dependent transport properties for a nanowire with an attractive impurity of strength $v_0 = -0.9$ and in the presence of Rashba spin-orbit coupling given by $\alpha_x = \alpha_y = 0.2$ at position $y_{imp} = 1.0\lambda_y$.(a) The spin-flip transmission, $T_{\uparrow\downarrow}$, presents a strong enhancement close to but below the threshold energy where it is fully suppressed. (b) At the threshold energy this percentage is zero, while below such threshold there is an energy at which all transmission allowed is spin-flip transmission.

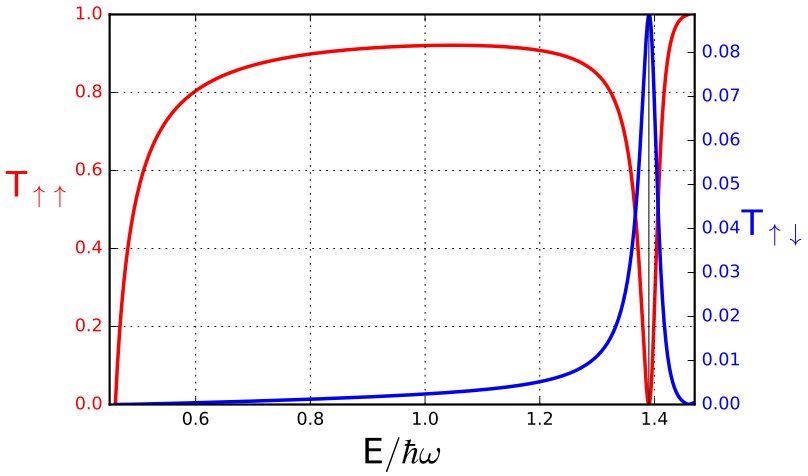

Figure 6.10: Resonant behavior in the transmissions for a n impurity of strength $v_0 = -0.9$ at position $y_{imp} = 1.0\lambda_y$ in a nanowire with Rashba parameters $\alpha_x = \alpha_y = 0.2$.Both the spin-conserved transmission (red line) and spin-flip transmission (blue line) present resonant behavior at the same energy below the threshold. When $T_{\uparrow\uparrow}$ is suppressed, $T_{\uparrow\downarrow}$ is enhanced. In addition, at the threshold energy this behaviour is reversed.

In Fig.6.10 we plot both the spin-conserved transmission $T_{\uparrow\uparrow}$ (red line) and the spin-flip transmission $T_{\uparrow\downarrow}$ (blue line). This confirms that at the resonant energy where the spin-conserved transmission is suppressed, the spin-flip transmission is enhanced. Similarly, for the threshold energy where the spin-conserved transmission reaches perfect transport, the spin-flip transmission is fully suppressed. Interpreting the spin-channels as independent, this result makes us conclude that the presence of the resonant dip is associated to quasi-bound states that affect spin-conserved transport by fully blocking the same-spin channel while not only allowing spin-flip transport but also enhancing it at the resonant energy below the threshold. Finally, to unify this result with the one on the charge transport from previous section, we compare the charge conductance (red line) to the total spin-flip transmission $T_{\uparrow\downarrow} + T_{\downarrow\uparrow}$ (blue line) in Fig. 6.11.

This result suggests that the impurity acts as a spin-filter if it is tuned to be at resonant energy, so that only spin-flip transmission is allowed. Furthermore, from the results of section 4.3.1, the impurity is at the origin of the torque generated in the presence of Rashba spin-orbit coupling

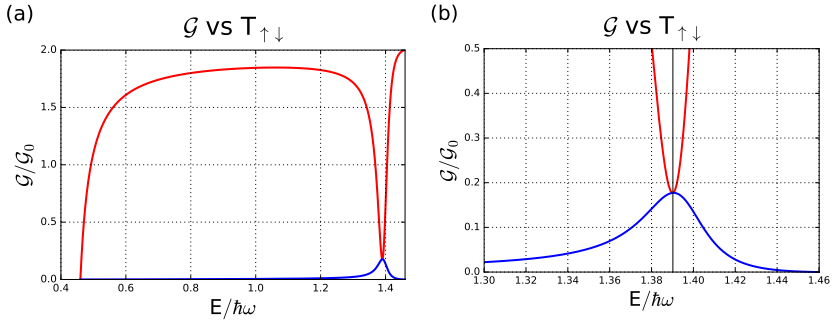

Figure 6.11: (a)Comparison between the conductance (red lines) and the spin-flip transmission,$T_{\uparrow\downarrow}$ (blue line). (b) Zoom iton the main feature of the resonant behavior. Both plots consider an attractive impurity potential of strength $v_0 = -0.9$ at position $y_{imp} = 1.0\lambda_y$ in a nanowire with Rashba parameters $\alpha_x = \alpha_y = 0.2$.

whenever a spin-bias is applied either on the left (V_L^s) or the right lead (V_R^s). Namely, by using the Landauer-Büttikker formalism we express the torque as,

$$T_0 = -\frac{e^2}{2\pi\hbar}\left[\left(t^\dagger_{\downarrow\uparrow}t_{\uparrow\downarrow} + t^\dagger_{\uparrow\downarrow}t_{\downarrow\uparrow} + r^\dagger_{\downarrow\uparrow}r_{\uparrow\downarrow} + r^\dagger_{\uparrow\downarrow}r_{\downarrow\uparrow}\right)V_L^s + \left(t'^\dagger_{\downarrow\uparrow}t'_{\uparrow\downarrow} + t'^\dagger_{\uparrow\downarrow}t'_{\downarrow\uparrow} + r'^\dagger_{\downarrow\uparrow}r'_{\uparrow\downarrow} + r'^\dagger_{\uparrow\downarrow}r'_{\downarrow\uparrow}\right)V_R^s\right] . \tag{6.15}$$

Clearly the torque depends only on the spin-flip transmission and reflection mechanisms, and hence it is enhance at the resonant energy where the spin-flip mechanisms reaches its maximum value.

We next study the spin-flip mechanism as a function of the lateral position of the impurity. This is shown in Fig.6.12.

When the impurity is situated in the middle of the nanowire ($y_{imp} = 0$), that is to say, in the middle of the harmonic confinement potential the symmetry of the even modes $\Phi_n(y_{imp})$ results in a suppression of the quasi-bound state and the dip associated with it as the evanescent and propagating modes are decoupled. Consequently, spin-conserved transmission is not suppressed and there is no spin-flip transmission. For out-of-center positions of the impurity we recover the features discussed for Fig.6.5(b). Firstly, the further away from the center the impurity is the higher the enhancement wich corresponds the a shallower dip in Fig.6.5(b).

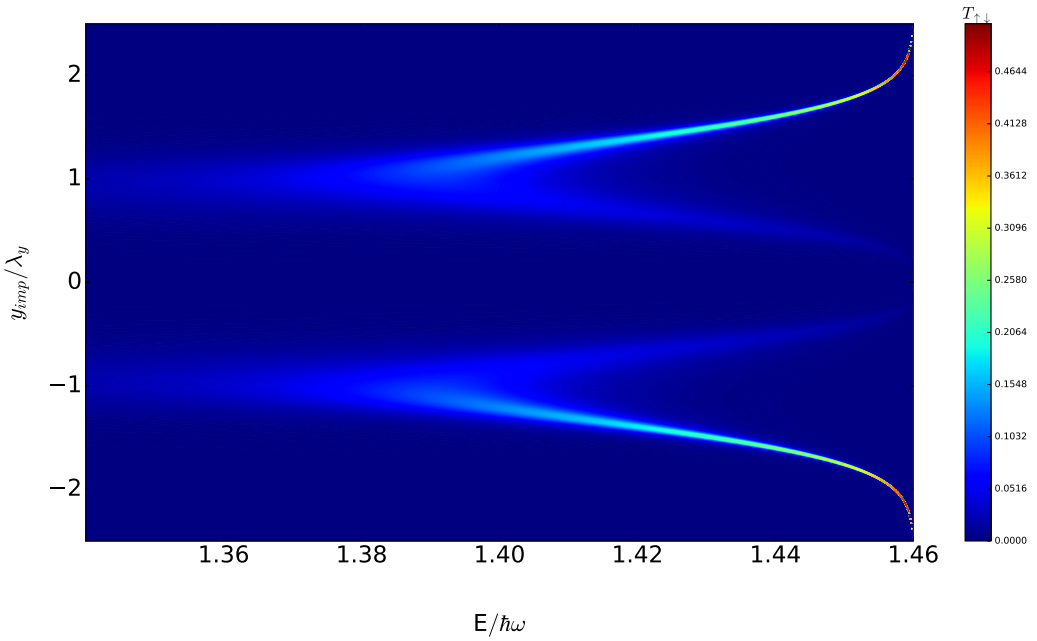

Figure 6.12: Spin-flip transmission as a function of energy and lateral position of the impurity in units of λ_y for an energy window close to the resonance. We find that at the center of the wire $y_{imp} = 0$ the spin-flip transmission is suppressed due to the symmetry of the lateral wavefunction. The further away from the center the higher the enhancement ot the spin-flip transmission. Regarding the energy axis, the position of the peak for the spin-flip transmission occurs the furthest from the threshold energy $\epsilon_0 = 1.46\hbar\omega_0$ at $y_{imp} \approx 1.0\lambda_y$. This means that at this position, the quasi-bound state energy is he highest.

And secondly, when we move away from the center of the nanowire the binding energy of the quasi-bound state E_{QBS} (energy difference between the threshold energy and the resonant energy), occurs at lower energies at first (and further away from the threshold energy) to later return back to the same value. Thus, one can track where the enhancement of the spin-flip conductance is at largest with respect to the Fermi energy. In other words, the position of the attractive impurity provides a tool for control of the spin degree of freedom.

Spin-flip transmission as a SU(2) probe

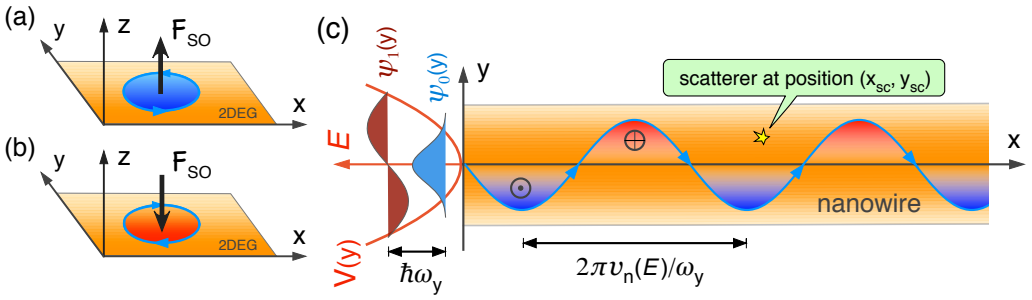

Figure 6.13: Behavior of the spin-orbit SU(2) gauge field for a nanowire in the xy-plane. (a) In the 2DEG, the electron cyclic motion on a closed path gives rise to a spin-orbital SU(2) field F_{SO}. (b) The field F_{SO} changes sign when the path is traversed in the opposite direction. (c) In the nanowire, the electron moving with speed $v_n(E)$ along x oscillates along y with frequency ω_y given by size quantization due to the potential $V(y)$. As a result,the field F_{SO} fluctuates, despite being zero on average, effectively coupling the electron spin to the central position y_0 of the electron wave function.

In this section we provide a physical picture that explains the found spin-flip mechanism. We find that in the process of transmission of an electron one to other side of the impurity, at certain resonant energy where there is a dip in the conductance, the transmission probability for the processes where the spin of the electron is flipped is enhanced, while the transmission probability of the process where the spin is conserved is completely suppressed. In this section we explain how this can be traced to the effects of a SU(2) field.

In systems with Rashba spin-orbit coupling, there is a contribution to spin currents from the SU(2) gauge field that gives rise to a spin-torque in the spin-transport (see Eq. (6.15)), consistent with the semi-classical theory. Similar to the electromagnetic field inducing forces on charge and charge current, one can derive forces acting on spin and spin currents induced by Rashba spin-orbit coupling [125, 126, 127, 128].

The underlying physics can be described by making use of the Yang-Mills gauge theory. Within a gauge theory, the dynamics of a system remain unchanged under some local transformation acting on a field (a fermionic field in the case of the Yang-Mills theory, $\psi = (\psi_1(x), \psi_2(x))^T$ which transform

into one another via a rotation [26],

$$\psi \to \mathrm{e}^{\mathrm{i}\alpha^i(x)\sigma^i/2}\psi \ , \tag{6.16}$$

with $i = x, y, z$. The rotation if the spin in the physical space is generated by the Puali matrices σ^i. In order to maintain the system invariant under a local gauge transformation we need to introduce the three-component gauge field $\mathcal{A}_\mu$ in the expression of the covariant derivative,

$$D_\mu = \partial_\mu - \mathrm{i}\mathcal{A}_\mu^i \frac{\sigma^i}{2} \ . \tag{6.17}$$

Mathematically, $\mathcal{A}_\mu$ is a *connection* and acts as a comparator of local symmetries. That is to say, the gauge field $\mathcal{A}_\mu$ is introduced as a way to compare how the transformation in Eq. (6.16) acts differently in different points in space. As a result of introducing this gauge field, the field-strength of the Yang-Mills theory adopts the following form

$$\mathcal{F}_{\mu\nu} = \partial_\mu \mathcal{A}_\nu - \partial_\nu \mathcal{A}_\mu - \mathrm{i}\left[\mathcal{A}_\mu, \mathcal{A}_\nu\right] \ . \tag{6.18}$$

The presence of the commutator term in Eq. (6.18) is a direct consequence of the non-commuting nature of the generators of the SU(2) symmetry, which is why it receives the name of non-Abelian gauge theory. For a nanowire with Rashba spin-orbit coupling described by Hamiltonian Eq. (5.17) [129], the gauge field components are given by

$$\mathcal{A}_x = -m_e^* \alpha_x \sigma^y \ , \tag{6.19}$$

$$\mathcal{A}_y = m_e^* \alpha_y \sigma^x \ . \tag{6.20}$$

Substituting Eq. (6.19) into the expression for the field-strenght in Eq. (6.18) we obtain an additional term responsible for the spin precession

$$-\mathrm{i}\left[\mathcal{A}_x, \mathcal{A}_y\right] = m_e^2 \left(2\alpha_x \alpha_y \sigma^z\right) \ . \tag{6.21}$$

We now write the semiclassical equation of motion for the trajectory of an electron in the nanowire

$$\ddot{\hat{y}} + \omega_0^2 \left[\hat{y} + \frac{2\alpha_x \alpha_y}{\hbar\omega_0^2} \hat{p}_x \hat{\sigma}_z\right] = 0 \ . \tag{6.22}$$

Eq. (6.22) reflects the oscillatory movement of an electron inside a confinement potential with the center displace by a factor proportional to

$(2\alpha_x\alpha_y\sigma^z)$ that appears in Eq. (6.21). The physical interpretation of this displacement is that depending on the orientation of the spin-orbit field $F_{SO} \sim (2\alpha_x\alpha_y\sigma^z)$ the particle will "see" the center of the confinement in one direction or the opposite.

In Fig.6.13 we illustrate the behaviour of the SU(2) field in the nanowire as an electron propagates along it. One see that an electron describing a cyclic motion on a closed path in the 2DEG ($xy-$ plane) gives rise to a spin-orbital SU(2) field F_{SO}, while in (b) the field F_{SO} changes sign when the path is traversed in the opposite direction. Fig.6.13(c) sketches an electron moving uniformly in the nanowire with speed $v_n(E)$ along x. The trajectory undergoes an oscillatory motion along y with frequency ω_0, as governed by size quantization due to the potential $V(y)$. The area swept by the radius-vector of the electron during its motion is oscillating about zero average value, resulting in a consistently positive (negative) F_{SO} for the lower (upper) half of the wire. The fluctuating field F_{SO}, despite being zero on average, couples the electron spin to the central position y_0 of the electron wave function that is displaced with respect to to the center of the wire according to the orientation of the F_{SO} field. We can see the emergence of the $\sim (2\alpha_x\alpha_y)$ with origin in the $SU(2)$ symmetry in Eq. (6.1). This equation directly relates the spin-flip transmission probability to the effect of $SU(2)$ gauge.

In Fig.6.14 we sketch the different transport processes that may occur for an electron traveling in the x-direction. If the electron is prepared with spin-up, and its trajectory is in the lower half of the nanowire plane that results in a positive $SU(2)$ field F_{SO}, then the electron will "see" the impurity potential as if it were displaced from its position by a quantity $y_0 \approx 2\alpha_x\alpha_y k_x/\omega_0^2$. On the other hand, if the electron is describing a trajectory in the upper half of the nanowire plane that results in a negative $SU(2)$ field F_{SO}, then the electron will "see" the impurity potential as if it were displaced from its position by a quantity $-y_0$. Upon interference of both possible tranmission paths, we pick up a phase φ resulting in a tilt of the spin. In other words, at the resonant energy where the only allowed tranmission is through spin-flip a measurement of the conductance would serve to probe the $SU(2)$ gauge field.

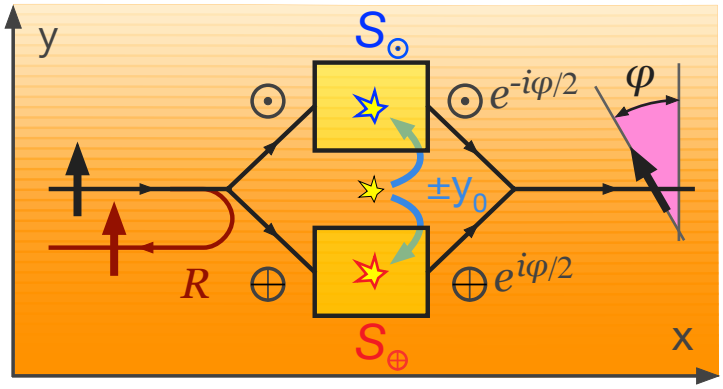

Figure 6.14: Transport mechanisms for an incoming spin-up state. Due to the $SU(2)$ there is a shift in the position of the impurity that depends on spin, as a consequence the spin picks up a phase translating in a tilt with respect to the quantization axis.

6.3 Conclusions

To summarize, in this the chapter we use the approaches developed in previous chapters of the thesis to study the transport properties of a nanowire with RSOC and a delta-like impurity. We first discuss the dip in the conductance that appears in the absence of Rashba spin-orbit interaction and its relation with the Fano resonance. In Subsection 6.1.2 we discuss the effect of RSOC on the transport and found a spin-flip transmission contribution as a consequence of the inter-band mixing mediated via an attractive impurity. As a consequence, we show that the presence of a quasi-bound state blocks the transmission channel that preserves spin, while it enhances the spin-flip transmission. In addition, we make a systematic study of the quasi-bound state resonant energy with respect to the lateral position and the strength of the impurity and recovering a result from the Chapter 4 that depends entirely on the spin-flip transmission, namely the torque. While there are effects of Rashba spin-orbit interaction of relevance in the charge conductance, our key result consists in finding the underlying relation between the spin-flip transmission and the $SU(2)$ field. At the resonant energy, the only

transmission allowed is through spin-flip permitting us to connect a physical quantity with the corresponding $SU(2)$ symmetry.

Chapter 7

Conclusions

The goal of this thesis is to formulate a theoretical model to study analytically electronic transport in quantum nanowires in the presence os Rashba spin-orbit interaction. The topic may have direct impact on the field of semiconducting and superconducting spintronics, and Majorana fermions. In general terms we have shown that the Rashba interaction in combination with an impurity and confinement potential affects drastically the charge and spin transport. At certain energies we found a hitherto unknown spin-flip transmission which is related to the appearance of a spin-orbit torque. Our theoretical results can be used in multiple ways to further studies on transport properties of confined systems in the presence of spin-dependent fields and impurities.

In the introductory Chapters 1 and 2, we describe the motivation behind our work and our goal of studying the properties of scattering from an impurity in a quasi-1D semiconducting nanowire with intrinsic spin-orbit coupling of Rashba type. We introduce the Lippmann-Schwinger equation, a useful method for the theoretical description of quantum scattering. In particular, we use this method to describe how the electronic transport is affected by the presence of the impurity in the nanowire. We first describe the approach in a general 3D system and later focus on scattering on a delta-potential in a purely 1D system, discussing the limitations of the Born approximation. Finally we focus on a more realistic nanowire described by a transverse confining potential, discussing the emergence of resonant behavior in the transmission as a consequence of quasi-bound states present in the nanowire. This effect arises from the localized impurity coupling the evanescent and propagating modes of the

nanowire. We focus the possible effects arising from the interplay between the Rashba interaction and the quasi-bound states.

Because the Rashba spin-orbit interaction plays a central role in this thesis, in Chapter 3 we provide an introduction in this topic. Specifically, we briefly discuss the spectral properties of a 2DEG with Rashba spin-orbit coupling before reviewing the complexities involved in the analytical solution of the model Hamiltonian for a quantum nanowire where the 2DEG is further confined. As a result of this confinement, the energy spectrum is strongly affected,as well as the spin polarization. The combined effect of RSOC and confinement gives raise to anti-crossings between branches of opposite spin and different band index, deforming the spectrum.These are a consequence of the subband mixing that couples propagating and evanescent states. We conclude that to address this problem enough subbands have to been taken into account. At the end of the chapter, we present an exact solution for the $k_x = 0$ that we use later as the zeroth order solution in our perturbation around the point $k_x = 0$. This calculation allows us to ensure the accuracy of our perturbative approach up to α^2 in Chapter 5.

In Chapter 4 we extend the widely used Landauer-Büttiker formalism to include the effect of the spin-orbit coupling for the description of the transport properties of the nanowire. We derive an expression for the spin current polarized along y-direction in the left lead considered to be far away from the impurity. This expression allow us to express such spin current as a function of the scattering coefficients of the S-matrix. Within this representation it is easy to track the contributions from the voltage and spin-biases. This result in combination with the expression for the spin current allowed us to describe the torque that arises at the impurity position, as a consequence of the spin-flip transport mechanisms resulting from the Rashba spin-orbit coupling. These mechanisms have important consequences on the conductance as discussed in subsequent chapters. Furthermore, we make a connection between our expressions and those obtained in the context of the spin-mixing conductance in magnetic hybrid structures.

In Chapter 5 we present a detailed derivation of the scattering coefficients for a short-range, delta- like impurity in a nanowire with Rashba spin-orbit coupling where electrons motion is confined in the y direction. We do this with the help of the Lippmann-Schwinger equation introduced in Chapter 2. The intersubband mixing, arising from the interplay between Rashba spin-orbit coupling and the harmonic

confinement, complicates the analytical solution of the equation. However, we deal with these difficulties by performing a Schrieffer-Wolff transformation. In this manner, we gauge away the intersubband mixing, up to second order in perturbation theory. As a result, the Green's function in the Lippmann-Schwinger can be obtained straightforwardly. On the other hand, the complexity is absorbed into the impurity potential or the eigenfunctions of the system. Consequently, the impurity, that is assumed from the beginning to be a scalar, acquires a spin-structure. From the form of the scattering coefficients we already understand that by scattering at the the impurity the electron spin may flip. Such spin-flip processes have important consequences on the transport properties of the wire, as discussed in the next chapter, where we use the results of Chapter 5 and previous chapters. We close the Chapter by describing a method to recover unitarity of the S-matrix within the perturbative approach used in the calculation.

Finally, we present the transport results in Chapter 6. Specifically, we use the approaches developed in previous chapters to study the transport properties of a nanowire with RSOC and a delta-like impurity. We first discussed the dip in the conductance that appears by scattering at a delta-like impurity in a nanowire in the absence of Rashba spin-orbit interaction and its relation with the Fano resonance. In Subsection 6.1.2 we discuss the effect of RSOC on the transport and found a spin-flip transmission contribution as a consequence of the inter-band mixing mediated via an attractive impurity. We show that the presence of a quasi-bound state blocks the transmission channel that preserves spin, while it enhances the spin-flip transmission. In addition, we make a systematic study of the quasi-bound state resonant energy with respect to the lateral position and the strength of the impurity. Another key result is the underlying relation between the spin-flip transmission and the $SU(2)$ field. At the resonant energy, the only transmission allowed is through spin-flip permitting us to connect a physical quantity with the corresponding $SU(2)$ symmetry.

Besides the effects discussed in this thesis, the methods developed here can be used in future research. We envision a possible application of the results from Chapter 6, namely the enhancement of spin-flip transmission, in the spirit of the Datta-Das spin-transistor introduced in Chapter 3. Indeed, one can design a device based on a nanowire in which one can externally tune the strength of the impurity potential and so, control the

spin-flip probability of injected electrons from a ferromagnetic lead. By tuning the chemical potential at the resonant energy, we can ensure that the spin of transmitted electrons is flipped. This application is in the spirit of previous works that extend the spin filter model to take advantage of Fano resonances in quantum dots [130] or side rings coupled to nanowires [131]. Moreover, the use these resonances has been already proposed in spin inversion devices based in semiconducting lattices with spin orbit-interaction and magnetic fields [132]. Furthermore, we can think of other ways to extend the study of disorder in nanowires. For example, placing a second defect and studying the possible spin-dependent transmission. In principle our methods, based on the scattering matrix, can be extended straightforwardly to two and more impurities.

One further perspective of the present work is its extension to include superconductivity and a Zeeman field and see what are the effects in the context of Majorana physics. Taking these two ingredients into account will be the next step in the theoretical approach to the scattering problem proposed in this thesis. Adding Zeeman to the Hamiltonian described in Eq.(5.1) would imply further work since the Greens function will be spin-dependent even in the absence of the impurity and additional terms in the Schriffer-Wolff transformation will appear. Moreover, introducing superconductivity require enlargement of the space to include the Nambu structure.

Another possible extension of our results, is the study of the Josephson current in a nanowire attached to two superconducting reservoirs. The Josephson current is an equilibrium current that can be determined from the knowledge of the subgap spectrum, Andreev bound sates . One can address the question how the quasi-bound states affects such spectrum and hence the Josephson current. According to Beennakker theory[133], the transport properties of such junction can be fully determine by the knowledge of the scattering matrix scattering matrix, that we know from our analysis. Moreover, if the superconducting leads consist of superconductors with a spin-split spectrum, induced by the proximity of a ferromagnetic insulating film [134], one can study how the Josephson current depends on the mutual direction of the magnetizations in the spin-split superconductors. By tuning the nanowire into the conductance dip, we know from our results, that transmission occurs together with spin-flip. This suggest that the Josephson current will be larger when the spin-split superconducting leads are in an antiparallel configuration. This

idea can be extended to multiterminal Josephson junctions where different topological states can be artificial created [135].

Bibliography

[1] R. M. Lutchyn, J. D. Sau, and S. Das Sarma, "Majorana fermions and a topological phase transition in semiconductor-superconductor heterostructures," *Phys. Rev. Lett.*, vol. 105, p. 077001, Aug 2010.

[2] Y. Oreg, G. Refael, and F. von Oppen, "Helical liquids and majorana bound states in quantum wires," *Phys. Rev. Lett.*, vol. 105, p. 177002, Oct 2010.

[3] A. Das, Y. Ronen, Y. Most, Y. Oreg, M. Heiblum, and H. Shtrikman, "Zero-bias peaks and splitting in an al–InAs nanowire topological superconductor as a signature of majorana fermions," *Nature Physics*, vol. 8, pp. 887–895, nov 2012.

[4] V. Mourik, K. Zuo, S. M. Frolov, S. R. Plissard, E. P. A. M. Bakkers, and L. P. Kouwenhoven, "Signatures of majorana fermions in hybrid superconductor-semiconductor nanowire devices," *Science*, vol. 336, pp. 1003–1007, apr 2012.

[5] M. T. Deng, C. L. Yu, G. Y. Huang, M. Larsson, P. Caroff, and H. Q. Xu, "Anomalous zero-bias conductance peak in a nb–InSb nanowire–nb hybrid device," *Nano Letters*, vol. 12, pp. 6414–6419, dec 2012.

[6] H. O. H. Churchill, V. Fatemi, K. Grove-Rasmussen, M. T. Deng, P. Caroff, H. Q. Xu, and C. M. Marcus, "Superconductor-nanowire devices from tunneling to the multichannel regime: Zero-bias oscillations and magnetoconductance crossover," *Phys. Rev. B*, vol. 87, p. 241401, Jun 2013.

[7] S. M. Albrecht, A. P. Higginbotham, M. Madsen, F. Kuemmeth, T. S. Jespersen, J. Nygård, P. Krogstrup, and C. M. Marcus, "Exponential

protection of zero modes in majorana islands," *Nature*, vol. 531, pp. 206–209, mar 2016.

[8] A. R. Akhmerov, J. P. Dahlhaus, F. Hassler, M. Wimmer, and C. W. J. Beenakker, "Quantized conductance at the majorana phase transition in a disordered superconducting wire," *Phys. Rev. Lett.*, vol. 106, p. 057001, Jan 2011.

[9] P. W. Brouwer, M. Duckheim, A. Romito, and F. von Oppen, "Probability distribution of majorana end-state energies in disordered wires," *Phys. Rev. Lett.*, vol. 107, p. 196804, Nov 2011.

[10] M. Wimmer, A. R. Akhmerov, J. P. Dahlhaus, and C. W. J. Beenakker, "Quantum point contact as a probe of a topological superconductor," *New Journal of Physics*, vol. 13, p. 053016, may 2011.

[11] J. Liu, A. C. Potter, K. T. Law, and P. A. Lee, "Zero-bias peaks in the tunneling conductance of spin-orbit-coupled superconducting wires with and without majorana end-states," *Phys. Rev. Lett.*, vol. 109, p. 267002, Dec 2012.

[12] F. Pientka, G. Kells, A. Romito, P. W. Brouwer, and F. von Oppen, "Enhanced zero-bias majorana peak in the differential tunneling conductance of disordered multisubband quantum-wire/superconductor junctions," *Phys. Rev. Lett.*, vol. 109, p. 227006, Nov 2012.

[13] D. Rainis, L. Trifunovic, J. Klinovaja, and D. Loss, "Towards a realistic transport modeling in a superconducting nanowire with majorana fermions," *Phys. Rev. B*, vol. 87, p. 024515, Jan 2013.

[14] D. I. Pikulin, J. P. Dahlhaus, M. Wimmer, H. Schomerus, and C. W. J. Beenakker, "A zero-voltage conductance peak from weak antilocalization in a majorana nanowire," *New Journal of Physics*, vol. 14, p. 125011, dec 2012.

[15] S. Datta and B. Das, "Electronic analog of the electrooptic modulator," *Applied Physics Letters*, vol. 56, no. 7, pp. 665–667, 1990.

[16] J. Nitta, T. Akazaki, H. Takayanagi, and T. Enoki, "Gate control of spin-orbit interaction in an inverted $\mathrm{in_{0.53}ga_{0.47}as/in_{0.52}al_{0.48}as}$ heterostructure," *Phys. Rev. Lett.*, vol. 78, pp. 1335–1338, Feb 1997.

[17] T. Schpers, G. Engels, J. Lange, T. Klocke, M. Hollfelder, and H. Lth, "Effect of the heterointerface on the spin splitting in modulation doped $\mathrm{In}_x\mathrm{Ga}_{1-x}\mathrm{As/InP}$ quantum wells for $b \to 0$," *Journal of Applied Physics*, vol. 83, no. 8, pp. 4324–4333, 1998.

[18] T. Schäpers, J. Knobbe, and V. A. Guzenko, "Effect of rashba spin-orbit coupling on magnetotransport in InGaAs/InP quantum wire structures," *Phys. Rev. B*, vol. 69, p. 235323, Jun 2004.

[19] A. V. Moroz and C. H. W. Barnes, "Effect of the spin-orbit interaction on the band structure and conductance of quasi-one-dimensional systems," *Phys. Rev. B*, vol. 60, pp. 14272–14285, Nov 1999.

[20] F. Mireles and G. Kirczenow, "Ballistic spin-polarized transport and rashba spin precession in semiconductor nanowires," *Phys. Rev. B*, vol. 64, p. 024426, Jun 2001.

[21] M. Governale and U. Zülicke, "Spin accumulation in quantum wires with strong rashba spin-orbit coupling," *Phys. Rev. B*, vol. 66, p. 073311, Aug 2002.

[22] C. A. Perroni, D. Bercioux, V. M. Ramaglia, and V. Cataudella, "Rashba quantum wire: exact solution and ballistic transport," *Journal of Physics: Condensed Matter*, vol. 19, p. 186227, apr 2007.

[23] P. F. Bagwell, "Evanescent modes and scattering in quasi-one-dimensional wires," *Phys. Rev. B*, vol. 41, pp. 10354–10371, May 1990.

[24] C. Kunze and R. Lenk, "A single scatterer in a quantum wire: Compact reformulation of scattering and transmission," *Solid state communications*, vol. 84, no. 4, pp. 457–461, 1992.

[25] M. Trif, V. N. Golovach, and D. Loss, "Spin dynamics in inas nanowire quantum dots coupled to a transmission line," *Physical Review B*, vol. 77, no. 4, p. 045434, 2008.

[26] M. E. Peskin, *An introduction to quantum field theory*. CRC Press, 2018.

[27] M. Moskalets, P. Samuelsson, and M. Büttiker, "Quantized dynamics of a coherent capacitor," *Physical review letters*, vol. 100, no. 8, p. 086601, 2008.

[28] C. H. L. Quay, T. L. Hughes, J. A. Sulpizio, L. N. Pfeiffer, K. W. Baldwin, K. W. West, D. Goldhaber-Gordon, and R. de Picciotto, "Observation of a one-dimensional spin–orbit gap in a quantum wire," *Nature Physics*, vol. 6, pp. 336–339, mar 2010.

[29] J. Kammhuber, M. C. Cassidy, F. Pei, M. P. Nowak, A. Vuik, D. Car, S. R. Plissard, E. P. M. Bakkers, M. Wimmer, and L. P. Kouwenhoven, "Conductance through a helical state in an InSb nanowire," *ArXiv e-prints*, Jan. 2017.

[30] J. Kammhuber, M. C. Cassidy, H. Zhang, Önder Gül, F. Pei, M. W. A. de Moor, B. Nijholt, K. Watanabe, T. Taniguchi, D. Car, S. R. Plissard, E. P. A. M. Bakkers, and L. P. Kouwenhoven, "Conductance quantization at zero magnetic field in InSb nanowires," *Nano Letters*, vol. 16, pp. 3482–3486, jun 2016.

[31] J. Gooth, V. Schaller, S. Wirths, H. Schmid, M. Borg, N. Bologna, S. Karg, and H. Riel, "Ballistic one-dimensional transport in InAs nanowires monolithically integrated on silicon," *Applied Physics Letters*, vol. 110, p. 083105, feb 2017.

[32] F. Bergeret, A. F. Volkov, and K. B. Efetov, "Odd triplet superconductivity and related phenomena in superconductor-ferromagnet structures," *Reviews of modern physics*, vol. 77, no. 4, p. 1321, 2005.

[33] J. Linder and J. W. Robinson, "Superconducting spintronics," *Nature Physics*, vol. 11, no. 4, pp. 307–315, 2015.

[34] M. Eschrig, "Spin-polarized supercurrents for spintronics," *Phys. Today*, vol. 64, no. 1, p. 43, 2011.

[35] F. Bergeret and I. Tokatly, "Spin-orbit coupling as a source of long-range triplet proximity effect in superconductor-ferromagnet hybrid structures," *Physical Review B*, vol. 89, no. 13, p. 134517, 2014.

[36] V. Gudmundsson, Y.-Y. Lin, C.-S. Tang, V. Moldoveanu, J. H. Bardarson, and A. Manolescu, "Transport through a quantum ring, dot, and barrier embedded in a nanowire in magnetic field," *Physical Review B*, vol. 71, no. 23, p. 235302, 2005.

[37] S. Tsukamoto and K. Hirose, "Electron-transport properties of na nanowires under applied bias voltages," *Physical Review B*, vol. 66, no. 16, p. 161402, 2002.

[38] J.-C. Weeber, A. Dereux, C. Girard, J. R. Krenn, and J.-P. Goudonnet, "Plasmon polaritons of metallic nanowires for controlling submicron propagation of light," *Physical Review B*, vol. 60, no. 12, p. 9061, 1999.

[39] C. Wan, J.-L. Mozos, G. Taraschi, J. Wang, and H. Guo, "Quantum transport through atomic wires," *Applied physics letters*, vol. 71, no. 3, pp. 419–421, 1997.

[40] D. C. Tsui, H. L. Stormer, and A. C. Gossard, "Two-Dimensional Magnetotransport in the Extreme Quantum Limit," *Phys. Rev. Lett.*, vol. 48, pp. 1559–1562, May 1982.

[41] B. L. Altshuler, P. A. Lee, and W. R. Webb, *Mesoscopic Phenomena in Solids.* Amsterdam: Elsevier Science, 2014. OCLC: 1044730981.

[42] A. B. Fowler, F. F. Fang, W. E. Howard, and P. J. Stiles, "Magneto-Oscillatory Conductance in Silicon Surfaces," *Phys. Rev. Lett.*, vol. 16, pp. 901–903, May 1966.

[43] E. Lifshits and A. Kosevich, "Theory of the Shubnikovde Haas effect," *Journal of Physics and Chemistry of Solids*, vol. 4, pp. 1–10, Jan. 1958.

[44] K. von Klitzing, "The quantized Hall effect," *Rev. Mod. Phys.*, vol. 58, pp. 519–531, July 1986.

[45] R. B. Laughlin, "Nobel Lecture: Fractional quantization," *Rev. Mod. Phys.*, vol. 71, pp. 863–874, July 1999.

[46] H. L. Stormer, D. C. Tsui, and A. C. Gossard, "The fractional quantum Hall effect," *Rev. Mod. Phys.*, vol. 71, pp. S298–S305, Mar. 1999.

[47] D. C. Tsui, "Nobel Lecture: Interplay of disorder and interaction in two-dimensional electron gas in intense magnetic fields," *Rev. Mod. Phys.*, vol. 71, pp. 891–895, July 1999.

[48] B. Van Wees, H. Van Houten, C. Beenakker, J. G. Williamson, L. Kouwenhoven, D. Van der Marel, and C. Foxon, "Quantized conductance of point contacts in a two-dimensional electron gas," *Physical Review Letters*, vol. 60, no. 9, p. 848, 1988.

[49] L. L. Sohn, L. P. Kouwenhoven, and G. Schn, *Mesoscopic Electron Transport.* Dordrecht: Springer Netherlands, 2010. OCLC: 958542184.

[50] S. Datta, *Electronic Transport in Mesoscopic Systems.* Cambridge: Cambridge University Press, 1995.

[51] T. Ando, A. B. Fowler, and F. Stern, "Electronic properties of two-dimensional systems," *Rev. Mod. Phys.*, vol. 54, pp. 437–672, Apr. 1982.

[52] D. á. Tsui, "Observation of surface bound state and two-dimensional energy band by electron tunneling," *Physical review letters*, vol. 24, no. 7, p. 303, 1970.

[53] C. Beenakker and H. van Houten, "Quantum Transport in Semiconductor Nanostructures," in *Solid State Physics*, vol. 44, pp. 1–228, Elsevier, 1991.

[54] D. K. Ferry, S. M. Goodnick, and J. P. Bird, *Transport in nanostructures.* Cambridge, UK ; New York: Cambridge University Press, 2nd ed ed., 2009. OCLC: ocn316824259.

[55] P. Havu, M. J. Puska, R. M. Nieminen, and V. Havu, "Electron transport through quantum wires and point contacts," *Phys. Rev. B*, vol. 70, p. 233308, Dec. 2004.

[56] J. J. Sakurai and E. D. Commins, "Modern quantum mechanics, revised edition," 1995.

[57] S. Gurvitz and Y. Levinson, "Resonant reflection and transmission in a conducting channel with a single impurity," *Physical Review B*, vol. 47, no. 16, p. 10578, 1993.

[58] E. Tekman and P. F. Bagwell, "Fano resonances in quasi-one-dimensional electron waveguides," *Physical Review B*, vol. 48, no. 4, p. 2553, 1993.

[59] C. S. Kim, O. Roznova, A. Satanin, and V. Stenberg, "Interference of quantum states in electronic waveguides with impurities," *Journal of Experimental and Theoretical Physics*, vol. 94, no. 5, pp. 992–1007, 2002.

[60] P. F. Bagwell, "Solution of dyson's equation in a quasi-1d wire," *Journal of Physics: Condensed Matter*, vol. 2, no. 28, p. 6179, 1990.

[61] E. Tekman and S. Ciraci, "Theoretical study of transport through a quantum point contact," *Physical Review B*, vol. 43, no. 9, p. 7145, 1991.

[62] C. Chu and R. Sorbello, "Effect of impurities on the quantized conductance of narrow channels," *Physical Review B*, vol. 40, no. 9, p. 5941, 1989.

[63] D. Boese, M. Lischka, and L. Reichl, "Resonances in a two-dimensional electron waveguide with a single δ-function scatterer," *Physical Review B*, vol. 61, no. 8, p. 5632, 2000.

[64] D. Boese, M. Lischka, and L. E. Reichl, "Scaling behavior in a quantum wire with scatterers," *Physical Review B*, vol. 62, no. 24, p. 16933, 2000.

[65] V. Vargiamidis, O. Valassiades, and D. Kyriakos, "Lippmann-schwinger equation approach to scattering in quantum wires," *physica status solidi (b)*, vol. 236, no. 3, pp. 597–613, 2003.

[66] A. Kumar and P. F. Bagwell, "Resonant tunneling in a quasi-one-dimensional wire: Influence of evanescent modes," *Physical Review B*, vol. 43, no. 11, p. 9012, 1991.

[67] C. S. Kim, A. M. Satanin, Y. S. Joe, and R. M. Cosby, "Resonant tunneling in a quantum waveguide: effect of a finite-size attractive impurity," *Physical Review B*, vol. 60, no. 15, p. 10962, 1999.

[68] C. Tang and C. Chu, "Coherent quantum transport in narrow constrictions in the presence of a finite-range longitudinally polarized time-dependent field," *Physical Review B*, vol. 60, no. 3, p. 1830, 1999.

[69] J. H. Bardarson, I. Magnusdottir, G. Gudmundsdottir, C.-S. Tang, A. Manolescu, and V. Gudmundsson, "Coherent electronic transport in a multimode quantum channel with gaussian-type scatterers," *Physical Review B*, vol. 70, no. 24, p. 245308, 2004.

[70] C. Kunze and P. F. Bagwell, "Fano resonances in the magnetoresistance of a quantum wire doped with magnetic impurities," *Physical Review B*, vol. 51, no. 19, p. 13410, 1995.

[71] H. Tamura and T. Ando, "Conductance fluctuations in quantum wires," *Physical Review B*, vol. 44, no. 4, p. 1792, 1991.

[72] P. F. Bagwell and R. K. Lake, "Resonances in transmission through an oscillating barrier," *Physical Review B*, vol. 46, no. 23, p. 15329, 1992.

[73] C. Chu and C. Tang, "Effects of a time-dependent transverse electric field on the quantum transport in narrow channels," *Solid state communications*, vol. 97, no. 3, pp. 243–247, 1996.

[74] H. A. Nilsson, P. Caroff, C. Thelander, M. Larsson, J. B. Wagner, L.-E. Wernersson, L. Samuelson, and H. Xu, "Giant, level-dependent g factors in insb nanowire quantum dots," *Nano letters*, vol. 9, no. 9, pp. 3151–3156, 2009.

[75] S. Nadj-Perge, V. Pribiag, J. Van den Berg, K. Zuo, S. Plissard, E. Bakkers, S. Frolov, and L. Kouwenhoven, "Spectroscopy of spin-orbit quantum bits in indium antimonide nanowires," *Physical review letters*, vol. 108, no. 16, p. 166801, 2012.

[76] S. E. Hernández, M. Akabori, K. Sladek, C. Volk, S. Alagha, H. Hardtdegen, M. Pala, N. Demarina, D. Grützmacher, and T. Schäpers, "Spin-orbit coupling and phase coherence in inas nanowires," *Physical Review B*, vol. 82, no. 23, p. 235303, 2010.

[77] R. Winkler, "Spin-orbit coupling effects in two-dimensional electron and hole systems," *Springer Tracts in Modern Physics*, vol. 191, pp. 1–8, 2003.

[78] G. Dresselhaus, "Spin-orbit coupling effects in zinc blende structures," *Physical Review*, vol. 100, no. 2, p. 580, 1955.

[79] Y. A. Bychkov and E. I. Rashba, "Oscillatory effects and the magnetic susceptibility of carriers in inversion layers," *Journal of physics C: Solid state physics*, vol. 17, no. 33, p. 6039, 1984.

[80] H. C. Koo, J. H. Kwon, J. Eom, J. Chang, S. H. Han, and M. Johnson, "Control of spin precession in a spin-injected field effect transistor," *Science*, vol. 325, no. 5947, pp. 1515–1518, 2009.

[81] P. Chuang, S.-C. Ho, L. W. Smith, F. Sfigakis, M. Pepper, C.-H. Chen, J.-C. Fan, J. Griffiths, I. Farrer, H. E. Beere, *et al.*, "All-electric all-semiconductor spin field-effect transistors," *Nature nanotechnology*, vol. 10, no. 1, p. 35, 2015.

[82] J. Nitta, T. Akazaki, H. Takayanagi, and T. Enoki, "Gate control of spin-orbit interaction in an inverted i n 0.53 g a 0.47 as/i n 0.52 a l 0.48 as heterostructure," *Physical Review Letters*, vol. 78, no. 7, p. 1335, 1997.

[83] T. Schäpers, G. Engels, J. Lange, T. Klocke, M. Hollfelder, and H. Lüth, "Effect of the heterointerface on the spin splitting in modulation doped in x ga 1- x as/inp quantum wells for b 0," *Journal of applied physics*, vol. 83, no. 8, pp. 4324–4333, 1998.

[84] D. Grundler, "Large rashba splitting in inas quantum wells due to electron wave function penetration into the barrier layers," *Physical review letters*, vol. 84, no. 26, p. 6074, 2000.

[85] J. Miller, D. Zumbühl, C. Marcus, Y. B. Lyanda-Geller, D. Goldhaber-Gordon, K. Campman, and A. Gossard, "Gate-controlled spin-orbit quantum interference effects in lateral transport," *Physical review letters*, vol. 90, no. 7, p. 076807, 2003.

[86] L. Meier, G. Salis, I. Shorubalko, E. Gini, S. Schön, and K. Ensslin, "Measurement of rashba and dresselhaus spin–orbit magnetic fields," *Nature Physics*, vol. 3, no. 9, p. 650, 2007.

[87] J. Alicea, Y. Oreg, G. Refael, F. Von Oppen, and M. P. Fisher, "Non-abelian statistics and topological quantum information processing in 1d wire networks," *Nature Physics*, vol. 7, no. 5, p. 412, 2011.

[88] N. Read and D. Green, "Paired states of fermions in two dimensions with breaking of parity and time-reversal symmetries and the fractional quantum hall effect," *Physical Review B*, vol. 61, no. 15, p. 10267, 2000.

[89] D. A. Ivanov, "Non-abelian statistics of half-quantum vortices in p-wave superconductors," *Physical review letters*, vol. 86, no. 2, p. 268, 2001.

[90] A. Stern, F. von Oppen, and E. Mariani, "Geometric phases and quantum entanglement as building blocks for non-abelian quasiparticle statistics," *Physical Review B*, vol. 70, no. 20, p. 205338, 2004.

[91] D. Bercioux and P. Lucignano, "Quantum transport in rashba spin–orbit materials: a review," *Reports on Progress in Physics*, vol. 78, no. 10, p. 106001, 2015.

[92] D. Sánchez and L. Serra, "Fano-rashba effect in a quantum wire," *Physical Review B*, vol. 74, no. 15, p. 153313, 2006.

[93] R. Landauer, "Spatial variation of currents and fields due to localized scatterers in metallic conduction," *IBM Journal of Research and Development*, vol. 1, no. 3, pp. 223–231, 1957.

[94] A. D. Stone and A. Szafer, "What is measured when you measure a resistance?the landauer formula revisited," *IBM Journal of Research and Development*, vol. 32, no. 3, pp. 384–413, 1988.

[95] M. Moskalets, *LandauerBttiker formalism*, pp. 1–33. 09 2011.

[96] X. Waintal, E. B. Myers, P. W. Brouwer, and D. Ralph, "Role of spin-dependent interface scattering in generating current-induced torques in magnetic multilayers," *Physical Review B*, vol. 62, no. 18, p. 12317, 2000.

[97] A. A. Kiselev and K. W. Kim, "T-shaped ballistic spin filter," *Applied Physics Letters*, vol. 78, no. 6, pp. 775–777, 2001.

[98] T. Pareek, "Pure spin currents and the associated electrical voltage," *Physical review letters*, vol. 92, no. 7, p. 076601, 2004.

[99] M. Wu and J. Zhou, "Spin-hall effect in two-dimensional mesoscopic hole systems," *Physical Review B*, vol. 72, no. 11, p. 115333, 2005.

[100] B. K. Nikolić, L. P. Zârbo, and S. Souma, "Mesoscopic spin hall effect in multiprobe ballistic spin-orbit-coupled semiconductor bridges," *Physical Review B*, vol. 72, no. 7, p. 075361, 2005.

[101] L. Sheng, D. Sheng, and C. Ting, "Spin-hall effect in two-dimensional electron systems with rashba spin-orbit coupling and disorder," *Physical review letters*, vol. 94, no. 1, p. 016602, 2005.

[102] P. Brusheim and H. Xu, "Spin filtering through magnetic-field-modulated double quantum dot structures," *Physical Review B*, vol. 73, no. 4, p. 045313, 2006.

[103] H.-F. Lü and Y. Guo, "Pure spin current in a three-terminal spin device in the presence of rashba spin-orbit interaction," *Applied Physics Letters*, vol. 91, no. 9, p. 092128, 2007.

[104] P. Brusheim, D. Csontos, U. Zülicke, and H. Xu, "Multiterminal multimode spin-dependent scattering matrix formalism: Electron and hole quantum spin transport in multiterminal junctions," *Physical Review B*, vol. 78, no. 8, p. 085301, 2008.

[105] K. Shen and M. Wu, "Robust strongly modulated transmission of a t-shaped structure with local rashba interaction," *Physical Review B*, vol. 77, no. 19, p. 193305, 2008.

[106] S. Bellucci and P. Onorato, "Spin filtering and spin hall accumulation in an interferometric ballistic nanojunction with rashba spin-orbit interaction," *Physical Review B*, vol. 77, no. 7, p. 075303, 2008.

[107] V. Fadeev and A. Umerski, "Application of the landauer formalism to the calculation of spin current," *arXiv preprint arXiv:1906.06097*, 2019.

[108] A. Brataas, Y. V. Nazarov, and G. E. Bauer, "Finite-element theory of transport in ferromagnet–normal metal systems," *Physical review letters*, vol. 84, no. 11, p. 2481, 2000.

[109] Y. M. Blanter and M. Büttiker, "Shot noise in mesoscopic conductors," *Physics reports*, vol. 336, no. 1-2, pp. 1–166, 2000.

[110] A. Prêtre, H. Thomas, and M. Büttiker, "Dynamic admittance of mesoscopic conductors: Discrete-potential model," *Physical Review B*, vol. 54, no. 11, p. 8130, 1996.

[111] G. Feve, W. Oliver, M. Aranzana, and Y. Yamamoto, "Rashba effect within the coherent scattering formalism," *Physical Review B*, vol. 66, no. 15, p. 155328, 2002.

[112] M. Eto, T. Hayashi, and Y. Kurotani, "Spin polarization at semiconductor point contacts in absence of magnetic field," *Journal of the Physical Society of Japan*, vol. 74, no. 7, pp. 1934–1937, 2005.

[113] J. R. Schrieffer and P. A. Wolff, "Relation between the anderson and kondo hamiltonians," *Physical Review*, vol. 149, no. 2, p. 491, 1966.

[114] S. Bravyi, D. P. DiVincenzo, and D. Loss, "Schrieffer–wolff transformation for quantum many-body systems," *Annals of physics*, vol. 326, no. 10, pp. 2793–2826, 2011.

[115] V. N. Golovach, M. Borhani, and D. Loss, "Electric-dipole-induced spin resonance in quantum dots," *Physical Review B*, vol. 74, no. 16, p. 165319, 2006.

[116] V. N. Golovach, A. Khaetskii, and D. Loss, "Spin relaxation at the singlet-triplet crossing in a quantum dot," *Physical Review B*, vol. 77, no. 4, p. 045328, 2008.

[117] S. Datta, M. Cahay, and M. McLennan, "Scatter-matrix approach to quantum transport," *Physical Review B*, vol. 36, no. 10, p. 5655, 1987.

[118] M. Cahay, M. McLennan, and S. Datta, "Conductance of an array of elastic scatterers: A scattering-matrix approach," *Physical Review B*, vol. 37, no. 17, p. 10125, 1988.

[119] A. E. Miroshnichenko, S. Flach, and Y. S. Kivshar, "Fano resonances in nanoscale structures," *Reviews of Modern Physics*, vol. 82, no. 3, p. 2257, 2010.

[120] U. Fano, "Effects of configuration interaction on intensities and phase shifts," *Physical Review*, vol. 124, no. 6, p. 1866, 1961.

[121] A. Rau, "Perspectives on the fano resonance formula," *Physica Scripta*, vol. 69, no. 1, p. C10, 2004.

[122] V. Vargiamidis, V. Fessatidis, and N. J. Horing, "Electric-field effects on fano resonances and transmission phase through quantum wires," *Journal of Applied Physics*, vol. 106, no. 4, p. 043710, 2009.

[123] D. Sánchez, L. Serra, and M.-S. Choi, "Strongly modulated transmission of a spin-split quantum wire with local rashba interaction," *Physical Review B*, vol. 77, no. 3, p. 035315, 2008.

[124] J. S. Lim, L. Serra, R. López, and R. Aguado, "Magnetic-field instability of majorana modes in multiband semiconductor wires," *Physical Review B*, vol. 86, no. 12, p. 121103, 2012.

[125] P.-Q. Jin, Y.-Q. Li, and F.-C. Zhang, "Su (2) xu (1) unified theory for charge, orbit and spin currents," *Journal of Physics A: Mathematical and General*, vol. 39, no. 35, p. 11129, 2006.

[126] A. Rebei and O. Heinonen, "Spin currents in the rashba model in the presence of nonuniform fields," *Physical Review B*, vol. 73, no. 15, p. 153306, 2006.

[127] N. Hatano, R. Shirasaki, and H. Nakamura, "Non-abelian gauge field theory of the spin-orbit interaction and a perfect spin filter," *Physical Review A*, vol. 75, no. 3, p. 032107, 2007.

[128] B. Leurs, Z. Nazario, D. Santiago, and J. Zaanen, "Non-abelian hydrodynamics and the flow of spin in spin–orbit coupled substances," *Annals of Physics*, vol. 323, no. 4, pp. 907–945, 2008.

[129] I. Tokatly, "Equilibrium spin currents: non-abelian gauge invariance and color diamagnetism in condensed matter," *Physical review letters*, vol. 101, no. 10, p. 106601, 2008.

[130] J. Song, Y. Ochiai, and J. Bird, "Fano resonances in open quantum dots and their application as spin filters," *Applied physics letters*, vol. 82, no. 25, pp. 4561–4563, 2003.

[131] M. Lee and C. Bruder, "Spin filter using a semiconductor quantum ring side coupled to a quantum wire," *Physical Review B*, vol. 73, no. 8, p. 085315, 2006.

[132] J. Cardoso and P. Pereyra, "Spin inversion devices operating at fano anti-resonances," *EPL (Europhysics Letters)*, vol. 83, no. 3, p. 38001, 2008.

[133] C. Beenakker, "Universal limit of critical-current fluctuations in mesoscopic josephson junctions," *Physical review letters*, vol. 67, no. 27, p. 3836, 1991.

[134] F. S. Bergeret, M. Silaev, P. Virtanen, and T. T. Heikkilä, "Colloquium: Nonequilibrium effects in superconductors with a spin-splitting field," *Reviews of Modern Physics*, vol. 90, no. 4, p. 041001, 2018.

[135] E. Strambini, S. D'Ambrosio, F. Vischi, F. Bergeret, Y. V. Nazarov, and F. Giazotto, "The ω-squipt as a tool to phase-engineer josephson topological materials," *Nature nanotechnology*, vol. 11, no. 12, p. 1055, 2016.

Appendix A

1D Green's function

For the resolution of the Lippmann-Schwinger equation for a 1D system, Eq.(2.16), we will need the Green's function for the Helmholtz equation,

$$\left(\nabla^2 + k^2\right) G_{\pm}\left(\mathbf{x}, \mathbf{x}'\right) = \frac{2m_e^*}{\hbar^2}\delta\left(\mathbf{x}, \mathbf{x}'\right) \ . \tag{A.1}$$

This requires the evaluation of,

$$G_{\pm}\left(\mathbf{x}, \mathbf{x}'\right) = \langle \mathbf{x}| \frac{1}{E - H_0 \pm \mathrm{i}\epsilon} |\mathbf{x}'\rangle \ . \tag{A.2}$$

Then,

$$\begin{aligned} G_{\pm}\left(\mathbf{x}, \mathbf{x}'\right) \quad &= \int_{-\infty}^{\infty} \frac{d\mathbf{p}}{2\pi\hbar} \langle \mathbf{x}| \frac{1}{E - H_0 \pm \mathrm{i}\epsilon} |\mathbf{p}\rangle\langle \mathbf{p}|\mathbf{x}'\rangle \\ &= \int_{-\infty}^{\infty} \frac{d\mathbf{K}}{2\pi} \frac{\mathrm{e}^{\mathbf{i}\mathbf{p}\mathbf{x}/\hbar}}{\frac{\mathbf{p}^2}{2m_e^*} - (E \pm \mathrm{i}\epsilon)} \mathrm{e}^{-\mathbf{i}\mathbf{p}\mathbf{x}'/\hbar} \\ &= \frac{1}{2\pi}\frac{2m_e^*}{\hbar^2} \int_{-\infty}^{\infty} d\mathbf{K} \frac{\mathrm{e}^{\mathbf{i}\mathbf{K}(\mathbf{x}-\mathbf{x}')}}{\mathbf{K}^2 - \frac{2m_e^*}{\hbar^2}\left(E \pm \mathrm{i}\epsilon\right)} \ , \end{aligned} \tag{A.3}$$

with poles given by

$$K = \pm k\sqrt{1 \pm \mathrm{i}\frac{2m\epsilon}{\hbar^2 k^2}} \simeq \pm k\left(1 \pm \mathrm{i}\frac{m_e^*\epsilon}{\hbar k}\right) \ . \tag{A.4}$$

The problem then can be solved using Cauchy's integral formula,

$$\oint_C f(z)\, dz = 2\pi\mathrm{i} \times (\text{sum of residues enclosed by C}) \ , \tag{A.5}$$

where C is the contour defining the path of integration, taken counter-clockwise for the upper half-plane and clockwise for the lower half-plane. For $E \geq 0$ and taking into account Eq.(A.5) for the poles in Eq. (A.4) in Eq.(A.3), then

$$\begin{aligned} G_{\pm}(\mathbf{x}, \mathbf{x}') &= \frac{2m_e^*}{\hbar^2}\frac{\mathrm{i}}{2k}\{\mp \mathrm{e}^{\pm \mathrm{i}k(x-x')}|_{x>x'} \mp \mathrm{e}^{\mp \mathrm{i}k(x-x')}|_{x<x'}\} \\ &= \mp\frac{2m_e^*}{\hbar^2}\frac{\mathrm{i}}{2k}\mathrm{e}^{\pm \mathrm{i}k|x-x'|} \ . \end{aligned} \tag{A.6}$$

The $\pm$ in the Green's function $G_{\pm}(\mathbf{x}, \mathbf{x}')$ corresponds to the incoming $(-)$ or outgoing $(+)$ boundary conditions, which means taht for the positive exponent we close in the upper half-plane and include the pole $(+k + \mathrm{i}\epsilon)$ and for the negative exponent we close in the lower half-pane and include $(-k - \mathrm{i}\epsilon)$.

Appendix B

Ensuring Kramers reversivility

The introduction of the notations $\langle\!\langle G_s \rangle\!\rangle$ and $\langle\!\langle \partial^2 G_a \rangle\!\rangle$ in Chapter 5, led us to the following expression for the bound-states,

$$1 + v_0 \left(\langle\!\langle G_s \rangle\!\rangle \pm \frac{2\alpha_x \alpha_y}{\omega_0^2} \langle\!\langle \partial^2 G_a \rangle\!\rangle \right) = 0 \, . \tag{B.1}$$

According to the Kramers theorem, the two solutions obtained from this equation (for the $\pm$ sign) must be degenerate. Therefore, we strongly suspect that $\langle\!\langle \partial^2 G_a \rangle\!\rangle$ has to vanish.

In Chapter 5 we introduce the short notations:

$$\langle\!\langle G_{\rm s} \rangle\!\rangle = \frac{1}{v_0} \int G_{\rm s}(\boldsymbol{r}_0, \boldsymbol{r}') V_{\rm imp}(\boldsymbol{r}') d^2 r', \tag{B.2}$$

$$\left\langle\!\!\left\langle \partial^2 G_{\rm a} \right\rangle\!\!\right\rangle = \frac{1}{v_0} \int \left[\partial_x \left(\partial_{y'} - \partial_y \right) G_{\rm a}(\boldsymbol{r}, \boldsymbol{r}') \right]\big|_{\boldsymbol{r}=\boldsymbol{r}_0} V_{\rm imp}(\boldsymbol{r}') d^2 r' \, . \tag{B.3}$$

$$\tag{B.4}$$

Let us model the scatterer potential as

$$\begin{aligned} V_{\rm imp}(x,y) &= V_0 e^{-\frac{(x-x_0)^2}{2\sigma^2}} e^{-\frac{(y-y_0)^2}{2\sigma^2}} \\ &= v_0 \delta_\sigma(x - x_0) \delta_\sigma(y - y_0), \end{aligned} \tag{B.5}$$

where $v_0 = 2\pi\sigma^2 V_0$ is the strenght of the impurity, V_0 is the height and we define the δ-like potential as

$$\delta_\sigma(x) := \frac{1}{\sqrt{2\pi}\sigma} e^{-\frac{x^2}{2\sigma^2}}. \tag{B.6}$$

The support of the integral, Eq.(B.2), is centered around $\boldsymbol{r}' = \boldsymbol{r}_0$ within a circle of radius $a \sim \sigma$.

The following integral is useful

$$\int_{-\infty}^{+\infty} dx' e^{ik_n|x_0-x'|}\delta_\sigma(x'-x_0) = e^{-\frac{1}{2}k_n^2\sigma^2}\left[1+\mathrm{erf}\left(i\frac{k_n\sigma}{\sqrt{2}}\right)\right]. \quad \text{(B.7)}$$

Since $\mathrm{erf}(0) = 0$ and the exponential tends to 1, we have this integral to be 1 in the limit $\sigma \to 0$. Another useful integral is

$$\begin{aligned}\int_{-\infty}^{+\infty} dy'\Phi_n^*(y')\delta_\sigma(y'-y_0) &= \frac{1}{\sqrt{2^n n!\sqrt{\pi}\lambda}}\sqrt{\frac{\lambda^2}{\lambda^2+\sigma^2}}\left(\frac{\lambda^2-\sigma^2}{\lambda^2+\sigma^2}\right)^{n/2} \\ &\times H_n\left(\frac{y_0\lambda}{\sqrt{\lambda^4-\sigma^4}}\right)\exp\left[-\frac{y_0^2}{2(\lambda^2+\sigma^2)}\right]. \quad \text{(B.8)}\end{aligned}$$

This integral in the limit $\sigma \to 0$ is equal to the transversal wavefunction at the impurity position $\Phi_n(y_0)$. As a result, from Eqs.(B.7) and (B.8) in the point-like limit, Eq. (B.2) becomes,

$$\langle\!\langle G_\mathrm{s}\rangle\!\rangle = \Phi_n^*(y_0)\,\Phi_n(y_0)\ . \quad \text{(B.9)}$$

For the calculation of Eq.(B.3) it is sufficient to focus on the y' integral. Taking into account that the partial derivative of G_a as defined in (5.54) is,

$$\partial_{y'}G_a = \frac{1}{\sqrt{2^n n!\sqrt{pi}\lambda}}\left\{\frac{2n}{\lambda}H_{n-1}(y'/\lambda) - \frac{y'}{\lambda^2}H_n(y'/\lambda)\right\}\mathrm{e}^{-y'^2/\lambda^2}\Phi_n(y)\ , \quad \text{(B.10)}$$

we can write the following integral for the y' dependence of Eq.(B.3),

$$\begin{aligned}\int_{-\infty}^{\infty} dy'(\partial_{y'}-\partial_y)G_a\delta_\sigma(y-y_0) &= \frac{\mathrm{e}^{-y_0^2/2\left(\lambda^2+\sigma^2\right)}\Phi_n(y_0)}{\sqrt{2^n n!\sqrt{pi}\lambda}} \\ &\times\left\{\frac{2n}{\lambda^2+\sigma^2}\left(\frac{\lambda^2-\sigma^2}{\lambda^2+\sigma^2}\right)^{n-1/2}H_{n-1}\left[\frac{\lambda y_0}{\sqrt{\lambda^4-\sigma^4}}\right]\right. \\ &-\frac{\sigma^2}{\lambda^2+\sigma^2}\left(\frac{\lambda^2-\sigma^2}{\lambda^2+\sigma^2}\right)^{n-1/2}H_{n-1}\left[\frac{\lambda y_0}{\sqrt{\lambda^4-\sigma^4}}\right] \\ &\left.-y_0\frac{1}{\lambda^2+\sigma^2}\sqrt{\frac{\lambda^2}{\lambda^2+\sigma^2}}\left(\frac{\lambda^2-\sigma^2}{\lambda^2+\sigma^2}\right)^{n/2}H_n\left[\frac{\lambda y_0}{\sqrt{\lambda^4-\sigma^4}}\right]\right\} \quad \text{(B.11)}\end{aligned}$$

Then, in the limit of $\sigma \to 0$ the term with factor $\sigma^2/\lambda^2 + \sigma^2$ becomes zero while the two other terms cancel each other by the recursion relation of the Hermite polynomials.

Appendix C

Effective One-Dimensional Impurity Potential

This result is used in Chapter 6. In this appendix we derive an effective 1D potential for a point-like impurity that takes into account the Rashba spin-orbit effect in the first subband with $n = 0$. We first calculate the matrix elements given by

$$V_{\sigma'\sigma}^{1D} = \langle \psi_{0\sigma'} | V_{imp} | \psi_{0\sigma} \rangle \ . \tag{C.1}$$

In a two-point representation the effective impurity potential is given by,

$$\hat{V}_{eff} = \int d\mathbf{x} d\mathbf{x}' \Psi_{\alpha'}^{\dagger}(\mathbf{x}') \, v_{\mathit{eff}}(\mathbf{x}', \mathbf{x}) \, \Psi_{\alpha}(\mathbf{x}) \ , \tag{C.2}$$

with $\alpha = n, k, \sigma$,

$$\Psi_{0k\sigma}(\mathbf{x}, \mathbf{y}) = \left[1 + i \frac{2\alpha_x \alpha_y}{\omega_0^2} (-i\partial_{\mathbf{x}}) (-i\partial_{\mathbf{y}}) \hat{\sigma}_z \right] \mathrm{e}^{\mathrm{i}\mathbf{k}\mathbf{x}} \Phi_0(\mathbf{y}) \, \chi_{\sigma}(s) \tag{C.3}$$

$$\Psi_{0k'\sigma'}^{\dagger}(\mathbf{x}, \mathbf{y}) = \left[1 - i \frac{2\alpha_x \alpha_y}{\omega_0^2} (i\partial_{\mathbf{x}}) (i\partial_{\mathbf{y}}) \hat{\sigma}_z \right] \mathrm{e}^{-\mathrm{i}\mathbf{k}'\mathbf{x}} \Phi_0(\mathbf{y}) \, \chi_{\sigma'}^{*}(s) \tag{C.4}$$

for the transformed problem $\Psi_{0k\sigma}(x,y) = [1-M]\,\tilde{\Psi}_{k\sigma}(\mathbf{x},\mathbf{y},s)$ with the Schrieffer-Wolff transformation matrix obtained in Eq.(5.14). Then,

$$\langle \Psi_{0k'\sigma'}|v|\Psi_{0k\sigma}\rangle = \int dxdy \Psi^{\dagger}_{0k'\sigma'}(\mathbf{x},\mathbf{y})\, v_0 \delta(x-x_0)\,\delta(y-y_0)\,\Psi_{0k\sigma}(\mathbf{x},\mathbf{y}) \tag{C.5}$$

$$= u_0 \Phi_0^2(y_0)\, \mathrm{e}^{\mathrm{i}(k-k')x_0} \tag{C.6}$$

$$- \mathrm{i}u_0 \frac{2\alpha_x\alpha_y}{\omega_0^2} \mathrm{i}(k+k')\, \mathrm{e}^{\mathrm{i}(k-k')x_0} \Phi_0(y_0)\,\partial_y\Phi_0(y_0)\,\sigma_z\ . \tag{C.7}$$

We Fourier transform back Eq.(C.5) and we obtain the following expression for the effective potential in the two-point representation,

$$\mathcal{V}_{eff}(\mathbf{x}',\mathbf{x}) = v_0\Phi_0^2(y_0)\,\delta(x-x_0)\,\delta(x'-x_0) - iv_0\frac{2\alpha_x\alpha_y}{\omega_0^2}\Phi_0(y_0)\,\partial_y\Phi_0(y_0)\,\sigma_z \times \left[\delta'_x(x-x_0)\,\delta_{x'}(x'-x_0) - \delta_x(x-x_0)\,\delta'_{x'}(x'-x_0)\right]\ . \tag{C.8}$$

The Lippmann-Schwinger equation for this effective potential in the two-point representation can be written in the position representation as

$$\langle x|\psi\rangle = \langle x|\phi\rangle + \int dx' \langle x|\frac{1}{E-H_0}|x'\rangle\langle x'|V|\psi\rangle = \langle x|\phi\rangle - \int dx' G(x,x') \int dx'' \langle x'|V|x''\rangle\langle x''|\psi\rangle\ . \tag{C.9}$$

resulting in

$$\psi(x) = \phi(x) - \int dx'dx'' G(x,x')\,V(x',x'')\,\psi(x'')\ . \tag{C.10}$$

Combining both Eq.(C.10) and Eq.(C.8) we obtain the following expression for the scatttering state at the impurity position:

$$\psi(x) = \phi(x) - v_0\Phi_0^2(y_0)\,G(x,x_0)\,\psi(x_0)\,\mathbb{1} - \mathrm{i}v_0\frac{2\alpha_x\alpha_y}{\omega_0^2}\left[\partial_y\Phi_0(y_0)\right]\Phi_0(y_0) \times \left\{\partial_{x_0}G(x,x_0)\,\hat{\sigma}_z\psi(x_0) - G(x,x_0)\,\hat{\sigma}_z\partial_{x_0}\psi(x_0)\right\}\ . \tag{C.11}$$

In order to obtain the value of the scattering state inside the impurity at $x = x_0$ we have to close the system of equations for $\psi(x_0)$ and $\partial_{x_0}\psi(x_0)$.

We do so by differentiating the expression in Eq. (C.11) and evaluating it at $x = x_0$:

$$\partial_x\psi(x) = \partial_x\phi(x) - v_0\Phi_0^2(y_0)\,\partial_x G(x,x_0)\,\psi(x_0)\,\mathbb{1} - \mathrm{i}v_0\frac{2\alpha_x\alpha_y}{\omega_0^2}\left[\partial_y\Phi_0(y_0)\right]\Phi_0(y_0) \times\left\{\partial_x\left[\partial_{x_0}G(x,x_0)\right]\hat{\sigma}_z\psi(x_0) - G(x,x_0)\,\hat{\sigma}_z\partial_{x_0}\psi(x_0)\right\}\ . \tag{C.12}$$

The Green's fuction for the 1D model transformed under the $SU(2)$ symmetry given by Eq.(5.34) as,

$$G(x,x') = g_0\mathrm{e}^{\mathrm{i}k_n|x-x'|}\left(\cos\left[k_R(x-x')\right] - \mathrm{i}\hat{\sigma}_y\sin\left[k_R(x-x')\right]\right)\ , \tag{C.13}$$

with $g_0 = \mathrm{i}/\hbar$ and $k_R = m_e^*\alpha_x/\hbar$. For the derivatives in Eq.(C.12), when $x \to x_0$:

$$\begin{aligned} G(x,x_0) &\to g_0 && \text{(C.14)}\\ \partial_{x_0}G(x,x_0) &\to \mathrm{i}g_0k_R\hat{\sigma}_y && \text{(C.15)}\\ \partial_x G(x,x_0) &\to \mathrm{i}g_0k_R\hat{\sigma}_y && \text{(C.16)}\\ \partial_x\left[\partial_{x_0}G(x,x_0)\right] &\to \infty && \text{(C.17)} \end{aligned}$$

It is worth noticing, that both derivatives $\partial_{x_0}G(x,x_0)$ and $\partial_x G(x,x_0)$ in Eq.(C.11) are of order $\mathcal{O}(\alpha_x^2\alpha_y)$ whereas the $\partial_x\left[\partial_{x_0}G(x,x_0)\right]$ as a term of order $\mathcal{O}\left(\alpha_x^2\alpha_y^2\right)$, and therefore they can all be neglected. Thus, we can write the solutions for the wavefunction and its derivative, $\psi(x_0)$ and $\partial_{x_0}\psi(x_0)$,as

$$\begin{aligned} \psi(x_0) &= \left[1 + v_0g_0\Phi_0^2\right]^{-1}\left\{\phi(x_0) + \mathrm{i}v_0\frac{2\alpha_x\alpha_y}{\omega_0^2}\left(\partial_y\Phi_0\right)\Phi_0g_0\hat{\sigma}_z\partial_{x_0}\phi(x_0)\right\}\\ \partial_{x_0}\psi(x_0) &= \partial_{x_0}\phi(x_0)\ , \end{aligned} \tag{C.18}$$

where we are only going to keep the terms up to second order in Rashba interaction, $\alpha_x\alpha_y$.

Finally, the scattering states are given by,

$$\begin{aligned} \psi(x) = \phi(x) &- \frac{v_0}{1 + v_0g_0\Phi_0^2(y_0)}\Phi_0^2(y_0)\,G(x,x_0)\,\phi(x_0)\,\mathbb{1}\\ &-\mathrm{i}\frac{v_0}{1 + v_0g_0\Phi_0^2(y_0)}\frac{2\alpha_x\alpha_y}{\omega_0^2}\left[\partial_y\Phi_0(y_0)\right]\Phi_0(y_0)\\ &\times\left\{\partial_{x_0}G(x,x_0)\,\hat{\sigma}_z\phi(x_0) - G(x,x_0)\,\hat{\sigma}_z\partial_{x_0}\phi(x_0)\right\}\ . \end{aligned} \tag{C.19}$$

If we write the Green's function as $G = \phi_{L0\sigma'}(x)\,\phi^*_{L0\sigma'}(x')$ with an incoming state propagating in the first band $\phi_{L0\sigma'}(x) = (\sqrt{\hbar/mk_0})\mathrm{e}^{\mathrm{i}(k_0 - k_R\hat{\sigma}_y)x}\chi_{\sigma'}$ we can probe (C.19) on the right side of the impurity by sending an incoming state from the left and looking at the asymptotic expression at $x \to \infty$,obtaining the transmission for the state scattering from left to right

$$t^{LR}_{0\sigma',0\sigma} = 1 - \frac{v_0}{1+g_0\Phi_0^2}\Phi_0^2\phi^*_{L0\sigma'}\phi_{L0\sigma} - \mathrm{i}\frac{v_0}{1+g_0\Phi_0^2}\frac{2\alpha_x\alpha_y}{\omega_0^2}\left(\partial_y\Phi_0\right)\Phi_0\left\{\partial_{x_0}\phi'^*_{L0\sigma'}\hat{\sigma}_z\phi_{L0\sigma} - \phi^*_{L0\sigma'}\hat{\sigma}_z\partial_{x_0}\phi'_{L0\sigma}\right\}. \tag{C.20}$$

The rest of the terms of the scattering matrix can be found in a similar fashion. We have to remember that we are dealing with spinors, and that this scattering coefficients are matrices in spin. Then, similarly for the reflexion coefficient from the left side $r^{LL}_{0\sigma',0\sigma}$, we write the Green's function as $G = \phi_{R0\sigma'}(x)\,\phi^*_{R0\sigma'}(x')$ with $\phi_{R0\sigma'}(x) = \sqrt{\frac{\hbar}{mk_0}}\mathrm{e}^{-\mathrm{i}(k_0 + k_R\hat{\sigma}_y)x}\chi_{\sigma'}$ we can probe (C.19) at $x \to -\infty$ by sending and incoming state from the left $\phi_{L0\sigma'}(x)$, such that

$$r^{LL}_{m\sigma',n\sigma} = -\frac{v_0}{1+g_0\Phi_0^2}\Phi_0^2\phi^*_{Rm\sigma'}\phi_{Ln\sigma} - \mathrm{i}\frac{v_0}{1+g_0\Phi_n^2}\frac{2\alpha_x\alpha_y}{\omega_0^2}\left(\partial_y\Phi_0\right)\Phi_0\left\{\partial_{x_0}\phi'^*_{R0\sigma'}\hat{\sigma}_z\phi_{L0\sigma} - \phi^*_{R0\sigma'}\hat{\sigma}_z\partial_{x_0}\phi'_{L0\sigma}\right\}. \tag{C.21}$$

The validity and limitations of this approach are discussed in Chapter 6.